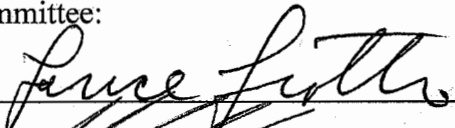
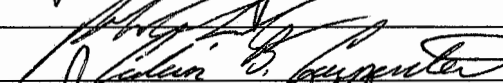
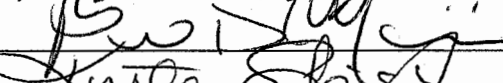
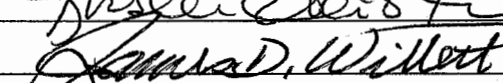


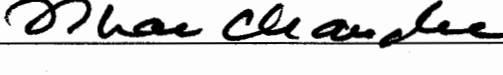
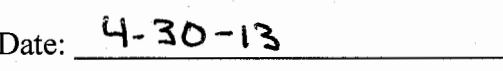


KILLING PRE-INVASIVE BREAST CANCER BY TARGETING AUTOPHAGY: A  
NEW VISION FOR CHEMOPREVENTION

by

Virginia Espina  
A Dissertation  
Submitted to the  
Graduate Faculty  
of  
George Mason University  
in Partial Fulfillment of  
The Requirements for the Degree  
of  
Doctor of Philosophy  
Biosciences

Committee:

	Dr. Lance A. Liotta, Dissertation Director
	Dr. Robin Couch, Committee Member
	Dr. Calvin Carpenter, Committee Member
	Dr. Brian D. Mariani, Committee Member
	Dr. Kirsten Edmiston, Committee Member
	Dr. James Willett, Director, School of Systems Biology
	Dr. Timothy L. Born, Associate Dean for Student and Academic Affairs, College of Science
	Dr. Vikas Chandhoke, Dean, College of Science

Date: 4-30-13

Spring Semester 2013  
George Mason University  
Fairfax, VA

Killing Pre-invasive Breast Cancer by Targeting Autophagy: A New Vision for  
Chemoprevention

A Dissertation submitted in partial fulfillment of the requirements for the degree of  
Doctor of Philosophy at George Mason University

by

Virginia Espina  
Master of Science  
Johns Hopkins University, 1999  
Bachelor of Science  
Rochester Institute of Technology, 1982  
Associate in Applied Science  
Rochester Institute of Technology, 1980

Director: Lance A. Liotta, Professor, School of Systems Biology and  
Biosciences

Spring Semester 2013  
George Mason University  
Fairfax, VA



This work is licensed under a [creative commons attribution-noncommercial 3.0 unported license](https://creativecommons.org/licenses/by-nc/3.0/).

Copyright 2013 Virginia Espina  
All Rights Reserved

## **DEDICATION**

To my family, Tito, Ben, Paul, Emily, and the cats.

## ACKNOWLEDGEMENTS

I would like to thank my dear husband Tito for his encouragement, loving support, and help with the household. His unwavering faith, confidence, and cooking, provided the mental and physical fuel needed to pursue this goal. My children, Ben, Paul and Emily, deserve untold gratitude for understanding the importance of *my* homework, in relation to *their* homework. Mary Anne and Len Schiff provided the early inspirational influence to pursue scientific research beyond the clinical laboratory bench. I would like to thank my committee, colleagues, faculty, and staff at George Mason University, for encouraging and supporting non-traditional graduate students. Daily scientific discussions with my committee director, Dr. Liotta, profoundly nurtured my theories and ideas. Dr. Liotta generously toiled alongside me as we collected tissue, injected mice, and cultured cells over the years. Dr. Mariani and Khoa Tran, Genetics & IVF Institute, performed the CytoSNP arrays and patiently taught me the technology. Dr. Mariani provided expert guidance regarding genomic technology for this project and shared invaluable career advice. Dr. Edmiston actively supported our clinical trial by recruiting patients, performing surgeries, and acting as Principal Clinical Investigator. Dr. Carpenter provided vital assistance with animal protocols. Dr. Couch offered unique biochemistry advice related to drug metabolism. Dr. Sulma Mohammed, Purdue University, kindly supplied the canine tissue blocks. Jianghong Deng provided statistical assistance. Claudius Mueller and Isela Gallagher skillfully assisted with cell culture, keeping my cells alive while I fulfilled by teaching/research/lab management obligations. Finally, I would like to thank all the patients who volunteered to participate in these research projects and our clinical trial.

The content of Chapters one through five was modified and reproduced from the following publications:

Espina V, Mariani BD, Gallagher RI, Tran K, Banks S, Wiedemann J, Huryk H, Mueller C, Adamo L, Deng J, Petricoin EF, Pastore L, Zaman S, Menezes G, Mize J, Johal J, Edmiston K, Liotta LA. Malignant precursor cells pre-exist in human breast DCIS and require autophagy for survival. PLoS One. 2010 Apr 20;5(4):e10240.

Espina V, Wysolmerski J, Edmiston K, Liotta LA. Attacking breast cancer at the preinvasion stage by targeting autophagy. *Womens Health (Lond Engl)*. 2013 Mar;9(2):157-70.

Espina V, Liotta LA. What is the malignant nature of human ductal carcinoma in situ? *Nat Rev Cancer*. 2011 Jan;11(1):68-75.

Espina V, Liotta LA. Chloroquine enjoys a renaissance as an anti-neoplastic therapy. *Clinical Investigation*. 2013 (submitted).

Mueller C, Edmiston KH, Carpenter C, Gaffney E, Ryan C, Ward R, White S, Memeo L, Colarossi C, Petricoin EF 3rd, Liotta LA, Espina V. One-step preservation of phosphoproteins and tissue morphology at room temperature for diagnostic and research specimens. *PLoS One*. 2011;6(8):e23780.

Mueller C, Liotta LA, Espina V. Reverse phase protein microarrays advance to use in clinical trials. *Mol Oncol*. 2010 Dec;4(6):461-81.

## TABLE OF CONTENTS

	Page
List of Tables .....	x
List of Figures .....	xi
List of Equations .....	xiii
List of Abbreviations and Symbols .....	xiv
Abstract .....	xvi
Chapter 1: Biological questions in breast cancer progression .....	1
Introduction .....	1
Current controversies in breast cancer .....	2
Breast physiology .....	5
Breast ductal structure and microenvironment .....	5
Evolution of the breast .....	9
Intraductal microcalcifications record long standing hypoxic stress .....	11
Breast cancer progression from atypia to invasive phenotype .....	13
Breast cancer statistics .....	14
Chapter 2: Isolation and Propagation of DCIS progenitor cells .....	17
Introduction .....	17
Breast stem cells .....	17
Phenotypic classification of putative stem cells .....	18
Transition from in situ to invasive phenotype .....	21
Materials and methods .....	23
Female human breast tissue .....	23
<i>Ex vivo</i> organoid culture .....	23
Xenograft Tumor Generation .....	24
Immunofluorescence .....	25
Results .....	26
Ex vivo organoid culture system for breast DCIS .....	26

Anchorage independent neoplastic epithelial cells spontaneously emerge in organoid culture of human DCIS .....	29
Generation of mouse mammary tumor xenografts from human DCIS .....	32
Discussion .....	36
Human Ductal Carcinoma In Situ contains malignant progenitor cells .....	37
Chapter 3: Proteomic analysis of DCIS Cells.....	41
Introduction .....	41
Protein signaling cascades .....	41
Materials and methods .....	43
Reverse Phase Protein Microarray (RPMA) .....	43
Immunohistochemistry .....	46
Immunofluorescence .....	47
Statistics.....	48
Results.....	48
Signal pathway proteomic analysis reveals augmentation of survival related pathways .....	48
Protein pathways intersecting with autophagy .....	52
Immune cells in the DCIS microenvironment.....	55
Disruption of autophagy in DCIS-derived spheroids .....	56
Discussion .....	57
Proteomic biomarkers in DCIS.....	57
Chapter 4: Molecular Cytogenetic characterization of DCIS cells.....	62
Introduction .....	62
Gene expression studies of human breast cancer .....	62
Genetic instability .....	63
Molecular karyotyping .....	64
Materials and methods .....	65
Samples.....	65
Molecular karyotyping via Single Nucleotide Polymorphism analysis .....	65
Immunohistochemistry .....	66
Results .....	66
DCIS derived tumorigenic spheroid forming cells are cytogenetically abnormal ....	66
Temporal comparison of molecular karyotyping .....	72



Abrogation of genetically unstable cells .....	75
Localization of SUPT3H in DCIS lesions .....	77
Discussion .....	78
Autophagy and genetic instability .....	78
Energy consumption for transcription, translation, remodeling, and DNA repair ....	80
Temporal variation in SNP microarray data .....	81
Chromosome 6 genes implicated in cancer .....	82
SUPT3H, chromatin modifications, epigenetic marks .....	84
Chapter 5: Autophagy as a therapeutic target in DCIS .....	87
Introduction .....	87
Cytoprotective Autophagy .....	87
Chloroquine: an anti-lysosomotropic agent .....	89
Development of medicinal 4-aminoquinolines .....	91
Chloroquine bioavailability/pharmacodynamics .....	92
Chloroquine metabolism and excretion .....	94
Materials and Methods .....	95
Chloroquine treatment of organoid cultures .....	95
Invasion/migration assay .....	95
Reverse Phase Protein Microarray .....	96
Immunohistochemistry .....	96
Statistics .....	96
Results .....	97
Autophagy is required for emergence and survival of DCIS tumorigenic spheroid cells .....	97
Chloroquine inhibits xenograft tumor formation .....	100
Chloroquine inhibits autophagy associated pathway proteins .....	100
Chloroquine treated cells fail to elicit a wound healing response <i>in vitro</i> .....	102
Autophagy is induced in a canine model of DCIS .....	104
Discussion .....	105
Cellular energy alterations during autophagy .....	105
Effects of ATP and nucleotide depletion on chromosomal stability .....	106
Chloroquine for chemoprevention of invasive breast cancer .....	109
Chapter 6: Efficacy of Chloroquine to treat DCIS in a Phase I/II Clinical TRial .....	110

Introduction .....	110
Rationale for a new clinical trial strategy .....	110
Preventing Invasive Neoplasia with Chloroquine (PINC) trial .....	112
Methods .....	117
Patient recruitment and tissue collection .....	117
Ex vivo organoid culture .....	118
Zymography of conditioned medium .....	118
Proliferation Index: Immunohistochemistry .....	119
Results .....	120
Patient enrollment .....	120
Diminished spheroid formation post treatment in <i>ex vivo</i> organoid culture .....	120
Matrix metalloproteinases in organoids and conditioned medium .....	123
Proliferation index reduction post anti-autophagy therapy .....	124
Pathologic response: Decrease in DCIS lesion volume .....	126
Discussion .....	128
Clinical trial progress to date .....	128
Proliferation index markers .....	130
Epidemiologic study of breast cancer prevalence in relation to Chloroquine use ...	131
Proposed epidemiologic study .....	133
Neuroendocrine axis and calcium regulation as new therapeutic targets .....	135
Summary .....	138
Index .....	140
References .....	143

## LIST OF TABLES

Table	Page
Table 1. Patient characteristics for generation of <i>ex vivo</i> organoid cultures. ....	28
Table 2. Mouse xenograft efficacy for lobular, invasive and pure DCIS breast tissue. ...	34
Table 3. Validated antibodies used with Reverse Phase Protein Microarrays.....	44
Table 4. Primary antibodies and heat induced epitope retrieval (HIER) conditions for immunohistochemistry.....	47
Table 5. Verification of DCIS stem-like cell phenotype. ....	51
Table 6. Immunohistochemical characterization of the primary human breast tissue (diagnostic specimen). ....	52
Table 7. Molecular karyotype of cultured human DCIS spheroid showing cytological location of chromosome aberrations (Corrected from reference <sup>10</sup> ). ....	70
Table 8. Mouse xenograft characteristics for chloroquine treated tissue implants.....	100
Table 9. Clinical data for PINC patients enrolled to date. ....	120
Table 10. Characteristics of organoid cultures from surgical tissue harvested post Aralen treatment. ....	121
Table 11. Pathologic response for PINC patients based on reduction in lesion area and proliferation index.....	127
Table 12. PINC trial outcome variables and statistical methods. ....	129

## LIST OF FIGURES

Figure	Page
Figure 1. The breast ductal carcinoma in situ microenvironment. ....	2
Figure 2. Schematic for emergence of invasive cells at the DCIS stage by either clonal evolution or cancer stem cells. ....	4
Figure 3. Human cadaver breast ductal tree. ....	6
Figure 4. Human breast duct anatomy and model of intra-ductal zones of stress. ....	8
Figure 5. New theory for emergence of invasive breast cancer. ....	14
Figure 6. Culture system for DCIS organoids. ....	27
Figure 7. Human DCIS tissue generates pseudoductal structures and spheroids in <i>ex vivo</i> culture. ....	28
Figure 8. Hematoxylin & Eosin stain of cultured human DCIS organoids. ....	30
Figure 9. Collagen type IV delineates intact basement membranes in pure DCIS lesions. ....	31
Figure 10. Human DCIS tissue generates spheroid and pseudoductal structures in <i>ex vivo</i> culture and forms xenograft tumors. ....	32
Figure 11. Representative tumor volume measurements for murine xenograft tumors from pure human DCIS cells. ....	33
Figure 12. Continuum of human breast cancer progression. ....	40
Figure 13. Signal pathway mapping by reverse phase protein microarray of DCIS organoid outgrowths. ....	50
Figure 14. Autophagy is activated in human DCIS lesions, spheroids, 3D structures, and xenograft tumors. ....	54
Figure 15. CD68 positive macrophages are located in the lumen and surrounding the periphery of the duct in DCIS lesions. ....	56
Figure 16. Autophagy pathway overview (Modified from reference <sup>157</sup> ). ....	61
Figure 17. Three independent patient's DCIS spheroids exhibited the same Chromosome 6p21.1-p12.3 copy number loss (deletion) <sup>10</sup> ....	69
Figure 18. Chromosome 17q shows extensive regions of copy number variation (gain) for spheroids from case 09-148. ....	70
Figure 19. Cell culture conditions did not induce genetic instability. ....	72
Figure 20. Copy Number Variation (CNV) summary of DCIS organoid cell cultures reflecting temporal aspects of <i>ex vivo</i> culture. ....	74
Figure 21. Copy number variation is not induced by chloroquine treatment in DCIS derived spheroids. ....	76
Figure 22. Molecular karyotype of chromosome 5 from chloroquine treated monolayer or untreated spheroids/3-D structures derived from human DCIS <sup>10</sup> ....	77

Figure 23. SUPT3H immunohistochemistry of case 09-148 shows rare cells with nuclear staining (black arrows) and numerous cells with cytoplasmic staining.....	78
Figure 24. Chemical structure of chloroquine diphosphate (Aralen, Sanofi-Aventis). ....	92
Figure 25. Chloroquine alters signal transduction pathways, suppresses DCIS neoplastic cell outgrowth, and spheroid formation. ....	99
Figure 26. Chloroquine increased levels of the apoptotic protein cleaved PARP Asp214 in human DCIS cultured cells and suppressed levels of proliferation associated proteins (n=3, mean $\pm$ SEM).....	101
Figure 27. Calcium export protein, PMCA2, is strongly expressed in cultured DCIS malignant progenitor cells.....	102
Figure 28. Migration assay in organoid culture. ....	103
Figure 29. Chloroquine prevented invasion/migration in an <i>in vitro</i> scratch assay.....	104
Figure 30. LC3B immunohistochemistry indicates up-regulation of autophagy in a canine model of breast cancer. ....	105
Figure 31. PINC trial design. ....	113
Figure 32. PINC trial workflow. ....	116
Figure 33. Lack of extensive 3-D structure formation and spheroid development in the organoid culture following 4 weeks of <i>in vivo</i> Chloroquine diphosphate (Aralen) therapy. ....	122
Figure 34. Matrix metalloproteinases are present in conditioned medium harvested from <i>ex vivo</i> cultures of patients treated with Aralen for 4 weeks. ....	124
Figure 35. The proliferation index is significantly reduced following a 4 week course of Aralen therapy in patients diagnosed with breast ductal carcinoma in situ. ....	125
Figure 36. PCNA proliferation index for PINC patients before (blue circles) and after Aralen treatment (red squares).....	126
Figure 37. Immunohistochemistry reveals a reduction in breast DCIS cell proliferation and autophagy following <i>in vivo</i> chloroquine treatment.....	128

## LIST OF EQUATIONS

Equation	Page
Equation 1. Cancer incidence rate .....	15
Equation 2. Proliferation Index.....	120

## LIST OF ABBREVIATIONS AND SYMBOLS

Adenosine Triphosphate .....	ATP
Atypical Ductal Hyperplasia.....	ADH
Atypical Lobular Hyperplasia.....	ALH
Autophagy Related Homolog 5 .....	Atg5
Autophagy Related Homolog 7 .....	Atg7
Biomarker and Histology Preservative .....	BHP
Bloom Syndrome, RecQ helicase-like .....	BLM
BRCA1/2.....	breast cancer 1/2, early onset
Calcium .....	Ca <sup>+2</sup>
Chloroquine .....	CQ
Cleaved Caspase 3 .....	CC3
Cleaved Caspase 9 .....	CC9
Confidence Interval.....	CI
Copy Number Variation.....	CNV
Diaminobenzidine .....	DAB
Ductal Carcinoma In Situ.....	DCIS
Dulbecco's Modified Essential Medium .....	DMEM
Epithelial Cell Adhesion Molecule.....	EpCAM
Estrogen Receptor .....	ER
Extracellular matrix .....	ECM
Extracellular signal Related Kinase .....	ERK
Focal Adhesion Kinase .....	FAK
Forkhead box protein .....	FOXO
Formalin Fixed Paraffin Embedded.....	FFPE
Hematoxylin and Eosin.....	H&E
Heat Induced Epitope Retrieval .....	HIER
Homeo-box domain .....	Hox
Hydroxychloroquine .....	HCQ
Hypoxia Inducible Factor .....	HIF-1
Immunofluorescence.....	IF
Immunohistochemistry .....	IHC
Invasive Ductal Carcinoma.....	IDC
Janus Kinase/Signal Activator and Transducer of Transcription .....	Jak/Stat
Lobular Carcinoma In Situ.....	LCIS
Loss of Heterozygosity .....	LOH
Magnetic Resonance Imaging.....	MRI

Major Histocompatibility Complex .....	MHC
Mammalian Target of Rapamycin .....	mTOR
Matrix Metalloproteinases .....	MMP
Matrix Metalloproteinase 9.....	MMP-9
Matrix Metalloproteinase 2.....	MMP-2
Matrix Metalloproteinase 14.....	MMP-14
Megabase .....	MB
Messenger RNA.....	mRNA
microtubule-associated protein-1 Light Chain 3 Beta .....	LC3B
Mitogen Activated Protein Kinase.....	MAPK
National Comprehensive Cancer Network .....	NCCN
National Institute of Health.....	NIH
Nuclear Factor KappaB.....	NF- $\kappa$ B
Non-obese Diabetic Severe Combined Immunodeficiency .....	NOD SCID
Plasma Membrane Calcium ATPase isoform2 .....	PMCA2
Phosphatidylinositol 3' Kinase .....	PI3K
Polycomb Group Repressor Complex .....	PGRC
Pre-B-cell leukemia transcription factor 1 .....	PBX1
Preventing Invasive breast Neoplasia with Chloroquine .....	PINC
Progesterone Receptor .....	PR
Proliferating Cell Nuclear Antigen .....	PCNA
Protein Kinase B .....	AKT
Response Evaluation Criteria In Solid Tumors .....	RECIST
Reverse Phase Protein Microarray.....	RPMA
Ribosomal RNA.....	rRNA
Runt related transcription factor 2 .....	RUNX2
Serine .....	Ser
Single Nucleotide Polymorphism .....	SNP
Suppressor of Ty3 Homolog.....	SUPT3H
SWItch/Sucrose NonFermentable.....	SWI/SNF
Terminal Ductal Lobulo-alveolar Units.....	TDLU
Threonine .....	Thr
Transcription Factor EB.....	TFEB
Tyrosine .....	Tyr
Ultrasound.....	US
$\alpha$ .....	alpha
$\beta$ .....	beta
$\delta$ .....	delta
$\kappa$ .....	kappa
$\mu$ .....	micro
$\pm$ .....	plus/minus



## ABSTRACT

### KILLING PRE-INVASIVE BREAST CANCER BY TARGETING AUTOPHAGY: A NEW VISION FOR CHEMOPREVENTION

Virginia Espina, Ph.D.

George Mason University, 2013

Dissertation Director: Dr. Lance A. Liotta

All invasive breast cancer is thought to be preceded by a pre-invasive state in which cells accumulate within the breast ductal niche. Breast cancer progression is thought to be a multi-step process involving a continuum of changes from a normal phenotype through hyperplastic lesions, carcinoma in situ, invasive carcinoma, to metastatic disease. Previously it was assumed that the invasive phenotype acquired major genetic changes during the phenotypic transition from ductal carcinoma in situ (DCIS) to invasive carcinoma. In direct contradiction to this previous assumption, herein we demonstrate, for the first time, the pre-existence of genetically abnormal, tumorigenic carcinoma progenitor cells within human breast DCIS lesions.

Human DCIS cells were cultivated *ex vivo* without a priori enzymatic treatment or sorting. The DCIS organoid cultures induced the emergence of neoplastic epithelial cells exhibiting the following characteristics: a) spontaneous generation of hundreds of

spheroids and duct-like 3-D structures in culture within 2-4 weeks, b) tumorigenicity in NOD SCID mice, and c) *in vitro* migration and invasion of autologous breast stroma. Proteomic characterization revealed that DCIS cells up-regulate signaling pathways directly, and indirectly, linked to cellular autophagy. Cells that proliferate and accumulate within the non-vascular intraductal space are under severe hypoxic and metabolic stress. Pre-invasive cells must adapt to hypoxic stress within the duct in order to survive and proliferate. Autophagy was found to be required for survival and anchorage independent growth, in the patient's original DCIS lesion and the mouse xenograft. Molecular karyotyping demonstrated DCIS cells to be cytogenetically abnormal (copy number loss or gain in chromosomes including 1, 5, 6, 8, 13, 17) compared to the normal karyotype of the non-neoplastic cells in the patient's breast tissue.

To demonstrate the dependence of the cytogenetically abnormal DCIS cells on autophagy as a survival mechanism, primary human DCIS cell cultures were treated with chloroquine phosphate, a lysosomotropic inhibitor of autophagy. Chloroquine treatment completely suppressed the generation of DCIS spheroids/3-D structures, suppressed *ex vivo* invasion of autologous stroma, induced apoptosis, suppressed autophagy associated proteins including Atg5, AKT/PI3 Kinase, and mTOR, eliminated cytogenetically abnormal spheroid forming cells from the organ culture, and abrogated xenograft tumor formation.

With the broad goal of arresting all breast cancer at the non-invasive, non-lethal stage, a phase I/II clinical trial (PINC; Preventing Invasive breast Neoplasia with Chloroquine) was established for clinical evaluation of the safety and efficacy of

chloroquine phosphate as a strategy to treat human breast Ductal Carcinoma in Situ (DCIS). Therapy that induces regression, or prevents progression, of occult or overt pre-invasive lesions could comprise a new treatment strategy for pre-invasive cancers independent of hormone receptor status.

## CHAPTER 1: BIOLOGICAL QUESTIONS IN BREAST CANCER PROGRESSION

### Introduction

The fundamental view of breast cancer progression at the time this project commenced was thought to be a multi-step process involving a continuum of genetic and/or proteomic changes from a normal phenotype through hyperplastic lesions, carcinoma in situ, invasive carcinoma, to metastatic disease<sup>1</sup>. Breast ductal carcinoma in situ (DCIS) morphologically appears as an accumulation of proliferating epithelial cells confined within the lumen of the breast duct. DCIS, by definition, has not invaded through the basement membrane encircling the duct, and might never invade the surrounding tissues (Figure 1)<sup>2</sup>. Even though DCIS is confined to the ductal lumen, there is clinical and experimental evidence to suggest that DCIS is a precursor lesion to most, if not all invasive breast cancer, including *BRCA1/2*-associated (breast cancer 1/2, early onset) carcinogenesis<sup>3-8</sup>. Nevertheless, the genetic step that transforms DCIS to an invasive cancer has not been elucidated because, delineated herein, DCIS cells already possess the capacity to invade but are held in check within the duct<sup>9-11</sup>. To decipher the molecular underpinnings of breast epithelial cells that accumulate within the breast duct at the DCIS stage, their capacity for invasion, and therapies that will kill pre-malignant lesions, one must first appreciate the controversies regarding breast cancer, the complex

female breast physiology, morphological heterogeneity of DCIS, and the reasons for the increased incidence of DCIS.

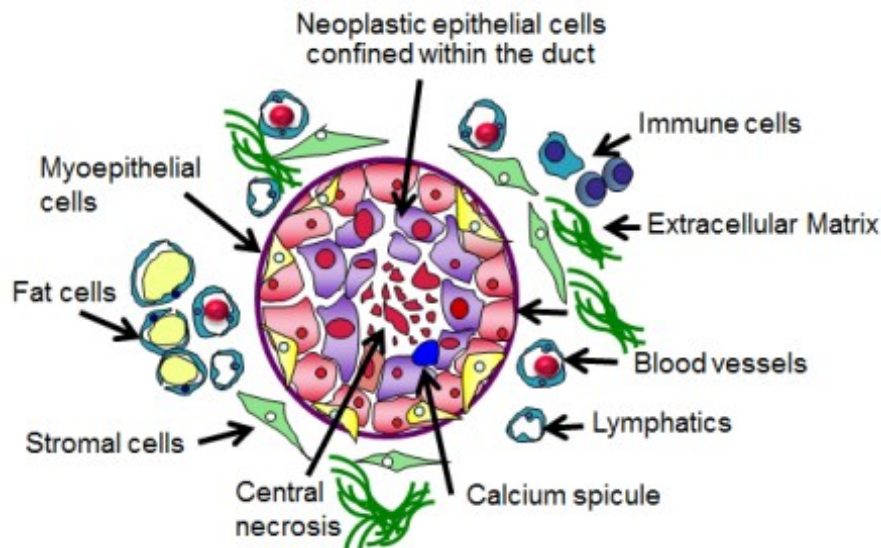


**Figure 1. The breast ductal carcinoma in situ microenvironment.** Breast epithelial cells proliferate within the confines of the duct basement membrane. Myoepithelial cells (yellow) adhere to the basement membrane. Luminal epithelium (pink) face the duct lumen. DCIS cells (purple) accumulate within the lumen. The duct is surrounded by adipose tissue, stromal fibroblasts, blood vessels, lymphatics, immune cells, and extracellular matrix. (Adapted from reference <sup>9</sup>, Espina V and Liotta LA (2011) Nature Reviews Cancer).

### **Current controversies in breast cancer**

How and why cells accumulate in the breast duct is unknown. Natural history studies of DCIS are rare due to historical diagnostic hurdles (prior to routine mammography/Magnetic Resonance Imaging (MRI)), reclassification of “benign DCIS” as atypical ductal hyperplasia, the spectrum of DCIS lesions (localized low grade through diffuse high grade, with/without necrosis), and a long clinical evolution to invasive carcinoma<sup>12</sup>. A follow-up study of 28 women treated for low grade DCIS by biopsy only

revealed that the natural history of localized low grade DCIS can extend over 40 years, and the risk of invasive cancer persists for 15 years or more following biopsy<sup>12</sup>.

This long clinical evolution fuels the controversy within the breast cancer field regarding ductal carcinoma in situ on two levels: 1) Is DCIS a carcinoma, implying the ability to become invasive, or is it a pre-invasive stage that requires accumulation of additional genetic changes to become invasive? and 2) Are we over-treating DCIS that may never progress to invasive cancer? Recommendations from the 2009 National Institutes of Health (NIH) breast ductal carcinoma in situ (DCIS) consensus conference have highlighted the clinical controversies surrounding the treatment of DCIS and the need to understand the malignant nature of DCIS<sup>13</sup>. While some members of the NIH DCIS conference proposed that the word 'carcinoma' should be removed from the term DCIS because DCIS is non-invasive and has a favorable prognosis, experimental studies of human and mouse DCIS lesions are showing the opposite: carcinoma precursor cells exist within human and mouse DCIS lesions, and the aggressive phenotype of breast cancer is pre-determined at the pre-invasive stage<sup>10,14-19</sup>.

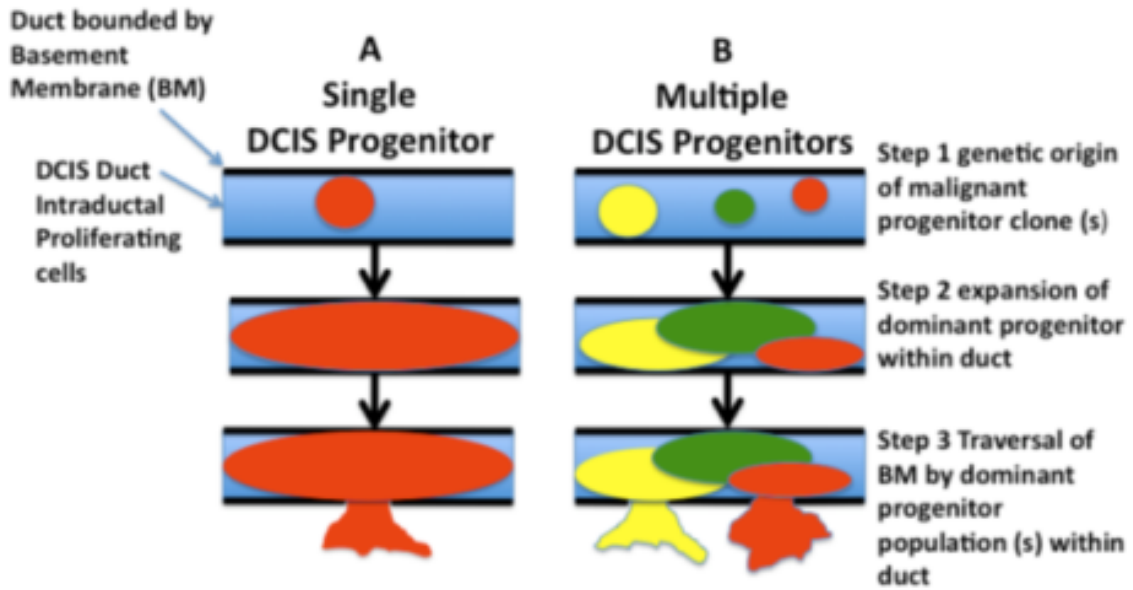


**Figure 2. Schematic for emergence of invasive cells at the DCIS stage by either clonal evolution or cancer stem cells.**  
**A) The clonal evolution theory stipulates that mutations accumulate over time allowing natural selection of competing clones. One cell acquires multiple mutations providing it with a survival advantage in the ductal niche. B) The cancer stem cell theory postulates that a population of progenitor cells with a stem cell-like phenotype drives tumor progression and generates tumor heterogeneity due to the existence of multiple stem-like cells with different mutations.**

Beyond the controversy of DCIS as “carcinoma” or “not carcinoma”, even the origin of carcinoma is arguable. The two competing theories on the evolution of carcinoma currently are the cancer stem cell theory and the clonal evolution model (Figure 2). The cancer stem cell theory postulates that a population of progenitor cells with a stem cell-like phenotype drives tumor progression and generates tumor heterogeneity due to the existence of multiple stem-like cells with different mutations<sup>1,20</sup>. Based on the cancer stem cell theory, an efficacious treatment would only need to kill the tumor stem cells. On the other hand, the clonal evolution model theorizes that mutations accumulate over time allowing natural selection of competing clones<sup>1,20</sup>. One cell acquires multiple mutations providing it with a survival advantage, while other non-

dominant clones may simultaneously exist but not predominate<sup>1,21</sup>. A curative therapy would therefore need to kill the dominant and non-dominant clonal populations. Both theories have merit, supporting the broad concepts of acquired genetic mutations, independent of the cell type in which the mutations occur, and the influence of the microenvironment on the tumor phenotype<sup>1,20</sup>. Regardless of the carcinoma evolution model, there is a need to identify successful therapies that impose lethal levels of cellular stress, or eradicate, the genetically abnormal cells capable of proliferating within their biological niche.

## **Breast physiology**

### **Breast ductal structure and microenvironment**

Human breast ductal tissue contains six distinct structures: 1) Terminal Ductal Lobulo-alveolar Units (TDLU) – alveoli clusters around a duct and ductal side branches, 2) Intra and Inter-lobular fibroblasts, 3) Ducts – branch-like tubules extending from the TDLU which empty into larger ducts called lactiferous ducts (Figure 3), 4) Lactiferous ducts – widen underneath the areola and nipple to become lactiferous sinuses, 5) Lactiferous sinuses – collect milk from lactiferous ducts and narrow to openings in the nipple (nipple pore), and 6) Basement membrane – extracellular collagen matrix that separates parenchymal cells from underlying connective tissue stroma<sup>20,22-24</sup>. Fibroblasts deposit type IV collagen providing a ductal substratum for mammary epithelium attachment and growth<sup>24</sup>. A normal duct is surrounded by an intact basement membrane. Contractile myoepithelial cells attach to the basement membrane providing tension and stretch receptors, while the secretory epithelial cells are apically located to the



myoepithelial cells<sup>5,25-28</sup> (Figure 4). Only the outside perimeter of the basement membrane interfaces with the connective tissue stroma, immune cells, lymphatics and vasculature<sup>5</sup>. Morphometric analysis of human breast tissue indicate that normal ducts are approximately 90 $\mu$ m in diameter, whereas ducts containing intraductal carcinoma have a mean diameter of 349  $\mu$ m<sup>29</sup>.

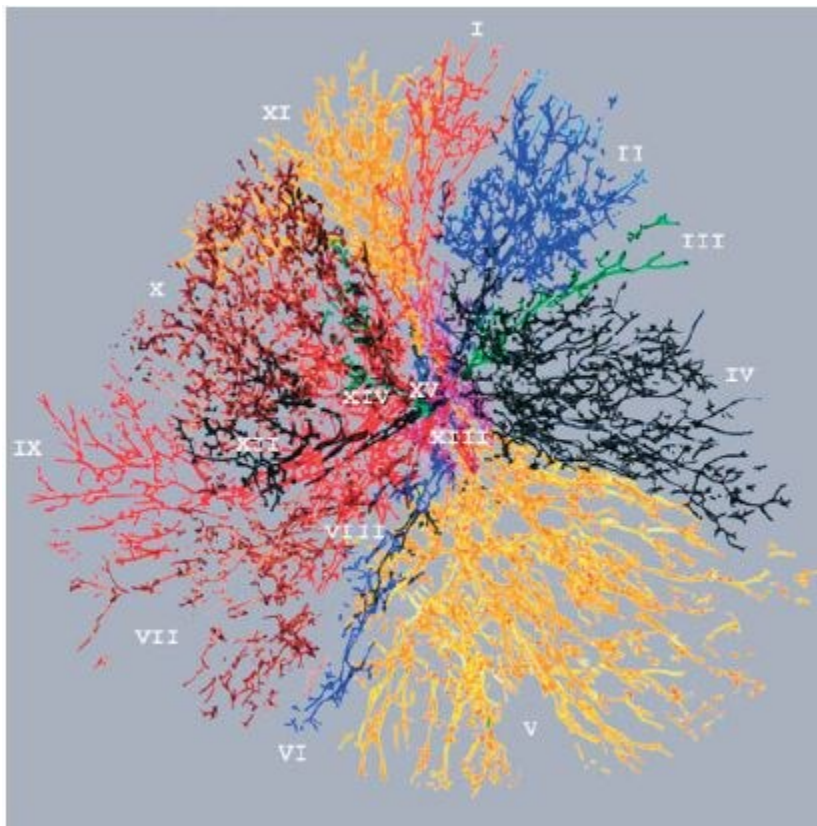


**Figure 3. Human cadaver breast ductal tree.**

**All ducts and their branches viewed en face. Each Roman numeral refers to a different independent duct system. Some colors are used for more than one duct system: II, VI, and XV (blue); III and XIV (green); IV and XII, black; V and XI (yellow); VII and X (brown); VIII and IX (red). I (orange) and XIII (purple) do not share their colors. Copyright © 2004 Pathological Society of Great Britain and Ireland. Published by John Wiley & Sons, Ltd.**

Beginning at puberty, the breast ducts proliferate into an expansive network of branches (Figure 3). Both the TDLU and duct have been identified as sources of adult mammary stem cells. The TDLU is composed of luminal cells responsible for milk production. Based on X-chromosome-linked gene inactivation studies, the TDLU has a clonal origin and may be the most likely site of adult stem cells responsible for the ductal proliferation during puberty, pregnancy, and menstrual cycles<sup>20</sup>. In contrast to the TDLU adult stem cell hypothesis, Villadsen *et al* showed that “stem cell zones” may be the source of adult breast stem cells<sup>30</sup>. Using enzymatically dissociated breast tissue, they classified cell populations using Keratin 14 as a myoepithelial marker and Keratin 19 as a marker of cell plasticity. They attributed stem-like qualities to the cells based on immunohistochemistry (IHC) of stage-specific embryonal antigen-4, keratins 6a, 15 and 5, Bcl-2, and chondroitin sulfate<sup>30</sup>. The duct derived cells exhibited clonal growth, self-renewal, and differentiation<sup>30</sup>. Regardless of the location of the mammary stem cell, *in vivo* disruption of the TDLU or duct basement membrane can conceivably liberate stem-like cells capable of invading the surrounding stroma<sup>9,10</sup>.

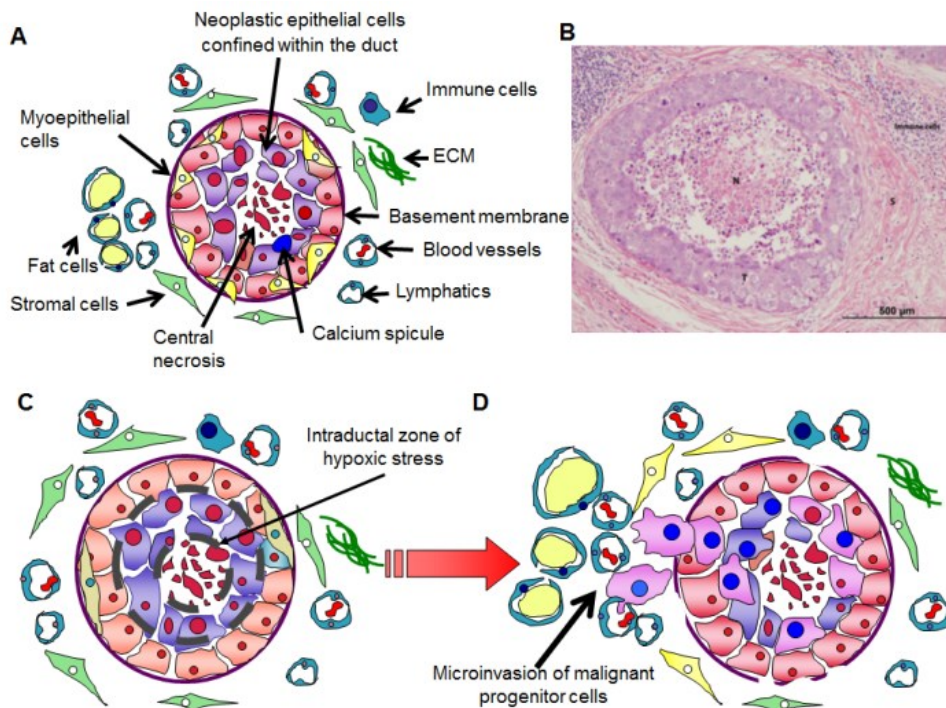


**Figure 4. Human breast duct anatomy and model of intra-ductal zones of stress.**  
**A.** Cells accumulate within the lumen of the duct in DCIS, which often has areas of central necrosis. **B.** Hematoxylin and Eosin (H&E) stained tissue section of DCIS with central necrosis and inflammatory cells surrounding the duct. **C-D.** Intraductal zones of stress due to loss of adhesion to the substratum, hypoxia, and nutrient deprivation. Adapted from reference <sup>9</sup>.

Five important aspects of breast anatomy related to DCIS are: 1) the ductal tree consists of multiple branches with minimal anastomoses<sup>31</sup>, 2) each human breast contains approximately 5-9 milk ducts that open on the nipple surface, 3) not all ducts have the same luminal diameter, 4) 10-15% of breast volume is epithelial components, and the remainder are stromal elements (connective and adipose tissue), and 5) ducts containing DCIS are 3-4 times the diameter of normal ducts<sup>22,23,32,33</sup>. Firstly, each duct is an individual microcosm, without connections to neighboring ducts. Hence, DCIS can develop in one duct or many ducts and the genetic lineage and phenotype of the DCIS cells may be heterogeneous. Secondly, not all ducts open to a nipple pore or have the

same lumen diameter. Therefore ductal lavage and peri-ductal sampling may not adequately represent all the ducts harboring DCIS. Thirdly, the percentage of adipose tissue in the breast stroma varies between individuals thus contributing different levels of adipokines/cytokines to the ductal niche<sup>34,35</sup>. Lastly, the diameter of the duct containing DCIS influences the intraductal zones of hypoxia and nutrient deprivation. The radius of the duct is a function of the radius of necrosis and the viable rim of epithelial/myoepithelial cells<sup>29</sup> (Figure 4B).

Ultrasound (US) imaging of breasts from healthy women, lactating women, and women with breast cancer reveal important features of breast anatomy for identifying potential DCIS. These features, in terms of interpreting US images, are: a) regularity, b) continuity, c) interruption, and d) disorder<sup>32,33</sup>. Normal mammary ducts appear isoechoic on US and the regularity and continuity of this pattern can be traced toward the nipple and toward the boundary with the lobes<sup>33</sup>. Sites of interruption can indicate pathological features such as cell accumulation or microcalcifications<sup>33,36</sup>. Regional variations in width may also indicate calcium deposits or abnormal cell accumulation, both of which are indicative of DCIS<sup>33,36</sup>.

### **Evolution of the breast**

Mammary glands are modified sweat glands that secrete proteins, water, minerals, and antibacterial enzymes<sup>22,37</sup>. The major protein components of human breast milk are beta-casein, alpha-lactalbumin, lactoferrin, immunoglobulin IgA, xanthine oxidoreductase, lysozyme, and serum albumin<sup>22,37</sup>. Breast myoepithelial cells also transport large quantities of calcium ( $\text{Ca}^{2+}$ ) against a gradient from the systemic

circulation into milk, and the cells must manage the large transcellular  $\text{Ca}^{2+}$  flux to avoid disruptions in  $\text{Ca}^{2+}$  signaling,  $\text{Ca}^{2+}$  toxicity, and apoptosis<sup>38</sup>. Calcium release post wounding serves as a second messenger in the inflammatory response, which provides evidence in favor of calcium as an immune mediator in the breast. Recent studies in *Drosophila* demonstrated that sudden bursts of calcium flow through intercellular junctions, which are equivalent to connexin gap junction proteins in human tissue<sup>39</sup>. These calcium flashes create cellular signaling waves resulting in cytokine (IL-1 $\beta$  and IL-18) and hydrogen peroxide release, which in turn initiate immune cell recruitment and activation<sup>39,40</sup>. Proteins that mediate inflammation, NF- $\kappa$ B and Jak/Stat, also regulate lactation<sup>41</sup>. Considering that mammary glands are unique to mammals, that their secretions contain evolutionarily conserved anti-microbial enzymes, and the secretions are regulated by inflammatory/stress related protein kinases and calcium, there is strong support for the theory that mammary glands evolved initially as innate immunity tissue<sup>41</sup>.

Even if this proposed evolutionary history is not entirely correct, human and mouse mammary glands undergo mini-evolutions during a female's life-time and life cycle<sup>42</sup>. Breast cell genetic plasticity and clonal expansion provide the molecular basis for normal breast biological processes<sup>43</sup>. Differential gene sets are activated during discrete phases of proliferation, differentiation, and apoptosis during cycles of pregnancy, lactation, and involution<sup>42</sup>. For example, histone acetylation and Switch/Sucrose non-fermentable (SWI/SNF) ATPase chromatin remodeling protein have been associated with the  $\beta$ -casein (milk protein) promoter in mammary epithelial cells and the ATPase domain is essential for  $\beta$ -casein transcription<sup>44</sup>.

Evidence of the importance of cycles of breast expansion/involution for normal mammary gland function relate to reproductive history as risk factors for invasive breast cancer. These risk factors include: young age at first menarche, older age at menopause, nulliparous, or giving birth to a first child after age thirty-five<sup>45</sup>. This reproductive history translates into comparatively long periods in which the breast epithelium has not undergone complete cycles of expansion and involution during lactation. These observations suggest that the number and frequency of ductal expansion/involution cycles, and the associated cycles of chromatin remodeling, gene transcription, and protein translation in the ductal epithelium/myoepithelium, may all be essential in maintaining normal breast parenchyma.

#### **Intraductal microcalcifications record long standing hypoxic stress**

Calcium metabolism may have a special relevance to pre-invasive breast cancer progression. Pathologists and surgeons have long questioned whether intraductal calcifications, the common radiologic diagnostic feature are a cause, or consequence, of breast cancer<sup>5</sup>. Ninety percent of DCIS mammographic diagnoses are based on the presence of microcalcifications<sup>46,47</sup>. Calcifications due to calcium oxalate are usually associated with benign lesions, whereas calcium phosphate crystals are associated with both benign and malignant breast lesions<sup>48,49</sup>. Lamellar calcifications (psammoma bodies) are often described in well-differentiated DCIS, whereas granular, amorphous calcium deposits are noted in poorly differentiated DCIS<sup>49</sup>.

While microcalcifications of all types are associated with a broad spectrum of breast lesions, and have a 30-40% overall specificity for malignancy<sup>5</sup>, the radiologic

location, shape, size, and density of the microcalcification can be highly specific to DCIS<sup>50</sup>. Fine linear, occasionally branching, microcalcifications, and pleomorphic small (<0.5mm) calcifications, are typically found within the ductal tree, and are associated with necrotic areas of high grade and intermediate grade DCIS. In contrast, microcalcifications restricted to the lobules, and not the ductal tree, are almost always associated with benign disease such as microcystic adenosis<sup>11</sup>.

The chemical composition of most DCIS associated microcalcifications is a subtype of calcium phosphate, hydroxyapatite, which is easily detectable by conventional light microscopy<sup>48</sup>. Upon histopathologic examination, psammoma bodies appear as flat, smooth pink ovals, while calcium oxalate forms amber colored pyramids<sup>51</sup>. Calcium phosphate appears as hematoxyphilic (blue) deposits present within the necrotic center of the DCIS lesion duct. The individual calcifications often appear concentrically layered, giving the impression that calcium deposition is accumulating over time<sup>48,49</sup>. Suspicious microcalcifications have been associated with the later stages of fat necrosis<sup>5</sup>, further supporting the concept that calcium phosphate deposition follows the accumulation of necrotic cellular material<sup>11</sup>. As such, microcalcifications provide an important clue about the age of intermediate and high grade DCIS lesions. Since hypoxia induced necrosis precedes calcium deposition, and calcium deposition occurs over time, we can conclude that most intermediate and high grade DCIS lesions are subjected to hypoxic stress for a long period of time prior to diagnosis. Intraductal microcalcifications record long standing hypoxic stress. Thus, microcalcifications can be a signature of ongoing conditions favoring genetic instability<sup>52</sup>. While it is unclear if microcalcifications are

related to the pathogenesis of DCIS, they may contribute to the persistence of the DCIS lesions. Insoluble calcium induces autophagy, and may contribute to the local oxidative or metabolic stress within the duct (Chapter 5: Autophagy as a therapeutic target in DCIS)<sup>53</sup>.

### **Breast cancer progression from atypia to invasive phenotype**

Women diagnosed with DCIS remain at high risk for subsequent development of invasive carcinoma, with lesion size, degree of nuclear atypia, and the presence of comedo necrosis being histopathological factors of DCIS identified as affecting this risk of recurrence<sup>6,54</sup>. Experimental approaches employing nuclear cytometry, loss-of-heterozygosity (LOH), and comparative genomic hybridization (CGH) provide strong evidence that DCIS and invasive carcinomas share similar genetic alterations<sup>55,56</sup>.

Additional support for a natural step-wise progression in breast tumorigenesis comes from studies demonstrating that some similar genetic abnormalities are found between normal lobular cells and adjacent carcinoma *in situ* lesions<sup>57</sup>. One drawback of these studies, however, is that they provide no information regarding specific molecules involved in tumorigenesis. More recent gene expression studies of a number of patient-matched tissues including atypical ductal hyperplasia (ADH), DCIS and invasive carcinoma revealed that the various stages of disease progression were very similar to each other at the level of the transcriptome and proteome<sup>16,17,58</sup>. These studies also show that the DCIS lesions at the level of gene expression are more similar to the invasive cancers in the same patient compared to DCIS lesions in other patients. This data supports the hypothesis that the invasive phenotype of cancers is already programmed at



the pre-invasive stages of disease progression. Thus, recent transcriptomic/proteomics studies challenge the conventional notion that DCIS requires additional genetic “hits” in order to express the propensity for invasion<sup>59</sup> (Figure 5).

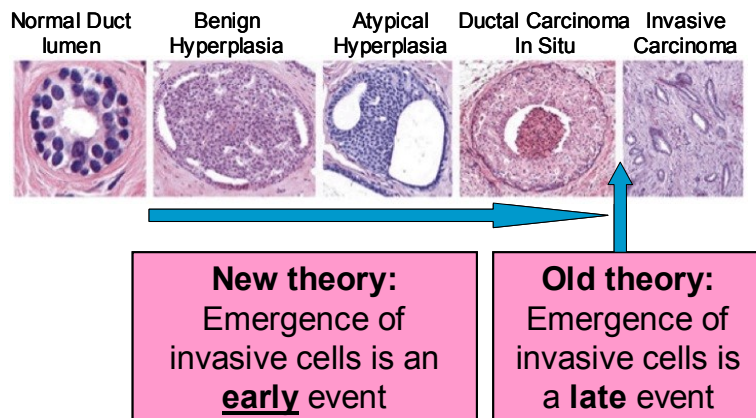


**Figure 5. New theory for emergence of invasive breast cancer.** The old theory states that invasive cancer progresses from an atypical stage, through ductal carcinoma in situ, with additional genetic mutations occurring along the continuum of morphologic alterations, prior to becoming an overt invasive tumor. The new theory postulates that cells with invasive potential exist in the early stages of cancer progression, but have not penetrated the ductal basement membrane.

### Breast cancer statistics

One-third of all newly diagnosed breast cancer cases in the US are pre-invasive cancer<sup>19</sup>. According to the SEER 18 (Surveillance, Epidemiology and End Results) data, the age-adjusted incidence rate of female in situ breast cancer in 2000 was 28.6 (95% C.I.=28.1-29.1), which increased to 32.9 (95% C.I.=32.4-33.5) by 2009 (Equation 1)<sup>60</sup>. Prior to general mammography screening (before 1980), DCIS accounted for only 2% of treated cancers<sup>61</sup>. Between 2002-2008, 60% of all breast cancers were diagnosed at the localized stage<sup>60</sup>.

**Equation 1. Cancer incidence rate**

$$\text{Incidence rate} = (\text{New cancers} / \text{Population}) \times 100,000$$

Pre-invasive breast neoplasms are non-obligate precursors to invasive and metastatic cancer<sup>5,8,12,26,62</sup>. Thus a sub-population of women with pre-invasive cancer will eventually go on to develop invasive carcinoma. Lesion size, degree of nuclear atypia, and the presence of comedo necrosis (central luminal inflammation interspersed with apoptotic cells) are histopathological parameters identified as affecting the risk of recurrence within the heterogeneous spectrum of pre-invasive breast lesions<sup>4,5,54,63-65</sup>. Compared to the general population, women harboring atypical ductal hyperplasia (ADH) and atypical lobular hyperplasia (ALH) have a 3.5 to 5 fold increased risk of developing invasive cancer<sup>19</sup>. A diagnosis of lobular carcinoma in situ (LCIS) increases the relative risk for invasive cancer by 7 to 9 fold and a diagnosis of DCIS represents a 4-12 fold increased risk<sup>19</sup>. Patients with high grade (comedo type, with necrosis) pre-invasive lesions have a greater risk of developing invasive cancer compared to patients with low grade lesions<sup>4,5,54,63-65</sup>.

The increase in incidence rate of DCIS and diagnosis of localized breast cancer may be attributed in part to screening programs, patient education, and enhanced imaging tools such as MRI<sup>61</sup>. However, the assumptions that breast MRI screening will prevent invasive disease have not been fulfilled<sup>66,67</sup>. Firstly, MRI screening cannot differentiate slow growing, indolent lesions from early stage aggressive tumors. Secondly, screening frequency for early disease detection should be often enough to prevent progression of localized, yet aggressive disease. Finally, screening fails to prevent the formation of the

initial DCIS lesion<sup>66,67</sup>. Consequently, an intervention therapy that directly kills all pre-invasive carcinoma lesions has the potential to eliminate the subset of precursor lesions that will become invasive cancer, possibly even before the lesion can be detected. But, the remaining unanswered questions are: a) at what stage of cell accumulation within the duct does the invasive potential begin?, b) what are the molecular characteristics of these precursor lesions?, and c) can a low toxicity therapy be found to prevent progression, or induce regression, of the pre-invasive lesion? Herein we establish the stage of invasive potential, the molecular pathway promoting cell survival within the duct, genetic and proteomic signatures of human DCIS, and present a clinical trial studying the safety and efficacy of a low toxicity therapy for pre-invasive breast lesions.

## CHAPTER 2: ISOLATION AND PROPAGATION OF DCIS PROGENITOR CELLS

### Introduction

#### Breast stem cells

Broad evidence supports the existence and role of stem cells both in normal mammary gland development and tumorigenesis<sup>20,27,68-70</sup>. Adult stem cells are defined as long-lived, generally quiescent cells capable of the process of self-renewal and the production of progeny which can differentiate into all the functional cell types of a particular tissue. Mouse and human breast stem/progenitor cells have been identified and purified by various means, primarily based on the presence/absence of specific marker proteins and/or dye-exclusion properties<sup>69,71-75</sup>. These isolated cells demonstrated self-renewal properties and were capable of differentiating into the various mammary cell types and reconstituting complete mammary structures *in vivo*<sup>20,27,68-70</sup>. While the concept that cancer arises from a small subpopulation of dysregulated tissue stem cells is not a new idea, the theory is controversial<sup>20,68,76,77</sup>. On one hand, the longevity properties of stem cells make them primary targets for mutation and transformation and thus, attractive candidates for the origins of cancer. Also, a number of commonalities between cancer cells and normal stem cells lend support to this idea. These include: 1) the capacity for self-renewal and molecular pathways controlling self-renewal, 2) the ability to differentiate, 3) activation of anti-apoptotic pathways, 4) increased membrane transport

protein activity, and 5) the ability to migrate and metastasize<sup>68,77</sup>. Large numbers of tumor cells are often required to transplant both human and rodent tumors, which supports the concept of a small subpopulation of tumor cells capable of regrowth. However, much of this evidence is circumstantial. Individual cells have not been identified in these studies and it could be argued that all tumor cells have a small probability of being able to recapitulate a tumor, rather than there being a small population capable of efficient tumor regrowth<sup>76</sup>.

### **Phenotypic classification of putative stem cells**

Despite these existing controversies, subpopulations of cancer cells with stem cell properties have been clearly demonstrated for hematopoietic cancers, and solid tumors, including brain and breast cancers<sup>71,78-82</sup>. Al-Hajj and colleagues successfully isolated a distinct population of cells from breast tumors capable of serial regrowth in mice<sup>71</sup>. Taking advantage of the heterogeneous expression of the cell surface markers CD44 and CD24 by human breast cells, they were able to isolate a CD44<sup>+</sup>/CD24<sup>-</sup>/Normal Lineage population of tumor cells that were able to form tumors in mice from as few as 100 cells. These tumorigenic cells generated additional CD44<sup>+</sup>/CD24<sup>-</sup> cells as well as phenotypically diverse, non-tumorigenic cells, suggesting that these cells exhibited self-renewal properties<sup>71</sup>. However, recent studies of the prevalence of CD44<sup>+</sup>/CD24<sup>-</sup> cells in human breast cancer specimens showed that there was no correlation between the percentage of CD44<sup>+</sup> /CD24<sup>-</sup> cells in a lesion and tumor progression, response to therapy, progression-free survival or overall survival<sup>83</sup>. A correlation with the presence of distant metastasis and a high percentage of CD44<sup>+</sup>/CD24<sup>-</sup> cells in the primary tumor

demonstrated that this subpopulation of cells may have increased invasive or metastatic potential<sup>83</sup>.

A key facet of CD44 antigenicity, namely recognizing extracellular matrix proteins, such as hyaluronic acid, collagen, laminin, and fibronectin, may explain why CD44<sup>+</sup> cells are frequently found in tumor metastasis<sup>84</sup>. Any CD44<sup>+</sup> cell would be capable of binding to, and thereby surviving, within the extracellular matrix. Although CD44 can activate stem cell regulatory genes, evidence supporting a role for CD44 in pluripotency and self-renewal is still lacking<sup>84</sup>.

The phenotypic emergence of normal and neoplastic adult stem cells may be regulated by the tissue microenvironment. The tissue microenvironment is known to play an important role in regulating cell proliferation and differentiation. Furthermore interactions between epithelial cells and the surrounding stroma are critical for maintaining tissue morphology and cellular function<sup>85-88</sup>. Just as tissue cells are influenced or controlled by the cells immediately surrounding them, stem cells are regulated by their immediate surrounding cells or “niche”. In breast tissue, the surrounding fibroblasts and myoepithelial cells maintain the stem cell population and also orient cell divisions in the stem cell “niche” in order to retain stem cells and release transit progenitor cells for amplification and differentiation<sup>25,77</sup>.

Numerous biochemical and histological markers have been proposed as prognostic and diagnostic markers of breast cancer. Invasive breast cancers have been categorized into 5 groups, luminal A, luminal B, basal, Her2-enriched, and claudin-low, based on gene expression signatures of heterogeneous human breast tissue<sup>89,90</sup>.

Luminal/basal designations apply to any secretory epithelial gland, such as prostate, pancreas, or breast and reflect embryological evolution more than a specific capacity for self-renewal. Basal cells line the basement membrane, with luminal cells layered on top, facing the lumen of the gland. Luminal A/B cells are estrogen receptor (ER) positive, with luminal A cells possessing a higher expression of ER-related genes and a lower expression of proliferation associated genes<sup>91</sup>. Basal like cells are ER negative. Claudin-low tumors express markers associated with epithelial to mesenchymal transition (EMT). Despite these classifications, breast tumor cell plasticity has confounded simple categorization of tumor initiating cells<sup>88,92</sup>. *BRCAl* mutations often lead to breast tumors with basal-like phenotypes, thus these tumors were thought to be derived from basal breast epithelium<sup>88</sup>. However, when tumors generated from a Big-Cre-*loxP* luminal cell mouse model (*Big-CreBrca1<sup>ff</sup> p53<sup>+/-</sup>*), under Big promoter control, were compared histologically to tumors from the same genetic model but under control of the basal cell Keratin 14 promoter, the luminal genotype (*Big-CreBrca1<sup>ff</sup> p53<sup>+/-</sup>*) tumors resembled human *BRCAl* tumors<sup>88</sup>. Another example of mistaken tumor cell classification was shown using milk mucin as a luminal-like cell lineage marker and CD271 as a basal cell lineage marker<sup>92</sup>. A generally accepted paradigm has been that tumor initiating cells show basal-like characteristics. Kim *et al* demonstrated that luminal-like cells can be tumorigenic and invasive in a NOD SCID mouse model, whether or not the luminal-like cells were differentiated or had acquired basal-like characteristics<sup>92</sup>.

Immunohistochemical analysis of pure DCIS, DCIS with invasion, and invasive ductal carcinoma has clearly demonstrated that the frequency of putative stem cell-like

markers, including CD44, ALDH1, and Claudin-7, vary based on tumor subtype and stage<sup>91,93</sup>. Immunohistochemical characterization of both breast tumor and stromal cell populations has revealed extensive heterogeneity in antigenic markers<sup>91,94</sup>. Using 6 markers (ER, Progesterone Receptor (PR), Androgen Receptor (AR), Bcl-2, p53, Her2), Meijnen *et al* classified DCIS into two groups and five subgroups<sup>91</sup>. However sub-classification of DCIS into molecular groups failed to provide additional information beyond the degree of cellular differentiation<sup>91,93</sup>. Gonzalez *et al* analyzed Matrix Metalloproteases (MMP) in tissue microarrays of pure DCIS or DCIS admixed with invasive ductal carcinoma to assess the proclivity for invasion based on the expression of degradative enzymes<sup>94</sup>. MMP are a class of proteins that degrade connective tissue stroma allowing invasion across basement membranes<sup>94</sup>. Fibroblasts, immune cells, and tumor cells exhibited overlapping MMP class activity, with the cell type being the dominant factor in the staining pattern<sup>94</sup>.

### **Transition from in situ to invasive phenotype**

Regardless of the molecular classification of the cell, DCIS cells accumulating within the duct may have already lost the requirement for basement membrane anchorage and are subjected to a non-vascular hypoxic environment<sup>87</sup>. In addition, myoepithelial cells may constitute a cellular suppressor of DCIS<sup>25</sup>. Therefore, in addition to physical confinement behind an intact basement membrane, other microenvironment cues may hold the invasive potential of DCIS cells in check. Adult stem cells have the capability to migrate from a site of clonal expansion, enter the circulation, and extravasate at a locus of tissue injury and repair. Thus adult stem cells possess the entire phenotype of invasive



cancer cells. The difference between DCIS, cancer stem cells, and normal adult stem cells may not be the physiologic program for invasion and migration, but instead may reside in a defect of the regulation of this program within the tissue microenvironment. Candidate cancer stem cells have been derived from human breast cancer and are thought to promote the unrestrained growth and invasion of breast cancer<sup>68,76</sup>. Clinical and experimental evidence suggests that DCIS is a precursor lesion to most, if not all, invasive carcinoma. It is generally accepted that women diagnosed with DCIS remain at high risk for subsequent development of invasive carcinoma<sup>15,16</sup>.

However, no information exists concerning the presence of cancer stem cells within human pre-invasive lesions such as DCIS, the time of onset of the malignant phenotype, or the triggering mechanism that switches in situ lesions to overt invasive breast carcinoma. The critical biologic questions, addressed in this study, are: Do invasive, cytogenetically abnormal neoplastic cells pre-exist in the pure intraductal DCIS lesion prior to the overt histologic transition to invasive carcinoma? If such precursor carcinoma cells pre-exist in DCIS, which biological processes support their survival in the face of nutrient deprivation and hypoxia?

Therefore, a wholly new system for culturing fresh, human DCIS tissue was devised to test the hypothesis that neoplastic cells pre-exist in pure intraductal DCIS lesions and to provide previously unobtainable information about the earliest breast cancer genetic/proteomic phenotypes that drive invasion.

## **Materials and methods**

### **Female human breast tissue**

Leftover breast tissue, not required for diagnosis, was obtained at the time of standard of care surgery (lumpectomy or mastectomy) for a suspicious breast lesion following institutional review board approved protocols with written informed patient consent. Inclusion criteria were: 1) Female; 2) Diagnosis of pure DCIS or DCIS admixed with Invasive Breast Cancer; 3) A signed consent and adequate sample of primary fresh or frozen tissue; 4) No history of an invasive cancer in the last 5 years with the exception of minimally invasive non-melanoma skin cancer; 5) At least 18 years of age; and 6) Non-pregnant/non-lactating. Exclusion criteria included: 1) Prior history of chemotherapy, hormonal therapy and/or radiation therapy; and 2) History of previous breast surgery in the immediately adjacent area.

Tissue sample sterility was maintained during the initial morphological assessment by the diagnostic pathologist. Areas of DCIS were identified by gross visual inspection of the tissue. Comedo DCIS lesions could be recognized in the gross specimen by their circular shape and characteristic pale friable center. Areas of tissue harboring discernible DCIS lesions were dissected into organoids approximately 3 mm<sup>2</sup>, containing one or more visible duct segments with associated stroma.

### ***Ex vivo* organoid culture**

Without collagenase or dispase enzymatic treatment, the intact organoids, containing one or more discernable duct segments with associated stroma, were grown in 115cm<sup>2</sup> TPP reclosable flasks (MidSci, St. Louis, MO) or 10cm<sup>2</sup> culture tubes (MidSci) in serum free DMEM/F12 medium supplemented with human recombinant EGF

(10ng/mL; Cell Signaling Technology, Danvers, MA), insulin (10 $\mu$ g/mL; Roche, Indianapolis, IN), streptomycin sulfate (100 $\mu$ g/mL; Sigma, St. Louis, MO) and gentamicin sulfate (20 $\mu$ g/mL; Sigma) (hereafter referred to as DMEM/F12+ factors), with or without 0.36% (v/v) murine Engelbreth-Holm-Swarm (EHS) derived, growth factor reduced, basement membrane extract (Trevigen, Gaithersburg, MD) at 37°C in a humidified 5.0% CO<sub>2</sub> atmosphere. Medium was replaced three times per week. Non-adherent organoids were removed from the culture flask and fixed immediately in Biomarker and Histology Preservative (BHP) to preserve histomorphology and phosphoproteins<sup>95</sup>. Biomarker and Histology Preservative was created as a separate project to meet the unmet need of one-step, room temperature preservation of tissue and cellular histomorphology, and simultaneous stabilization of proteins and their post-translational modifications<sup>96-98</sup>.

### **Xenograft Tumor Generation**

Human DCIS tumor tissue, propagated organoid tissue, or spheroids generated from primary DCIS organoid cultures were transplanted transdermally into the mammary fat pad of female NOD SCID mice (NOD.CB17-*Prkdc*<sup>scid</sup>/NCrHsd; Harlan or The Jackson Laboratory) with or without a 17 $\beta$  Estradiol pellet (Innovative Research of America, Sarasota, FL; 60 day release, 1.7mg/pellet). Immunodeficient mice were maintained in sterile housing and all manipulations were performed under aseptic techniques. The DCIS organoids, prior to transplantation into the murine mammary fat pad, were incubated in serum-free DMEM/F12 medium supplemented with EGF, insulin,

streptomycin, gentamicin, or estrogen (Sigma) for 6 to 18 hours. The study was conducted under a contract with Biocon Inc., Rockville, MD<sup>10</sup>.

Survival, weight, and condition of all mice were monitored daily and palpable tumor masses were measured with calipers (length/width) twice weekly. Mice exhibiting evidence of tumor growth were sacrificed as necessary or after 120 days. Complete necropsies were performed for evidence of metastasis. Clinical evidence of tumor metastasis was based on the following criteria a) visible secondary tumor growths distinct from the primary transplant, or b) shortness of breath or neurologic symptoms (e.g. circling, tremors, seizures) suspected as being due to pulmonary metastasis or brain metastasis. Tumor tissue, when present, was either excised for immunohistochemical analysis or injected into a different NOD SCID mouse for propagation of the tumor.

### **Immunofluorescence**

Spheroids were aspirated directly from the culture flask under direct microscopic visualization, mounted on positively charged glass microscope slides, fixed in 16% paraformaldehyde (Fisher Scientific), and stored with desiccant at 4°C. FFPE murine xenograft tissue sections were deparaffinized in xylene (2 x 15min), and rehydrated in graded alcohols (100%, 95%, 70% ethanol). Spheroids and FFPE sections were incubated at room temperature with anti-human specific epithelial cell adhesion molecule (EpCAM) conjugated to FITC (EpCAM-FITC, 5 µg/mL) (Abcam, Cambridge, MA), or mouse immunoglobulin IgG1 as a negative control (Dako). Slides were rinsed in borate buffer pH 8, then nuclear counterstained with ProLong Gold+DAPI (Invitrogen). Images were captured with a Nikon Eclipse C1si confocal microscope in different channels for

EpCAM-FITC (pseudo-colored green, 488nm) and DAPI (psuedo-colored blue, 408nm) using the 20x objective.

## **Results**

### **Ex vivo organoid culture system for breast DCIS**

Originally, we followed established protocols for mammosphere generation and culture using collagenase and dispase disruption of breast tissue followed by subsequent culture in chemically defined medium<sup>71,99,100</sup>. These initial attempts were unsuccessful in generating any cellular growth or spheroids from DCIS containing tissue, therefore we devised a new system based on the principle of cell streaming/migration. The discernible breast ducts, and surrounding stroma were submerged in a minimum volume of serum-free medium (just enough to cover the duct fragments) to maximize gas exchange, with the cut surface of the duct exposed to the culture medium, but in no specific orientation in the flask (Figure 6). This culture system allowed cells to migrate out of the duct and into/onto the autologous stroma. Submerging the duct segments in a larger volume of media (more than 3 times the height of the fragments) did not yield epithelial or fibroblast outgrowth.

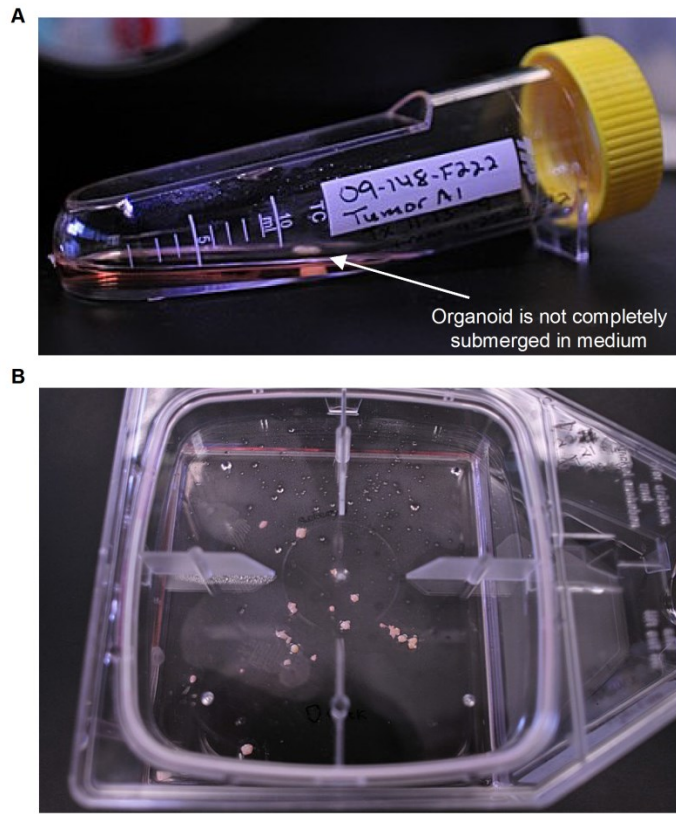


**Figure 6. Culture system for DCIS organoids.**

**Human DCIS tissue was cultured in tissue culture flasks or dishes without prior enzymatic digestion of the tissue. A minimal amount of serum-free culture medium supported cellular growth while maintaining an air-liquid interface around the organoid.**

Seven organoid cultures generated from non-invasive primary human breast lesions were maintained for more than 12 months (Table 1). The culture conditions consistently generated a high yield of DCIS epithelial cell outgrowths for each patient, even with small volumes of starting tissue (Figure 7).

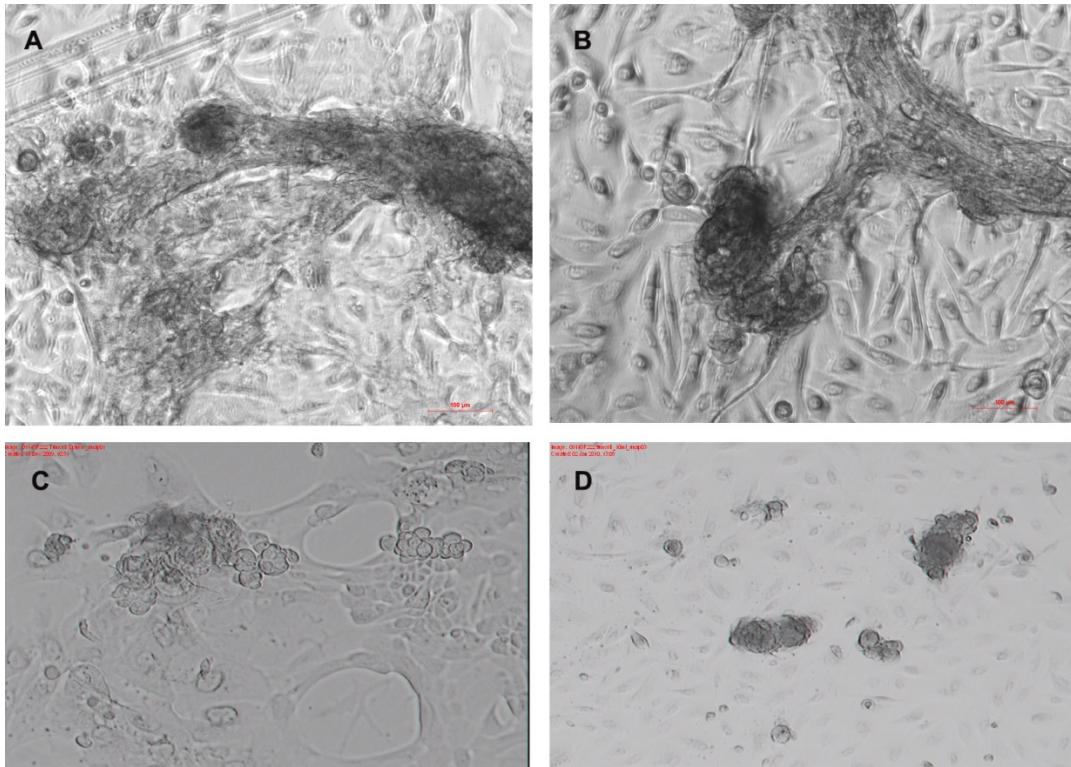


**Figure 7. Human DCIS tissue generates pseudoductal structures and spheroids in *ex vivo* culture. A & B) Organoid culture of human DCIS lesions in serum free conditions spontaneously form pseudoductal structures with lumen formation (case 08-352, 20x), and C & D) epithelial monolayers with spheroids (case 09-148).**

**Table 1. Patient characteristics for generation of *ex vivo* organoid cultures.**

<b>Sample</b>	<b>Age</b>	<b>Diagnosis</b>	<b>Histology</b>	<b>Grade</b>	<b>ER</b>	<b>PR</b>	<b>Time in culture as of Dec. 2010</b>
08-183	47	DCIS	CN/CR	3	30%	Neg	6 months
08-352	42	DCIS	CR extended	3	50%	50%	12 months
09-091	68	DCIS/ADH	CR	2/3	Pos	Pos	8 months
09-118	49	ADH*	Stromal fibrosis AH	2	Pos	N/A	8 months
09-148	45	DCIS	Solid and CR	3	90%	90%	7 months
09-301	34	DCIS	Solid and CR	2	90%	90%	4 months
09-327	57	DCIS	Cribriform with IP	2	Pos	Neg	2 months

\* Previous history of DCIS, patient treated with Tamoxifen citrate.

DCIS - ductal carcinoma in situ; ADH - Atypical ductal hyperplasia; ER - Estrogen Receptor;

PR - Progesterone Receptor; + indicates positive result, no cell percentage specified; CN - Comedo necrosis; CR – Cribriform; CR-extended = extension into lobules with no evidence of invasion; AH - Pseudoangiomatoid hyperplasia; IP - Intraductal papilloma

### **Anchorage independent neoplastic epithelial cells spontaneously emerge in organoid culture of human DCIS**

Proliferative cells were observed to migrate out of the DCIS organoids grown in culture for as little as 2 weeks (within 2-4 weeks). Hematoxylin and eosin (H&E) staining of formalin fixed paraffin embedded (FFPE) organoid sections indicated that the organoids contained ducts harboring DCIS, stroma, normal appearing ducts or lobules, and some adipose elements (Figure 8). DCIS cultured neoplastic epithelial cells migrated over the surface of autologous stroma and formed multilayered colonies with clear epithelial morphology (Figure 1C). Invasive foci beneath these outgrowths within autologous stroma were verified by absence of type IV collagen basement membrane (Figure 9). Sub-passage of DCIS organoids reconstituted the 3-D ductal and spheroid phenotypes, which reproducibly invaded inward from the surface of autologous stroma in organoid culture. Histomorphology of the duct fragments revealed, by type IV collagen immunohistochemistry, that intact basement membrane, epithelium and myoepithelium were retained for at least 12 weeks under the serum-free culture conditions employed (Figure 9).



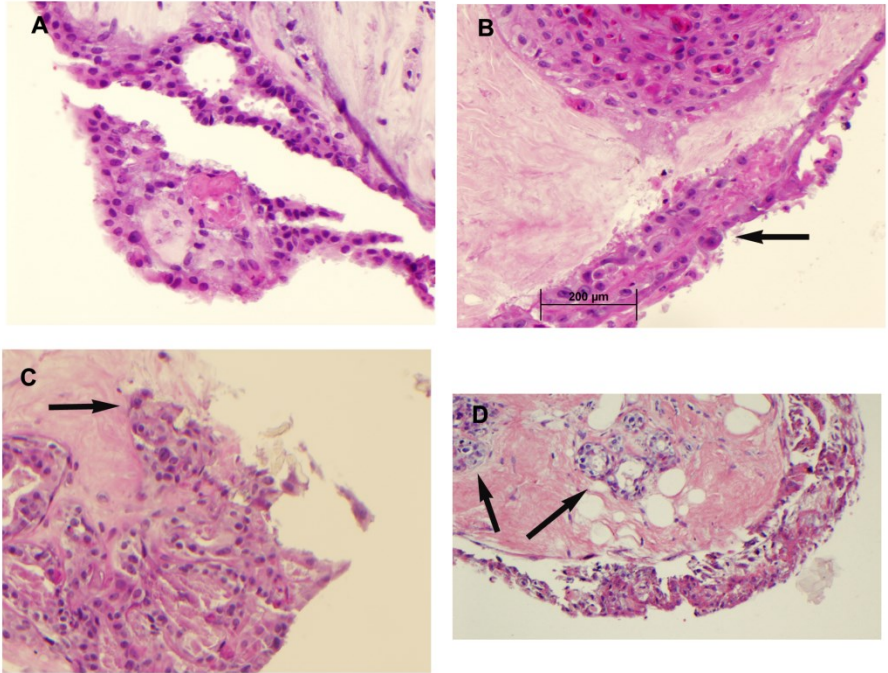


**Figure 8. Hematoxylin & Eosin stain of cultured human DCIS organoids.**  
**A & B) Multi-layered pleomorphic epithelial cells consistently grow on the surface of autologous breast stroma after 12 weeks in culture (20x). C) DCIS cultured neoplastic cell exhibit autologous stromal invasion (20x). D) Ductal architecture remains intact with viable cells in the organoid culture.**

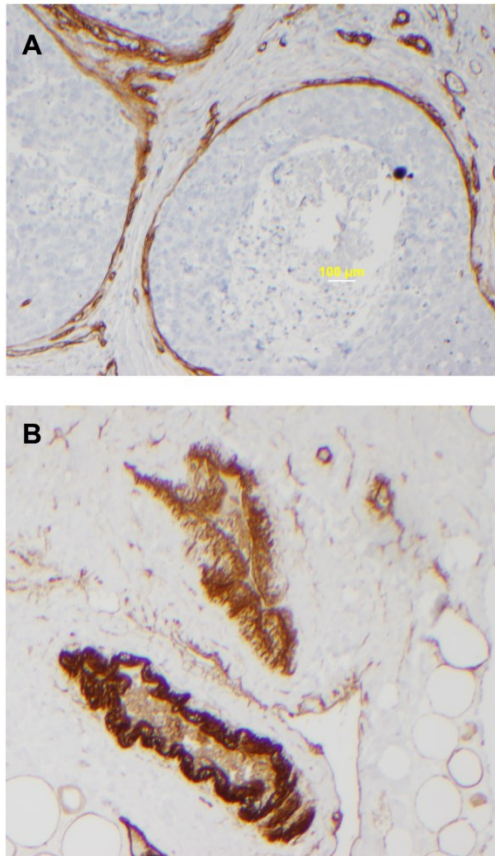


**Figure 9. Collagen type IV delineates intact basement membranes in pure DCIS lesions.**  
A) Collagen type IV immunohistochemistry demonstrates intact basement membrane surrounding breast ducts (brown staining) in the primary sample prior to culture (case 08-352 FFPE scale bar 100μm, magnification 10x). B) The basement membrane surrounding the duct remains intact during breast organoid culture for 12 weeks (case 09-148, magnification 20x).

Continued *in vitro* organoid cultivation successfully propagated DCIS derived epithelial cells with anchorage independent growth, defined as upward growing and expanding spheroids, and lobulated, duct-like 3-D formations with pseudo lumens, in serum free medium supplemented with EGF and insulin (Figure 10).

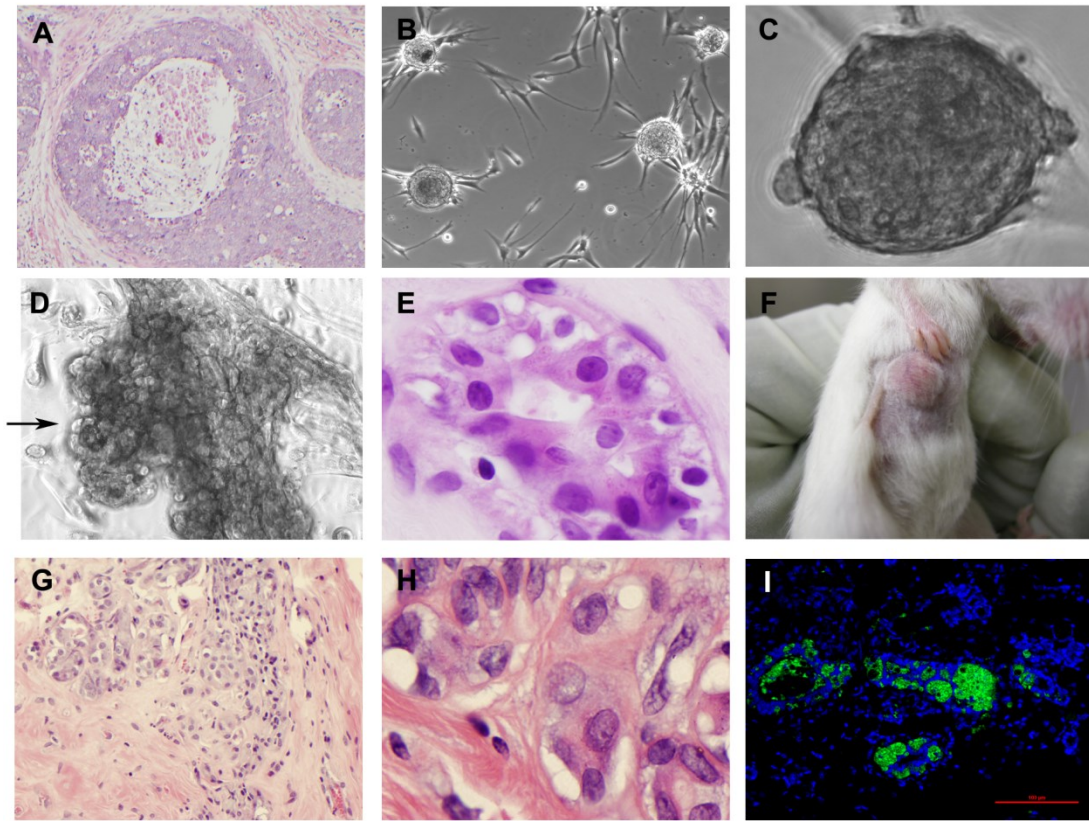


**Figure 10. Human DCIS tissue generates spheroid and pseudoductal structures in *ex vivo* culture and forms xenograft tumors.**

A) H&E stain of human breast tissue, DCIS, high grade with comedo necrosis (case 08-352) that represent the primary surgical source material for our DCIS organoid culture system. B) Epithelial spheroids (10x). C) A single large spheroid (40x). D) Pseudoductal structures with lumen formation. E) H&E stain of human breast tissue following organoid culture (case 08-352, 100x). F) Example xenograft tumor induced by DCIS epithelial cells or spheroids in a NOD SCID mouse mammary fat pad. G & H) H&E stain of murine xenograft tumor (20x and 100x respectively) with pleomorphic epithelial cells with prominent nucleoli, stromal invasion, and partial glandular differentiation. I) Murine xenograft tumors derived from human DCIS were shown to be of human origin by the presence of human specific epithelial cell adhesion molecule (EpCAM) in formalin fixed paraffin embedded tissue sections. EpCAM-FITC (pseudo-colored green, 488nm) and DAPI nuclear counterstain (pseudo-colored blue, 408nm) (20x) (Adapted from reference<sup>10</sup>).

### **Generation of mouse mammary tumor xenografts from human DCIS**

The existence of tumorigenic cells within fresh human DCIS involved duct segments was tested using xenotransplantation<sup>101</sup>. Multiple independent xenograft transplants of human DCIS organoids, with no histological evidence of invasive carcinoma, generated tumors within 1 to 2 months in NOD SCID mice (Figure 10).

Xenograft tumors arising from pure DCIS tissue contained partially formed ductal structures with stromal infiltration<sup>10</sup>. The xenograft tumors were confirmed to be of human origin by the presence of human specific epithelial cell adhesion molecule EpCAM within the xenograft tumor (Figure 10 I). Xenograft tumors were greater than 16mm<sup>2</sup> (length x width) as measured with calipers (Figure 11).

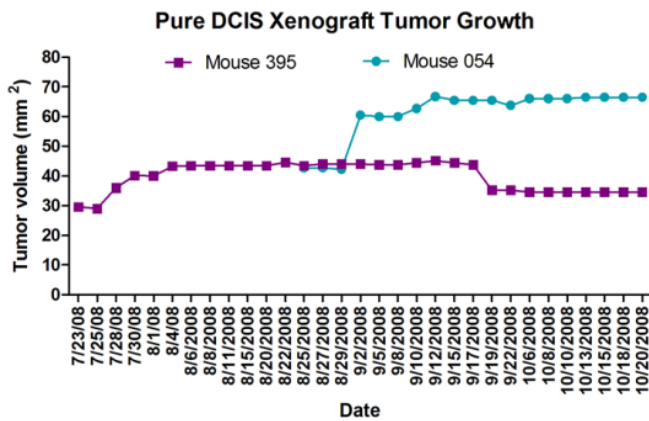


Figure 11. Representative tumor volume measurements for murine xenograft tumors from pure human DCIS cells. The apparent decrease in tumor volume for mouse 395 (purple square) may have been due to inter-observer variation.

Xenograft transplants generated from invasive breast carcinoma or DCIS with invasive components were used as positive controls under the assumption that invasive tumors manifested a more aggressive phenotype compared to pure DCIS and thus were more likely to generate a tumor xenograft. The number of positive control tumors observed for mixed DCIS or invasive breast carcinoma tissue was 9 of 20 transplanted (45%).

58 mice were transplanted with either freshly procured DCIS duct segments, propagated xenograft tumors, or organoids and/or human primary cultured cells generated from the DCIS tissue (Figure 10). The number of tumors generated within 3 months of injection was 44/58. The number of tumors observed for pure DCIS tissue, which included cribriform DCIS as well as DCIS intermediate and high grades, was 18 of 22 transplanted (81%). The number of tumors observed from cultured primary cells and/or spheroids was 20 of 29 transplanted (68.9%). No evidence of organ metastasis was noted at necropsy. Xenograft propagated tumors, which were derived initially from pure DCIS tissue, produced tumors in 6 out of 7 mice for 2 generations (Table 2).

These data clearly demonstrate that both DCIS tissue and cultured DCIS spheroid structures were capable of inducing tumors with comparable tumorigenic potential.

**Table 2. Mouse xenograft efficacy for lobular, invasive and pure DCIS breast tissue.**

<b>Mouse DOB</b>	<b>NOD SCID Mouse Vendor</b>	<b>Date of Implant</b>	<b>Mouse ID</b>	<b>Tissue Type/Histology of transplanted tissue</b>	<b>Xenograft Tumor Formation</b>
12/25/07	Jackson	2/14/08	<b>963</b>	Lobular breast carcinoma	No
12/25/07	Jackson	2/14/08	<b>962</b>	Lobular breast carcinoma	Yes
12/25/07	Jackson	2/21/08	<b>964</b>	infiltrating DCIS	Yes
12/25/07	Jackson	2/21/08	<b>965</b>	infiltrating DCIS	No
12/25/07	Jackson	3/5/08	<b>961</b>	Lobular invasive carcinoma	N/A
1/22/08	Jackson	3/5/08	<b>301</b>	Lobular breast carcinoma	No
1/22/08	Jackson	4/2/08	<b>102</b>	infiltrating DCIS	Yes
1/22/08	Jackson	4/2/08	<b>103</b>	infiltrating DCIS	Yes
1/22/08	Jackson	4/2/08	<b>104</b>	infiltrating DCIS	N/A
1/22/08	Jackson	4/2/08	<b>105</b>	infiltrating DCIS	No
1/22/08	Jackson	4/17/08	<b>104</b>	DCIS	No
1/22/08	Jackson	4/17/08	<b>105</b>	DCIS	No
3/10/08	Harlan	4/30/08	<b>306</b>	infiltrating DCIS	No
3/10/08	Harlan	4/22/08	<b>307</b>	propagated xenograft infiltrating DCIS	Yes
3/10/08	Harlan	5/22/08	<b>308</b>	infiltrating DCIS	No

3/10/08	Harlan	5/22/08	<b>309</b>	infiltrating DCIS	No
3/10/08	Harlan	4/30/08	<b>310</b>	infiltrating DCIS	No
3/10/08	Harlan	4/30/08	<b>311</b>	cultured xenograft cells	No
3/31/08	Harlan	6/18/08	<b>395</b>	DCIS	Yes
3/31/08	Harlan	6/18/08	<b>398</b>	DCIS	Yes
3/31/08	Harlan	6/27/08	<b>400</b>	invasive ductal carcinoma with DCIS	Yes
3/31/08	Harlan	6/27/08	<b>396</b>	invasive ductal carcinoma with DCIS	Yes
3/31/08	Harlan	6/27/08	<b>399</b>	infiltrating DCIS, Her2+, cribriform variant	No
3/31/08	Harlan	6/27/08	<b>397</b>	infiltrating DCIS, Her2+, cribriform variant	Yes
3/31/08	Harlan	7/1/08	<b>397</b>	DCIS	Yes
3/31/08	Harlan	7/1/08	<b>400</b>	DCIS	Yes
1/22/08	Jackson	7/1/08	<b>101</b>	DCIS	Yes
5/26/08	Harlan	7/23/08	<b>876</b>	DCIS, grade 2, can't rule out invasion	Yes
5/26/08	Harlan	7/23/08	<b>581</b>	DCIS+adipose tissue	Yes
5/26/08	Harlan	7/23/08	<b>379/579</b>	DCIS	Yes
5/26/08	Harlan	8/7/08	<b>877</b>	propogated from mouse 102	Yes
6/16/08	Harlan	8/14/08	<b>054</b>	DCIS	Yes
6/16/08	Harlan	8/29/08	<b>051</b>	propogated from mouse 399	Yes
6/16/08	Harlan	9/16/08	<b>055</b>	DCIS	Yes
7/7/08	Harlan	10/22/08	<b>392</b>	proagated from mouse J4395	Yes
7/7/08	Harlan	10/22/08	<b>393</b>	proagated from mouse J4397	No
7/7/08	Harlan	10/22/08	<b>391</b>	proagated from mouse 055	Yes
7/7/08	Harlan	10/22/08	<b>394</b>	proagated from mouse 054	Yes
7/7/08	Harlan	10/22/08	<b>395</b>	proagated from mouse J4397	Yes
7/7/08	Harlan	11/19/08	<b>396</b>	DCIS	Yes
9/19/08	Harlan	11/19/08	<b>795</b>	DCIS	No
9/19/08	Harlan	11/19/08	<b>791</b>	DCIS	Yes
9/19/08	Harlan	11/19/08	<b>794</b>	DCIS	No
9/19/08	Harlan	11/19/08	<b>793</b>	Normal breast tissue	No
9/19/08	Harlan	11/19/08	<b>792</b>	DCIS	Yes
11/4/08	Jackson	12/18/08	<b>080</b>	DCIS,extension into lobules, no invasive component	Yes
11/4/08	Jackson	12/18/08	<b>081</b>	DCIS,extension into lobules, no invasive component	Yes
11/4/08	Jackson	12/18/08	<b>082</b>	DCIS,extension into lobules, no invasive component	Yes
11/4/08	Jackson	12/18/08	<b>783/763</b>	DCIS,extension into lobules, no invasive component	Yes
11/4/08	Jackson	12/18/08	<b>079</b>	DCIS,extension into lobules, no invasive component	Yes
12/8/08	Harlan	1/16/09	<b>687</b>	08-352 cell culture	No
12/8/08	Harlan	1/16/09	<b>686</b>	08-352 cell culture + organoid	No
12/8/08	Harlan	1/16/09	<b>684</b>	08-352 organoid	Yes
12/26/08	Harlan	2/5/09	<b>634</b>	08-352 organoid in gel foam	Yes
12/26/08	Harlan	2/5/09	<b>632</b>	08-352 organoid in gel foam	Yes

12/26/08	Harlan	2/17/09	<b>633</b>	08-352 cell culture	Yes
12/26/08	Harlan	2/27/09	<b>631</b>	08-352 cell culture in gel foam	Yes
12/26/08	Harlan	2/27/09	<b>635</b>	08-352 cell culture in gel foam	Yes
2/6/2009	Harlan	3/23/09	<b>530</b>	08-352 cell culture in gel foam	Yes
2/6/2009	Harlan	3/23/09	<b>528</b>	08-352 cell culture in gel foam	Yes
2/6/2009	Harlan	04/17/09	<b>526</b>	08-352 spheroids and epithelial cells	Yes
2/6/2009	Harlan	04/17/09	<b>527</b>	08-352 spheroids and epithelial cells	Yes
2/6/2009	Harlan	04/17/09	<b>529</b>	08-352 spheroids and epithelial cells	Yes
12/5/2008	Harlan	04/17/09	<b>683</b>	08-352 spheroids and epithelial cells	Yes
3/16/2009	Harlan	05/04/09	<b>171</b>	08-352 cell culture	Yes
3/16/2009	Harlan	05/13/09	<b>170</b>	08-352 cell culture	No
3/16/2009	Harlan	05/13/09	<b>170</b>	08-352 organoid, not attached to flask	Yes
4/13/2009	Harlan	06/08/09	<b>580</b>	09-118 spheroids+epithelial cells	No
4/13/2009	Harlan	06/08/09	<b>583</b>	09-118 spheroids+epithelial cells	No
4/13/2009	Harlan	06/08/09	<b>582</b>	09-148 organoid	Yes
4/13/2009	Harlan	07/02/09	<b>581</b>	09-118 spheroids	Yes
4/13/2009	Harlan	07/02/09	<b>579</b>	09-091 spheroids	Yes
7/10/2009	Harlan	08/26/09	<b>K4635</b>	09-118 cell culture	No
7/10/2009	Harlan	08/26/09	<b>650</b>	09-148 cell culture	N/A
10/9/2009	Harlan	12/01/09	<b>473</b>	09-118 cell culture	Yes
10/9/2009	Harlan	12/01/09	<b>473</b>	09-118 cell culture	No
10/9/2009	Harlan	12/01/09	<b>471</b>	09-148 cell culture	No
10/9/2009	Harlan	12/01/09	<b>471</b>	09-148 cell culture	Yes
10/10/2009	Harlan	12/18/09	<b>472</b>	09-301 cell culture	N/A
10/10/2009	Harlan	12/18/09	<b>470</b>	09-148 propagated culture, single large spheroid	Yes

In some cases, the same mouse was injected with more than one sample, from different patient source material, because either the initial injection did not produce a measurable tumor, or different patient samples were injected on the right, compared to the left, mammary fat pad. Therefore, in Table 2, identical mouse identification numbers may be listed as both affirmative and negative for xenograft tumor formation.

## Discussion

Breast cancer progression has previously been theorized to be a multi-step process involving a continuum of changes from the normal phenotype to hyperplastic lesions,

carcinomas in situ, invasive carcinoma, and finally to metastatic disease<sup>2</sup>. Under this model additional genetic alterations are required before neoplastic cells in a DCIS lesion can progress to an invasive and metastatic carcinoma. However, more recent refinements of this model indicate that the aggressive phenotype of breast cancer is determined at the premalignant stage, much earlier than previously thought. Experimental approaches employing loss-of-heterozygosity (LOH), and comparative genomic hybridization (CGH) provide strong evidence that DCIS and invasive carcinomas in the same patient share similar genetic alterations<sup>14-17</sup>. Damonte *et al*, employing the 'MINO' (mammary intraepithelial neoplasia outgrowth) mouse model of DCIS, concluded that malignant aggressiveness is pre-programmed in the pre-cancer stem cell<sup>15</sup>. Taken together, these data support the hypothesis that the invasive phenotype of human breast cancer is already programmed at the pre-invasive stages of disease progression.

### **Human Ductal Carcinoma In Situ contains malignant progenitor cells**

We have successfully developed a novel *ex vivo* breast organoid culture system to isolate, propagate and enrich spheroid-forming, invasive, carcinoma stem cells from fresh human breast ductal tissue prior to the overt *in vivo* emergence of stromal invasion, and/or lymphatic and vascular dissemination. This is the first study to establish the existence of human DCIS derived progenitor cell lines<sup>10</sup>.

Fresh human DCIS lesions reproducibly generate *in vitro* anchorage independent, neoplastic epithelial cells that generate 3-D structures including spheroids and duct-like structures. Neoplastic cells with this phenotype can emerge from a high proportion of replicate DCIS lesion samples from the same patient, and can be serially propagated for



at least one year. No anchorage independent cells arose from tissue containing histologically verified normal appearing glands and adipose tissue. The anchorage independent epithelial cells were observed to arise from all grades of DCIS including ADH (Table 1).

It is unlikely that the invasive cell strains propagated from fresh human DCIS ducts are isolates of micro-invasion areas or invasive cancer in the original histopathology. The patient source material was verified histologically to be devoid of microinvasion or invasive cancer before and after DCIS lesion tissue procurement. Verification was assessed by an independent pathologist with no knowledge of the research findings for the individual specimen. The DCIS lesion source material was evaluated by IHC for type IV collagen and was found to contain an intact basement membrane (Figure 9). If the neoplastic, cytogenetically abnormal cells isolated in this study represented areas of microinvasion, this would be expected to be a rare event, but this was not the case.

Evaluation of nodules/tumors in xenograft models requires confirmatory studies to verify that the observed palpable mass is actually a tumor and not a granuloma or abscess<sup>102</sup>. Palpable nodules may grow quickly or slowly in immune compromised xenograft mouse models. To verify that the nodules present in our xenografts recapitulated characteristic features of the primary DCIS tissue, we performed H&E and EpCAM stains on the xenograft tissue sections. EpCAM is a transmembrane glycoprotein whose expression pattern changes from basolateral membrane to uniform membranous expression in carcinoma<sup>103</sup>. EpCAM has been associated with less differentiated breast

tumors, and recently was shown to exhibit differential ability to support tumor growth in epithelial versus mesenchymal cell phenotypes<sup>103</sup>. Knock-down of EpCAM in MCF7 and T47D breast cell lines produced smaller, less invasive tumors, compared to mesenchymal MDA-MD-231 cell lines, suggesting that cells with a mesenchymal phenotype may be independent of EpCAM during invasion<sup>103</sup>.

The non-obese diabetic severe combined immunodeficient (NOD SCID) mouse model does not appear to contribute diabetic-mediated metabolic factors that could positively influence tumor growth<sup>104,105</sup>. The SCID model lacks T cells and B cells and has impaired natural killer cells, with normal/low glucose levels and elevated insulin levels<sup>104</sup>. NOD SCID mice do not develop diabetes because they lack immune cells that cause autoimmune destruction of the  $\beta$  cells in the pancreas<sup>104,105</sup>. However, diabetes can be induced in the NOD SCID mouse by adoptive transfer of pancreatic  $\beta$  cells from immune competent mice<sup>105</sup>.

Generation of spheroids and 3-D structures arose spontaneously from multiple, independent human DCIS duct tissue fragments from the same patient and from different patients. These results demonstrate that progenitor cells with invasive potential pre-exist within the human breast DCIS duct but are apparently held in check by the ductal niche and can be coaxed to emerge in organoid culture. These cells constitute a new category of breast stem-like cells that exist prior to the overt manifestation of the malignant phenotype<sup>10</sup>.

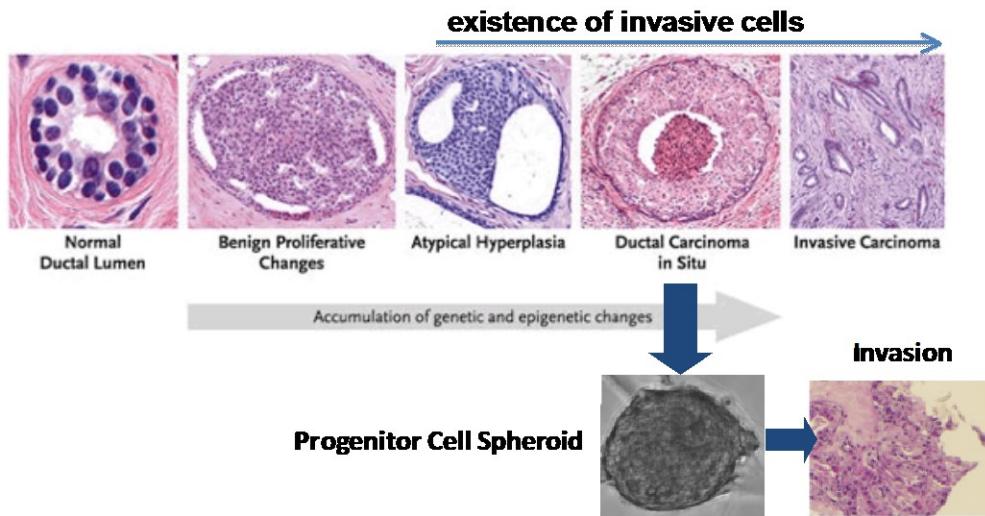


Figure 12. Continuum of human breast cancer progression. Cells capable of invasion exist within the breast duct at the atypical hyperplasia and DICS stages.

## CHAPTER 3: PROTEOMIC ANALYSIS OF DCIS CELLS

### Introduction

#### Protein signaling cascades

Proteins are the verbs of the cell, translating the DNA template into functional molecules. Network maps of cell signaling proteins, and their post-translational modifications, permit recreation of cellular networks that reflect the state of the cells at the time of harvesting/preservation. Numerous proteins known to function as tumor suppressors or drivers, such as BRCA1, Forkhead box proteins (FOXO1/03), Homeobox (Hox) family, Polycomb Group Complex 2 (PRC2), which mediate cell function by modulating chromatin binding<sup>106-111</sup>. Mutations in *BRCA1* contribute to hereditary breast cancer due to defects in DNA repair and recent evidence shows that BRCA1 loss results in deubiquitylation of histone H2A and opening of heterochromatin, but it is unknown at what stage of tumor progression each of these factors has the greatest effect<sup>111</sup>.

Chromatin structure, gene transcription, and transcription factor binding events modulate gene expression in an interdependent manner. *Hox* genes provide control of cellular patterning in vertebrate bodies and a high ratio of *HoxB13:IL17* gene expression is a prognostic indicator for ER positive, lymph node negative breast cancer patients<sup>112-114</sup>. Upon activation, *Hox* gene clusters are enriched with repressive Polycomb group proteins and methylated histone H3 on lysine 27 (H3K27me3). Methylation on lysine 27 is an epigenetic marker of gene silencing. On the other hand, recruitment of a Ubiquitously

Transcribed Tetratricopeptide Repeat X (UTX) protein complex causes H3K27 demethylation with methylation of H3K4, an activation mark<sup>107</sup>. This illustrates the complex interplay between gene expression and protein function in either promoting or inhibiting cell growth and differentiation and highlights the importance of quantifying proteins and post-translational modification for deciphering cellular biology.

In addition to HOX and polycomb group proteins, FOXA1 and Pre-B-cell leukemia transcription factor 1 (PBX1) are pioneer factors that remodel chromatin allowing recruitment of ER $\alpha$  to specific regions of the cistrome within the nucleus<sup>115</sup>. Many PBX1 proteins are cofactors for Hox transcription factors. Although FOXA1 and PBX1 have overlapping binding sites, PBX1 was shown to be essential for MCF7 breast cell line proliferation and as a marker of functional ER $\alpha$  binding sites. Functionally, PBX1 was found to open chromatin at H3K4me2 regulatory elements<sup>115</sup>. These insights suggest that *Hox* genes may play a role in gene activation state changes during cycles of breast ductal involution. An absence of involution cycles may alter the normal patterning events in breast epithelium, creating a cascade of signals that either inappropriately stalls/activates gene transcription, or activates/represses inappropriate gene sets, which could be evident by levels of protein cell signaling kinases.

Within the organoid cultures we sought to characterize the functional signal pathways that may be involved in the phenotype of these cells. It would not be possible to measure a large number of protein signal pathway endpoints and post-translational modifications by conventional flow cytometry following enzymatic dissociation, even within hundreds of spheroids. Consequently we used Reverse Phase Protein Microarray

(RPMA) analysis of 59 cell signaling kinase endpoints, representing stem cell markers, autophagy, adhesion, invasion, and pro-survival pathways. RPMA technology has the required sensitivity and precision for small numbers of cells and provides a means of quantifying protein post-translational modifications indicative of activated signal pathways<sup>116-118</sup>.

## **Materials and methods**

### **Reverse Phase Protein Microarray (RPMA)**

Cellular outgrowths were removed from the culture flask by scraping or aspiration with a pipette and were spun briefly to pellet the cells. Medium was removed by aspiration and the cell pellet was subjected to lysis with a 10% (v/v) solution of Tris(2-carboxyethyl)phosphine (TCEP; Pierce, Rockford, IL) in Tissue Protein Extraction Reagent (T-PER™, Pierce)/ Tris-glycine 2X SDS buffer (Invitrogen). Cell lysates were stored at -80°C prior to microarray construction. Cellular lysates were printed on glass backed nitrocellulose array slides (FAST Slides, Whatman, Florham Park, NJ) using an Aushon 2470 arrayer (Aushon BioSystems, Burlington, MA) equipped with 350µm pins as previously described<sup>116,118</sup>. Immunostaining was performed on a Dako Autostainer per manufacturer's instructions (CSA kit, Dako)<sup>118</sup>. Each slide was incubated with a single primary antibody at room temperature for 30 minutes. Polyclonal and monoclonal antibodies are listed in Table 3. Antibodies were validated by western blotting as previously described<sup>118</sup>. The negative control slide was incubated with antibody diluent. Secondary antibody was goat anti-rabbit IgG H+L (1:7,500) (Vector Labs, Burlingame, CA) or rabbit anti-mouse IgG (1:10) (Dako). Subsequent signal detection was amplified

via horseradish peroxidase mediated biotinyl tyramide deposition with chromogenic detection (Diaminobenzidine) per manufacturer's instructions (Dako).

Total protein per microarray spot was determined with a Sypro Ruby protein stain (Invitrogen/Molecular Probes) per manufacturer's directions and imaged with a CCD camera (NovaRay; Alpha Innotech, San Leandro, CA). Signal intensity of each RPMA spot was quantified with ImageQuant ver5.2 (GE Healthcare), with mean local area background subtraction. Data was compiled using a VBA Excel macro for non-specific antibody staining subtraction, and normalization to  $\beta$ -Actin.

**Table 3. Validated antibodies used with Reverse Phase Protein Microarrays.**

<b>Antibody</b>	<b>Vendor</b>	<b>Polyclonal/ Monoclonal</b>	<b>Function</b>
Beta Actin	CST	Polyclonal	Cytoskeletal
AKT	CST	Polyclonal	Growth/Prosurvival
AKT Ser473	CST	Polyclonal	Growth/Prosurvival
AKT Thr308	CST	Polyclonal	Growth/Prosurvival
AMPK alpha1 Ser485	CST	Polyclonal	Hypoxia/Stress
AMPK beta1 Ser108	CST	Polyclonal	Hypoxia/Stress
Atg5	CST	Polyclonal	Autophagy
Bak	CST	Polyclonal	Apoptosis
Bad Ser136	CST	Polyclonal	Apoptosis
BCL-XL	CST	Polyclonal	Apoptosis
Bcl-2 Ser70	CST	Polyclonal	Apoptosis
Bcl-2 Thr56	CST	Polyclonal	Apoptosis
Beclin1	CST	Polyclonal	Autophagy
B-Raf Ser445	CST	Polyclonal	Growth/Prosurvival
c-Raf Ser338	CST	Polyclonal	Growth/Prosurvival
Caspase-9, cleaved Asp330	CST	Polyclonal	Apoptosis
Beta Catenin Ser33/37/Thr41)	CST	Polyclonal	Adhesion/Differentiation
CD133 (W6B3C1)	Miltenyi	Monoclonal	Stem cell marker

CD24 (FL-80)	Santa Cruz Bio.	Polyclonal	Stem cell marker
CD44 (156-3C11)	CST	Monoclonal	Stem cell marker
Cox-2	BD Biosciences	Monoclonal	Stress/inflammation
E-Cadherin	CST	Polyclonal	Adhesion
EGFR Tyr992	CST	Polyclonal	Growth factor receptor
EGFR Tyr1045	CST	Polyclonal	Growth factor receptor
EGFR Tyr1068	CST	Polyclonal	Growth factor receptor
EGFR Tyr1148	Invitrogen	Polyclonal	Growth factor receptor
EGFR Tyr1173	CST	Polyclonal	Growth factor receptor
EGFR	CST	Polyclonal	Growth factor receptor
ErbB2/HER2	CST	Polyclonal	Growth factor receptor
ErbB2/HER2 (Y1248)	Millipore	Polyclonal	Growth factor receptor
ErbB3/HER3 (Y1289) (21D3)	CST	Polyclonal	Growth factor receptor
ERK 1/2 Thr202/Tyr204)	CST	Polyclonal	Growth/Prosurvival
FAK Tyr576/577	CST	Polyclonal	Adhesion
Fibronectin	Abcam	Monoclonal	Adhesion
FOXO1 Thr24/FOXO3a Thr32	CST	Polyclonal	Cycle cell arrest/Apoptosis
Gab1 Tyr627	CST	Polyclonal	Adaptor protein/signal transduction
Grb2	CST	Polyclonal	Adaptor protein/signal transduction
GSK-3alpha Tyr279/beta Tyr216	Invitrogen	Polyclonal	Glucose Metabolism
GSK-3alpha/beta Ser21/9	CST	Polyclonal	Glucose Metabolism
Integrin alphaV beta5	Millipore	Monoclonal	Adhesion
IGF-1R Tyr1131/IR Tyr1146	CST	Polyclonal	Insulin Receptor
IRS-1 Ser612	CST	Polyclonal	Glucose Metabolism
LC3B	CST	Polyclonal	Autophagy
MAPK pTEpY	Promega	Polyclonal	Growth/Differentiation
MEK1/2 Ser217/221	CST	Polyclonal	Growth/Prosurvival
Met Tyr1234/1235	CST	Polyclonal	Epithelial/Mesenchymal Transition
MMP-14	Abcam	Monoclonal	Invasion
MMP-9	CST	Polyclonal	Invasion
mTOR Ser2448	CST	Polyclonal	Growth/Prosurvival



Musashi	CST	Polyclonal	Stem cell marker
Nanog	CST		Stem cell marker
N-Cadherin	CST	Polyclonal	Adhesion
NF-kappaB Ser536	CST	Polyclonal	Proteasome Degradation/Inflammation
Nodal	Millipore	Monoclonal	Stem cell marker
p38 Thr180/Tyr182	CST	Polyclonal	Stress/inflammation
p70 S6 Kinase Thr389	CST	Polyclonal	Growth/Prosurvival
PARP, cleaved (D214)	CST	Polyclonal	Apoptosis
PI3 Kinase	BD Biosciences	Monoclonal	Growth/Prosurvival
PTEN	CST	Polyclonal	Tumor suppressor
PTEN Ser380	CST	Polyclonal	Tumor suppressor
Smad2 Ser465/467	CST	Polyclonal	Growth/Differentiation
Src Tyr416	CST	Polyclonal	Growth/Differentiation
STAT3 Ser727	CST	Polyclonal	Stress/Inflammation
STAT3 Tyr705 (9E12)	CST	Polyclonal	Stress/Inflammation
STAT5 Tyr694	CST	Polyclonal	Stress/Inflammation
SUPT3H	Abnova	Monoclonal	Transcription
Survivin	CST	Polyclonal	Apoptosis
TIMP2	Abcam	Monoclonal	Invasion

### **Immunohistochemistry**

Formalin fixed murine tissue or DCIS organoids were processed and paraffin embedded by commercial laboratories (AML Laboratories, Inc, Baltimore, MD or Bi-Biomics, Nampa, ID). Formalin fixed paraffin embedded (FFPE) tissue sections (5µm thickness) mounted on positively charged glass slides were baked at 56°C for 20 min., deparaffinized in xylene and rehydrated in a series of graded alcohols (100%, 95%, and 70%) with a final rinse in wash buffer (Dako, Carpinteria, CA). Antigen retrieval, when necessary, was performed with proteinase K or heat induced epitope retrieval (HIER). HIER was performed for 20 minutes at 95°C in a water bath. Immunostaining was

performed on a Dako Autostainer with an Envision+HRP staining kit (Dako) per manufacturer's instructions. Primary antibodies are listed in Table 4. Stained tissue sections were counterstained with Hematoxylin (Dako), rinsed in distilled water and developed in Scott's Tap Water Substitute solution. Coverslips were applied using aqueous mounting medium (Faramount, Dako). Images were captured with an Olympus BX51 microscope using 4x, 10x, 20x, or 100x objectives.

**Table 4. Primary antibodies and heat induced epitope retrieval (HIER) conditions for immunohistochemistry.**

<b>Antibody</b>	<b>Vendor</b>	<b>Species</b>	<b>Dilution</b>	<b>Proteinase K</b>	<b>HIER</b>
Atg5	Abcam	Rabbit	1:300	None	pH6
Atg7	Sigma	Rabbit	1:25	5 min	None
Beclin-1	Sigma	Rabbit	1:750	5 min	None
CD44	CST	Mouse	1:50	5 min	None
Collagen IV	Dako	Mouse	1:25	5 min	pH6
LC3B	CST	Rabbit	1:25	None	pH9
SUPT3H	Abnova	Mouse	1:50	5 min	None
CD68 (clone PG-M1)	Fisher	Mouse	1:50	None	pH6

### **Immunofluorescence**

LysoTracker Red (Invitrogen; 75 nM) and nuclear counterstain Hoechst 33258 pentahydrate (Invitrogen; 5 µg/mL) were added to serum-free DMEM/F12 culture medium as described in Chapter 2 and incubated with live human DCIS organoid cell cultures for 0.5 hour. Medium containing dye was removed and replaced with fresh medium. Images were captured with either a Nikon Eclipse C1si confocal or a Nikon Eclipse TE200 microscope in different channels for LysoTracker Red (psuedo-colored

red, 561nm) and Hoechst 33258 (pseudo-colored blue) using either the 10x or 20x objective.

### **Statistics**

Standard deviation (SD) or standard error of the mean (SEM) was calculated for small group comparisons. The Student t-test, two tailed with Welch's correction, was used to calculate the p-value. p values <0.05 were considered significant (GraphPad Prism ver 5.03, GraphPad Software).

### **Results**

#### **Signal pathway proteomic analysis reveals augmentation of survival related pathways**

The activation state of signaling pathways in the DCIS spheroids was compared to the anchorage dependent cells in organoid culture to functionally characterize the two cell populations<sup>10</sup>. The mixed cell culture model we devised provided an advantage over standard single cell or 3-D co-culture systems because we did not need to introduce foreign cells, such as irradiated fibroblasts. Our system supported growth of epithelial and fibroblasts from the same patient, thus providing a spatial and temporal context for orchestrating cellular organization and function, similar to the extracellular matrix.

48 endpoints were analyzed representing total or post-translationally modified proteins. Spheroids, the epithelial monolayer, and distinct cuboidal monolayer cells from the same DCIS organoid culture were procured using sterile technique, under direct microscopic visualization. Approximately 25 spheroids were analyzed and each sample was analyzed in duplicate. Data was normalized to  $\beta$ -Actin per microarray spot as described in VanMeter *et al*<sup>118</sup>.

Comparison of the spheroids to the flat, single layer epithelial cells in the same culture revealed a set of activated signaling pathways in the spheroids consistent with a progenitor-type classification. Macroautophagy, herein termed autophagy, is a dynamic, catabolic process of cellular self-cannibalization in which the cell sequesters organelles, such as mitochondria, or cytoplasmic proteins in double-membrane vesicles, to generate ATP during periods of nutrient limitation<sup>119-121</sup>. First coined by de Duve, autophagy (*auto-* “self”, *-phagy* “eating”) is an evolutionarily conserved endoplasmic reticulum-lysosomal pathway response for degrading protein aggregates, and recycling non-essential intracellular organelles and cytoplasmic proteins<sup>122-126</sup>.

Autophagy markers (Atg5 and LC3B) were elevated in the spheroids in comparison to the epithelial and cuboidal monolayer cells. p38 MAPK Thr180/Tyr182 and SMAD2 Ser465/467, cell signaling proteins associated with survival and stress, were elevated in the spheroids in comparison to the epithelial and cuboidal monolayers. The spheroids exhibited progenitor cell characteristics as evidenced by up-regulation of stem cell markers (CD44), down-regulation of cell adhesion markers (E-Cadherin), up-regulation of invasion related matrix metalloproteinases (MMP14), and up-regulation of COX-2 (Figure 13).

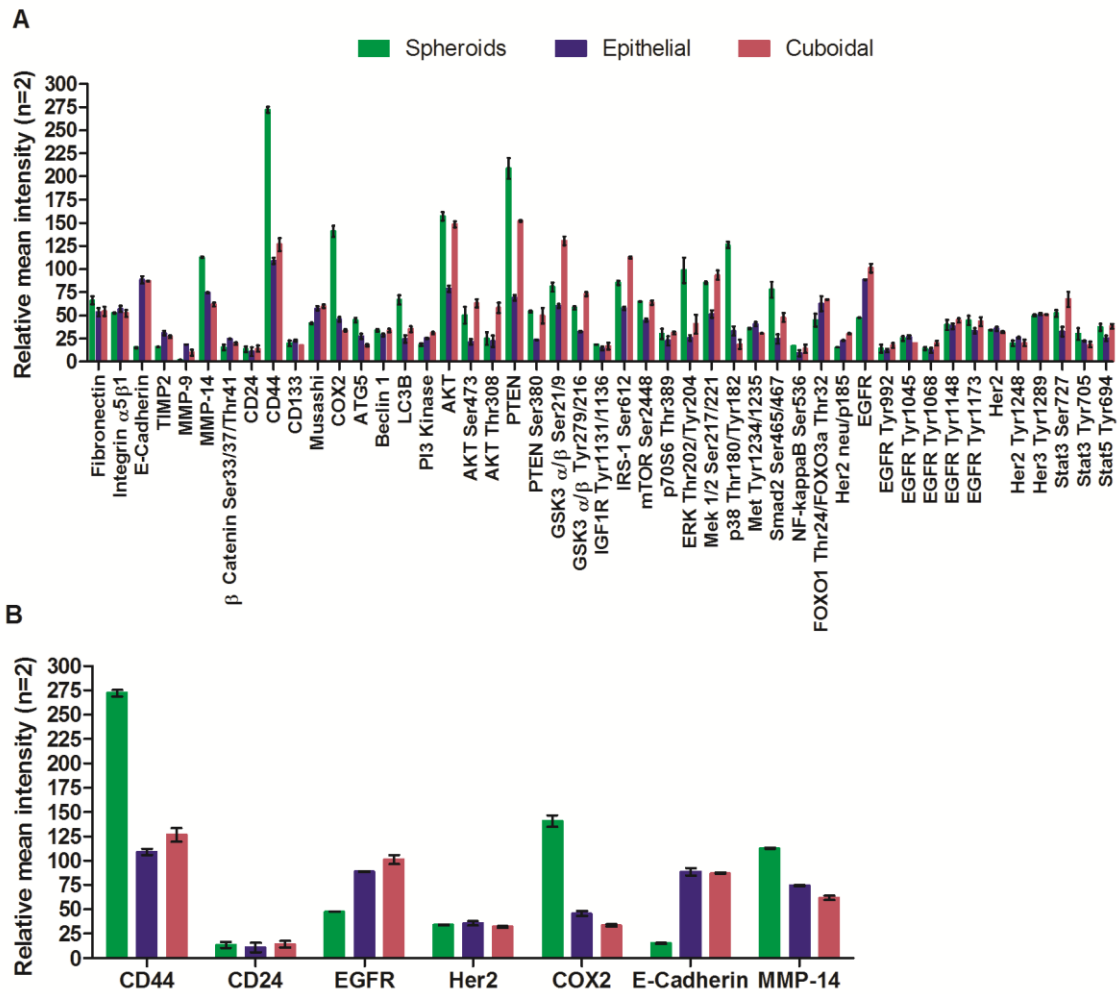


**Figure 13. Signal pathway mapping by reverse phase protein microarray of DCIS organoid outgrowths.** A) Comprehensive depiction of cell signaling kinase activity for spheroids (green), epithelial (blue) and cuboidal (red) cell populations reveal differential up-regulation of proteins involved in autophagy, stress, pro-survival and invasion. B) The spheroids exhibited progenitor cell characteristics as evidenced by augmentation of CD44, COX-2, and matrix metalloproteinase (MMP-14), with associated reduction of E-Cadherin (relative mean intensity, n=2,  $\pm$ SEM).

To test whether these differences in cell signaling proteins were a stable characteristic of the observed phenotype, we conducted an independent verification analysis. RPMA was performed on a different set of harvested cultured spheroids, epithelial cells, and stromal fibroblasts from the same patient derived cultures that were propagated over several months (Table 1). Autophagy, adhesion, and pro-survival

signaling proteins remained elevated in the spheroids compared to the epithelial and fibroblast cells (Table 5). Levels of putative stem cell markers, CD44 and CD133, and MMPs were also elevated in the spheroids indicating potential proliferative and invasive capacity.

**Table 5. Verification of DCIS stem-like cell phenotype.**

Protein	Epithelial Cells (n=6)			Spheroids (n=2)			Fibroblasts (n=2)		
	Mean	SD	SEM	Mean	SD	SEM	Mean	SD	SEM
AMPKa1 Ser485	22.45	6.69	2.73	65.15	24.73	17.49	12.72	0.10	0.07
Atg5	85.64	63.55	25.94	474.40	277.66	196.34	224.17	82.82	58.56
Beclin-1	17.92	5.98	2.44	42.33	35.91	25.39	2.63	3.72	2.63
Nanog	46.67	14.44	5.89	223.97	11.73	8.30	75.05	19.71	13.93
LC3B	79.35	30.13	12.30	384.78	91.57	64.75	267.72	14.68	10.38
N-Cadherin	25.47	6.15	2.51	152.13	20.91	14.79	27.92	17.45	12.34
p53 Ser15	27.87	9.84	4.02	188.05	114.83	81.20	66.33	27.00	19.09
TLR3	93.45	27.22	11.11	1693.65	1559.64	1102.83	4.49	ND	ND
SUPT3H	50.11	5.91	2.41	161.95	62.96	44.52	15.45	0.27	0.19
LAMP2	59.95	15.43	6.30	406.00	292.15	206.58	59.13	ND	ND
Fibronectin	121.74	107.31	43.81	165.32	11.04	7.81	562.55	224.45	158.71
Laminin5, gamma-2 chain	89.82	68.59	28.00	512.06	214.00	151.32	175.99	95.61	67.61
CD44	71.61	8.54	3.48	220.39	113.82	80.49	68.95	ND	ND
CD133	27.78	4.78	1.95	137.60	1.14	0.81	26.40	ND	ND
AKT Ser473	49.55	53.56	21.87	78.41	58.06	41.05	62.48	0.88	0.62
AKT Thr308	35.27	7.82	3.19	282.85	106.47	75.29	120.72	13.56	9.59
BetaCatenin Ser33	43.38	14.46	5.90	257.14	64.63	45.70	62.61	16.18	11.44
EGFR	87.51	21.35	8.72	335.33	46.13	32.62	102.48	10.01	7.08
FOXO1/O3a Thr24/Thr32	77.47	39.10	15.96	311.64	53.66	37.95	83.74	6.33	4.47
Her2	4.44	3.92	1.60	13.35	13.80	9.76	ND	ND	ND
IRS-1 Ser612	54.10	43.00	17.56	236.34	56.47	39.93	147.73	48.01	33.95
MEK1/2 Ser217	132.24	109.07	44.53	637.07	125.06	88.43	341.91	11.55	8.17
Met Y1234/1235	42.76	8.91	3.64	228.73	2.94	2.08	44.70	7.31	5.17
MMP-9	15.40	3.06	1.25	58.18	17.62	12.46	27.55	10.42	7.37
MMP-14	42.06	8.73	3.56	217.25	7.73	5.46	82.60	11.10	7.85

<b>mTOR Ser2448</b>	<b>67.05</b>	24.14	9.86	<b>272.57</b>	88.76	62.76	<b>89.77</b>	0.50	0.35
<b>p38 Thr180/Tyr182</b>	<b>80.13</b>	63.31	25.85	<b>409.66</b>	142.67	100.88	<b>286.35</b>	17.65	12.48
<b>PTEN Ser380</b>	<b>80.71</b>	61.82	25.24	<b>227.33</b>	136.84	96.76	<b>133.70</b>	3.81	2.70
<b>PTEN</b>	<b>242.38</b>	307.58	125.57	<b>843.56</b>	292.85	207.08	<b>857.90</b>	166.71	117.88
<b>Integrin alpha5beta1</b>	<b>31.97</b>	8.54	3.49	<b>244.21</b>	99.29	70.21	<b>100.61</b>	53.00	37.48

### Protein pathways intersecting with autophagy

Based on RPMA phenotype characterization, we noted that cell signaling pathways intersecting with autophagy were up-regulated in the cultured spheroids and 3-D structures. To determine if autophagy was activated *in vivo*, we performed immunohistochemical staining for proteins involved in autophagic flux (LC3B) and initiation of autophagosome formation (Beclin1 and Atg5). CD44 immunohistochemical analysis was performed to determine the prevalence of a stem-cell like marker in our sample cohort (Table 6). Immunohistochemical markers of autophagy were examined in primary DCIS lesions, mouse xenograft tumors, and DCIS *ex vivo* generated spheroids/pseudoductal structures<sup>10</sup>.

**Table 6. Immunohistochemical characterization of the primary human breast tissue (diagnostic specimen).**

<b>Sample ID</b>	<b>Diagnosis</b>	<b>LC3B</b>	<b>Beclin1</b>	<b>Atg5</b>	<b>CD44</b>
08-183	DCIS	1+	3+	3+	Positive
08-352	DCIS	1+	3+	3+	Positive
09-091	DCIS/ADH	0	1+	1+	Negative
09-118	ADH	N/A	1+	1+	Positive
09-148	DCIS	0	2+	1+	Positive
09-301	DCIS	0	2+	1+	Positive
09-327	DCIS	0	2+	1+	Negative

Intermediate and high-grade DCIS lesions were positive by immunohistochemistry for autophagy pathway proteins Atg5, Beclin-1 and LC3B, which are involved in the nucleation of autophagosomes. CD44 positivity was not associated with autophagy up-regulation, nor was it a consistent characteristic of the ADH/DCIS samples. Autophagosome accumulation, as demonstrated by fluorescence microscopy and immunohistochemistry of endogenous LC3B, showed an increase in punctate LC3B staining<sup>10</sup> (Figure 14). LC3B is a hallmark of autophagy induction because following lipidation of LC3-I, LC3-II (LC3B) co-localizes on the inner and outer membranes of the autophagosomes (Figure 16)<sup>53,127</sup>.



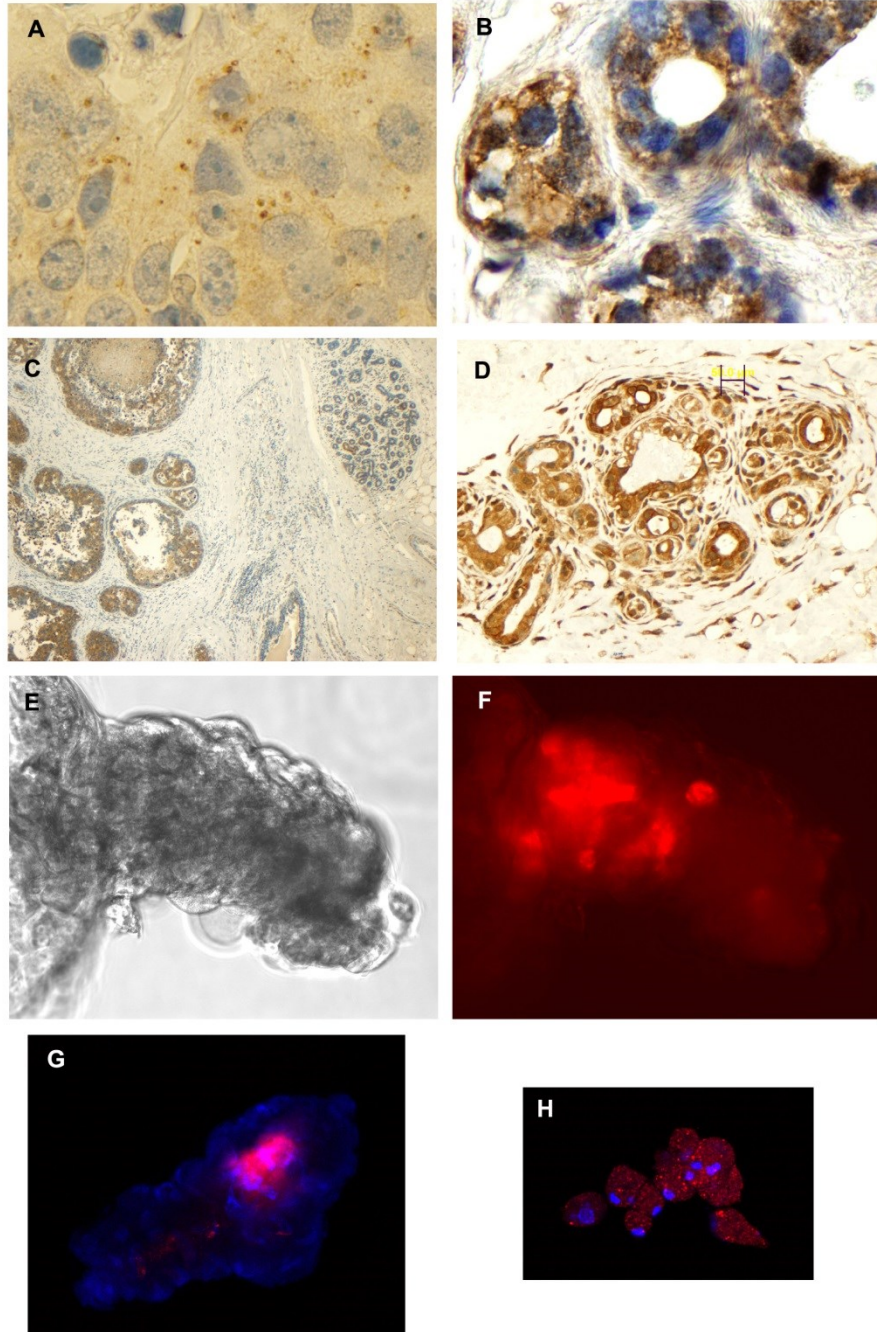


**Figure 14. Autophagy is activated in human DCIS lesions, spheroids, 3D structures, and xenograft tumors. A) IHC of a primary DCIS lesion showing punctate staining within the cytoplasm for LC3B (anti-LC3B, 100x). B) Beclin1 positive human DCIS derived mouse xenograft tissue (100x). C) Case 08-352 surgical specimen is positive for Atg5 staining in comedo DCIS human breast glands (DCIS) compared to adjacent non-neoplastic ductal elements (NL) (10x). D) Positive Atg5 staining of a DCIS organoid after 12 weeks in culture (20x). E) A bright field image of a multi-cellular pseudoductal structure (20x). (F) Fluorescence microscopy shows accumulation of LysoTracker Red dye within the organelles of the inner cell mass of the structure shown in panel E (20x). (G) LysoTracker Red dye accumulation within the central cell mass of a spheroid**

(red=LysoTracker Red; blue=DAPI nuclear counterstain, 20x) demonstrates enhanced phagosome and lysosomal activity in the region of the aggregate expected to be most hypoxic. H) Chloroquine inhibits autophagy by preventing the fusion of autophagosomes and lysosomes in the dynamic, multi-step autophagy cascade. An organoid culture was maintained in medium supplemented with chloroquine phosphate (50  $\mu$ M) for 2 weeks. Dissociation of the spheroid, and diffuse accumulation of LysoTracker Red in autophagic compartments and lysosomes were observed (red=LysoTracker Red; blue=DAPI nuclear counterstain, 20x, Nikon Eclipse TE200 microscope)<sup>10</sup>.

### **Immune cells in the DCIS microenvironment**

In mouse models of DCIS, mammary macrophages support stem cell activity in reconstituting mammary ducts and provide essential tissue remodeling during involution<sup>128,129</sup>. Infiltrating leukocytes on the periphery of breast ducts are often seen during pathologic examination of H&E stained breast tissue sections<sup>130</sup>. The immunophenotypic profile of immune cells in 53 mastectomy samples representing normal breast, benign breast disease, DCIS and infiltrating DCIS has shown that invasion may be a common immune-mediated response<sup>130</sup>. To determine if macrophages were present in the immune cell milieu of our DCIS patient cohort, FFPE and/or BHP fixed tissue sections of DCIS lesions were immunostained for CD68, a 110kDa transmembrane glycoprotein. A macrophage –specific antibody clone, PG-M1, was used to prevent cross-reactivity with neutrophils. CD68 positive macrophages were localized in the duct periphery, outside the basement membrane, of duct alveoli (Figure 15). Numerous macrophages were found in the infiltrating lymphocyte populations surrounding ducts with DCIS and were present in the surrounding adipose tissue. Intraluminal macrophages were observed as well as macrophages interspersed between the luminal epithelium. The presence of CD68+ macrophages in the DCIS microenvironment could contribute to autophagy activation via chemokine release.

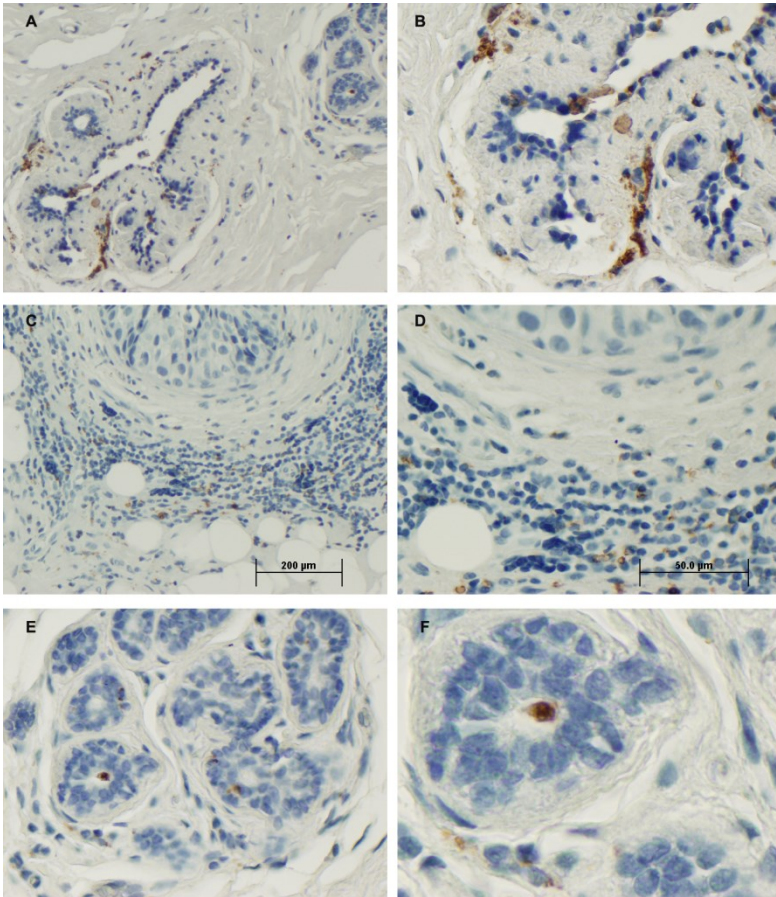


Figure 15. CD68 positive macrophages are located in the lumen and surrounding the periphery of the duct in DCIS lesions.

A & B) Macrophages (brown staining) are localized on the periphery of duct alveoli and are scattered among the luminal epithelial cells (20x and 40x magnification). C & D) Infiltrating lymphocytes (case 10-134) harbor numerous macrophages (20x and 40x magnification). E & F) Intra-luminal macrophages (40x and 100x magnification).

### **Disruption of autophagy in DCIS-derived spheroids**

Autophagy activation increases the number of autophagosomes within a cell.

Acidotropic dyes can be used to qualitatively assess autophagy activation. The acidotropic dye, LysoTracker Red (Invitrogen), which accumulates in intracellular autophagosomes/lysosomes was used to image live DCIS organoid culture cell

outgrowths, including spheroids and 3-D structures (Figure 14). In the spheroids generated from DCIS lesions, lysosomal and/or autophagosome activity was up-regulated in the central region of the spheroid as shown by strong fluorescence intensity with LysoTracker Red (Figure 14 F&G) and by distinct immunohistochemical staining of LC3B and Atg5 in FFPE tissue sections (Figure 14 A & C).

Chloroquine inhibits autophagy by preventing the fusion of autophagosomes and lysosomes in the dynamic, multi-step autophagy cascade. An organoid culture was maintained in medium supplemented with chloroquine phosphate (50  $\mu$ M) for 2 weeks. Dissociation of the spheroid, and diffuse accumulation of LysoTracker Red in autophagic compartments and lysosomes were observed (Figure 14 H). Accumulation of autophagosomes and lysosomes is consistent with altered autophagic flux, either due to lack of fusion with the lysosome or decreased lysosomal degradation<sup>127</sup>. Regardless of the mechanism disrupting autophagic flux, accumulation of autophagosomes/lysosomes indicated that autophagy was activated in the spheroids. Up-regulation of autophagy promotes survival in the hypoxic and nutrient deprived center of the spheroid in culture and the intraductal DCIS microenvironment<sup>10</sup>.

## **Discussion**

### **Proteomic biomarkers in DCIS**

Extensive studies characterizing breast mammary cells both functionally and structurally have yielded many putative prognostic and diagnostic markers of breast cancer, including cytokeratin profiling<sup>72,112-114,131-133</sup>. For clinical diagnosis of invasive breast cancer, Ki-67, ER, PR, and Her2 status are commonly evaluated, but considerable

debate remains surrounding the most appropriate biomarkers for DCIS<sup>134</sup>. Several classification schemes for pre-invasive breast lesions arose in an attempt to distinguish indolent precursor lesions from those lesions likely to progress to invasive cancer<sup>54,134-137</sup>. The Van Nuys Prognostic Index utilizes tumor size, nuclear grade, comedo-necrosis and surgical margin width to classify samples as low, intermediate, or high risk of local recurrence<sup>136,137</sup>. An enhanced DCIS prognostic classification that includes the DCIS lesion architecture has been proposed<sup>138</sup>. Despite the plethora of putative biomarkers and classification schemes, we analyzed the underlying cell signaling pathways within the DCIS microenvironment without any pre-conceived hypotheses as to which proteins were the most reliable biomarker.

Functional characterization of the DCIS cells using reverse phase protein microarrays provided quantitative comparison of the proteins supporting the growth and proliferation of the DCIS cells *in vivo* as well as in culture. Reverse phase protein microarrays provide clinical grade assay sensitivity and precision for quantifying proteins and their post-translational modifications from a small number of cells<sup>98,139</sup>.

When and why human DCIS cells with pre-existing invasive potential eventually breach the ductal basement membrane is a central question. The absence of suppressive factors produced by the duct myoepithelial cells, the basement membrane, or the stromal cells are likely to have a role<sup>140,141</sup>. Suppressive factors may include myoepithelial cell -- glandular epithelial cell interactions, soluble factors secreted by reactive or activated stromal cells, mesenchymal cells, or immune cells, loss or enhancement of ECM tropic factors, or composition of the ECM<sup>27,62,63,140-143</sup>. However, autophagy was up-regulated in

diagnostic specimens, *ex vivo* cultured organoids, and mouse xenograft tumors. Thus we have shown, for the first time, that activation of autophagy in the neoplastic epithelial cells has a central role as a cell survival strategy within human DCIS lesions<sup>10</sup>. Gong *et al* recently reported similar requirements for autophagy in maintaining mammospheres derived from MCF7 and BT474 (Lapatinib resistant) human breast cancer cell lines<sup>144</sup>. Substantiation of our findings support the concept of generalized cell signaling pathway alterations in pre-malignant lesions and cells under stress, rather than a single dominant protein.

Autophagy optimizes nutrient utilization in growing cells faced with hypoxic or metabolic stresses (Figure 16). During autophagy, macroautophagosomes (also referred as autophagosomes) are formed as double membrane-bound vesicles that engulf cytoplasmic constituents and/or cytoplasmic organelles. Autophagosomes fuse with lysosomes to degrade the contents of the autophagic vesicle and provide molecular breakdown products to either feed the cell or enable cell death. Accumulation of autophagosomes can be due to reduced turnover of autophagosomes or increased autophagic activity (autophagic flux)<sup>127</sup>. Cancer cells may undergo autophagic cell death associated with extreme autophagic degradation after exposure to several cancer therapies<sup>145</sup>. While some initial studies described autophagy as a tumor suppressor mechanism<sup>146-148</sup>, the autophagic response can also function as a protective mechanism allowing the recycling of proteins and cellular components to facilitate cell survival during the severe cellular stress of cytotoxic therapy<sup>149</sup>. We have shown that “protective autophagy” might also sustain the survival of pre-invasive or invasive stem-like cells within the intraductal

environment of the DCIS lesion. High grade DCIS is associated with central necrosis in the duct, and the accumulation of cellular degradation products such as lipofuscin.

Autophagy is a plausible means for DCIS neoplastic cells, accumulating in the duct, to survive in the face of severe metabolic, oxidative, and hypoxic stress.

In the breast microenvironment, macrophages perform vital tissue repair and remodeling functions<sup>150,151</sup>. Macrophages degrade and deposit extracellular matrix, stimulate angiogenesis and lymphangiogenesis, and remove necrotic cell debris<sup>150,151</sup>. Macrophages can be alternately activated to either M1 or M2 phenotypes by interferon gamma/tumor necrosis factor or IL-33/IL-1/IL21 cytokines, respectively<sup>150,151</sup>. Immune cells and cytokines can create cellular stress which in turn induces autophagy<sup>152-154</sup>. IL-2 activates autophagy through classic autophagy/stress related cell signaling cascades - Ras, PI-3K, AKT, the Janus associated kinases (JAK1-JAK3), and STAT5 (a transcription factor). IL-2 activates natural killer (NK) cells and promotes maturation of T-reg cells. This global stress response promotes “immune cell-mediated autophagy”, which is cell contact dependent and contributes to vascular leak and organ dysfunction<sup>152,155</sup>. In hypoxic conditions, HIF-1 induces expression of chemokines and chemokine receptors (CXCR4 and CXCL12), further promoting macrophage tissue remodeling<sup>150,156</sup>. In addition to their role in breast organogenesis and involution, macrophages help to sustain autophagy activation.

Chloroquine, a lysosomotropic inhibitor, was shown in our *in vitro* model to disrupt autophagic flux in the DCIS-derived spheroid culture. Chloroquine inhibits both the fusion of autophagosomes to the lysosome and enzymatic degradation of lysosomal

contents, providing dual avenues for disrupting cellular homeostasis in cells dependent on autophagy for survival (Figure 16).

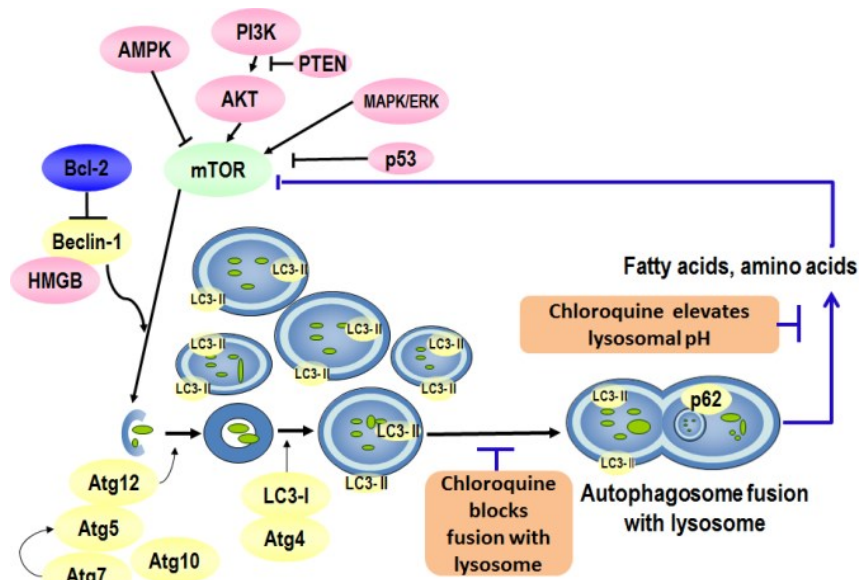


Figure 16. Autophagy pathway overview (Modified from reference <sup>157</sup>).



## CHAPTER 4: MOLECULAR CYTOGENETIC CHARACTERIZATION OF DCIS CELLS

### Introduction

#### Gene expression studies of human breast cancer

Gene expression studies of human breast cancer progression found similarities at the gene transcript level for ductal hyperplasia, ductal carcinoma in situ, and invasive breast tumors, whereas different grades of breast tumors were found to have distinct transcriptome signatures<sup>17</sup>. In the clonal evolution model, multiple, genetically abnormal, malignant progenitor cells arise within an individual patient's intraductal microenvironment. Each of these clones is different depending on the stage of differentiation they were in when the founding oncogenic genetic event took place<sup>1,21,158,159</sup>. The malignant progenitor clones compete for dominance before and after overt basement membrane and stromal invasion. During the course of disease, and during therapy induced regression and recurrence, the relative dominance of pre-existing malignant clones changes, giving rise to drug resistance and recurrence<sup>1,21,158,159</sup>. The aggressive phenotype of a patient's tumor, and treatment susceptibility, is therefore predestined very early as a product of the genetic changes first created within the ductal niche. Support for this model stems from the apparent clinical success of predictive gene signatures of invasive breast cancer recurrence, such as the 21-gene score used in *Oncotype DX*<sup>160,161</sup>.

**Genetic instability**

Genetic instability (chromosomal instability) is thought to be caused by chromosome missegregation during mitosis (non-homologous recombination), chromosome breaks, and inadequate or inefficient repair of DNA damage<sup>162-164</sup>.

Chromosomal instability exists in pre-malignant breast and prostate lesions and is not associated with loss of p53 tumor suppressor function<sup>164</sup>. Immunohistochemical analysis of centrosomes in premalignant lesions of breast and prostate tissue has shown abnormally large centrosomes, increased numbers of centrosomes, plus mitotic spindle abnormalities<sup>164</sup>. The number of defects correlated with increasing histological grade of in situ carcinomas<sup>164</sup>.

A cell's ability to modulate chromatin structure and function via epigenetic marks and ATP-dependent remodeling proteins depends on an abundant energy supply (ATP) and amino acid/nucleotide pool<sup>165</sup>. Autophagy ('auto' – 'self', 'phagy' – 'eating') maintains cellular homeostasis during nutrient starvation, hypoxia, or cellular stress, such as during chemotherapy<sup>166-169</sup>. One can hypothesize that prolonged autophagy could potentially increase genetic instability by altering chromatin remodeling and gene transcriptional states due to a lack of abundant ATP, selective degradation of cytoplasmic proteins, free radical accumulation, and a decreased amino acid/nucleotide pool. Surges in ATP production due to autophagy may indirectly increase reactive oxygen species, contributing to genetic instability<sup>170,171</sup>. ATP level fluctuations could have many implications regarding epigenetic modifications such as altering nuclear pore transport of trans-acting transcription factors, reducing nucleosome mobility, inhibiting ATP-dependent chromatin remodeling enzymes, and altering the cytoplasmic/nuclear

distribution of transcription factors. Furthermore, the stressful DCIS microenvironment could promote genetic instability through deregulation at various cellular levels including gene specific mutational events, alterations in signal transduction to avoid hypoxia induced apoptosis and oxidative damage, or dysfunctional DNA synthesis and repair mechanisms<sup>10</sup>.

### **Molecular karyotyping**

Stephens *et al* mapped chromosomal abnormalities in cell lines and primary breast tumors using paired-end sequencing methods to identify somatic rearrangements<sup>172</sup>. The advantage of sequence-based mapping is the fact that actual chromosome fusion points can be identified and characterized, however the cost of sequencing each sample is tremendously expensive. Since many chromosomal alterations manifest themselves as changes in copy number, such as amplifications, duplications, and deletions, the single nucleotide polymorphism (SNP) array is a cost effective technology for detecting copy number variation<sup>173-175</sup>. SNPs are stable polymorphisms that occur in 1% or more of the population. The prevalence of copy number variation and SNPs in the healthy population, and the importance of LOH in tumor suppressor genes, indicate that these genetic alterations have a role in carcinogenesis<sup>173,176</sup>. SNP arrays measure allele-specific copy number by comparing signal intensity from SNP probes designated as SNP A and SNP B. Variations in the signal intensity between the two probes allows detection of copy number alterations and allelic imbalance<sup>175</sup>.

To detect cytogenetic abnormalities within the DCIS organoid outgrowths, we performed molecular karyotyping with CytoSNP arrays (Illumina, Inc.).

## **Materials and methods**

### **Samples**

Human breast tissue and/or cellular outgrowths from *ex vivo* cultures, including spheroids, epithelial cell monolayers, 3-D structures and fibroblasts, were harvested by either aspirating cells with a manual pipette or by scraping the desired cell population with a tissue scraper from the tissue culture flask. Conditioned medium in the vicinity of the cells was removed concurrently with the cells. The samples were spun at 14,000rpm for 20 seconds, the majority of media was removed and discarded. The cell pellet plus a small volume of residual conditioned medium was frozen at -80°C prior to nucleic acid isolation.

### **Molecular karyotyping via Single Nucleotide Polymorphism analysis**

Nucleic acid preparations derived from human breast tissue and/or cell culture outgrowths were tested using quantitative PCR (qPCR), PicoGreen (Invitrogen) staining and fluorometry (FLx800 fluorescence plate reader, BioTek, Winooski, VT). Microarray-based genomic analysis was performed using CytoSNP-12 beadchips (Illumina, Inc.) and analyzed on an Illumina BeadStation 500 GX laser scanner<sup>177-179</sup>. Briefly, the microarray process involved sample DNA amplification, followed by DNA fragmentation, hybridization of samples to beadchips, single-nucleotide extension, antibody-based labeling, and finally two-color fluorescence scanning and computer-based raw data collection.

The DNA extraction and purification was performed using a DNA purification column (QIAmp DNA Mini Kit, Qiagen, Valencia, CA). Approximately 200 ng of DNA at a concentration of 50 ng/μL was amplified, fragmented, precipitated, re-suspended, and

hybridized to the Illumina CytoSNP-12 beadchips. After single-base extension, sample DNA was stained and the chip was washed, dried, and scanned for the resulting 300,000 SNP calls and copy number values.

Raw fluorescence data was converted to genotypic data using the Illumina GenomeStudio software program. Data analysis was performed using the Illumina KaryoStudio software program that converts genotypic and signal intensity data into a “molecular karyotype” showing B allele frequency, Log R ratio, LOH score and Copy Number Score. Log R ratio, which is the log (base 2) ratio of the normalized R value, was used for comparisons. A Log R Ratio  $\geq 2$  was considered to represent a true amplification and Log R Ratio  $\leq -1.5$  was considered to represent a probable homozygous deletion. B allele frequency data were used to identify regions of copy-neutral and hemizygous LOH<sup>10</sup>.

### **Immunohistochemistry**

SUPT3H antigen retrieval was performed with ProteinaseK treatment for 5 minutes at room temperature. Immunostaining was performed for on a Dako Autostainer with an Envision+HRP staining kit (Dako) per manufacturer’s instructions. Primary antibody (Abnova) dilution was 1:50, 60 minutes incubation. Tissue was counterstained with Hematoxylin and a cover slip was applied with aqueous mounting medium (Faramount, Dako).

### **Results**

#### **DCIS derived tumorigenic spheroid forming cells are cytogenetically abnormal**

The molecular karyotype of the isolated DCIS spheroid forming cells was evaluated and compared to the non-neoplastic tissue from the same patient. The spheroid

forming DCIS epithelial cells were found to be cytogenetically abnormal compared to the normal karyotype of the anchorage dependent monolayer cells cultured from the same patient's breast tissue lesion<sup>10</sup>. Full genotypic data output included allele calls from "tagged" single nucleotide polymorphism (SNP) sites and signal intensity values from non-polymorphic sites to determine DNA copy number values (CytoSNP-12 beadchips (Illumina, Inc.)). Molecular cytogenetic profiles demonstrated cytogenetic alterations in the isolated DCIS spheroids (3-5 spheroids per prep) and isolated pseudoductal structures compared to the non-neoplastic, normal karyotype cells in the same patient's DCIS breast tissue. The abnormal karyotype signature of the spheroids included loss of copy number on chromosomes 5, 6, 8, and 13, and gain of copy number on chromosomes 1, 5, and 17<sup>10</sup>. Abnormalities were present in all DCIS cell spheroids and 3-D cell complexes (Table 7) and arose in a background of cells with a normal karyotype from the same patient.

Table 7 summarizes gain (3 or more copies) or loss (0 or 1 copy) of DNA > 3 million base pairs. If gains or losses greater than 1 million base pairs were used as the cutoff, then, at this higher resolution, anchorage independent spheroid cells from 3 different patient DCIS lesions all showed narrow copy number loss of chromosome 6 (p21.1/p12.3). This region includes the transcription factor SUPT3H (protein coding GIFTs:59, GC06M044904, UniProtKB/Swiss-Prot: SUPT3\_HUMAN, O75486) (Figure 17)<sup>10</sup>. SUPT3H is a component of the STAGA transcription factor complex and has a putative tumor suppressor function. RUNX2 regulates cell fate and has been implicated as either an oncogene or a tumor suppressor<sup>180-186</sup>.

A second region of aberration was observed in a single patient on the p-arm of chromosome 5 entailing extended regions of gain and loss of chromosomal content. Chromosomal bands from 5p12 to 5p13.3 were present in 3 copies and a distal segment of 5p13.3 included 4 copies. Bands 5p14.1 and 5p14.3 on the same chromosome however showed loss of DNA content as represented by homozygous and hemizygous deletions, respectively (Table 7). This same patient's cultured DCIS cells showed a 14 Megabase (Mb) region of trisomy on chromosome 17, extending from 17q22 to 17q25.1 (Figure 18)<sup>10</sup>.

The SNP data indicated, for all matched samples, that the DCIS cultured cells were derived from the donor patient tissue and were not a contaminating cell line. The normal epithelial and stromal cells of the donor tissue grown for the same length of time in culture possessed a fully normal karyotype. In all cases the propagated DCIS cells forming 3-D structures and exhibiting invasion, showed copy number gain or loss in one or more genetic loci indicative of a neoplastic mutational event (Table 7)<sup>10</sup>. Multiple isolates from different regions of the DCIS lesion, for the same patient, yielded spheroids with the same abnormal molecular karyotype. Thus, cytogenetically abnormal, DCIS derived, spheroid forming epithelial cells emerged spontaneously from organoids in culture and were responsible for the tumorigenic and invasive phenotype observed (Figure 10).

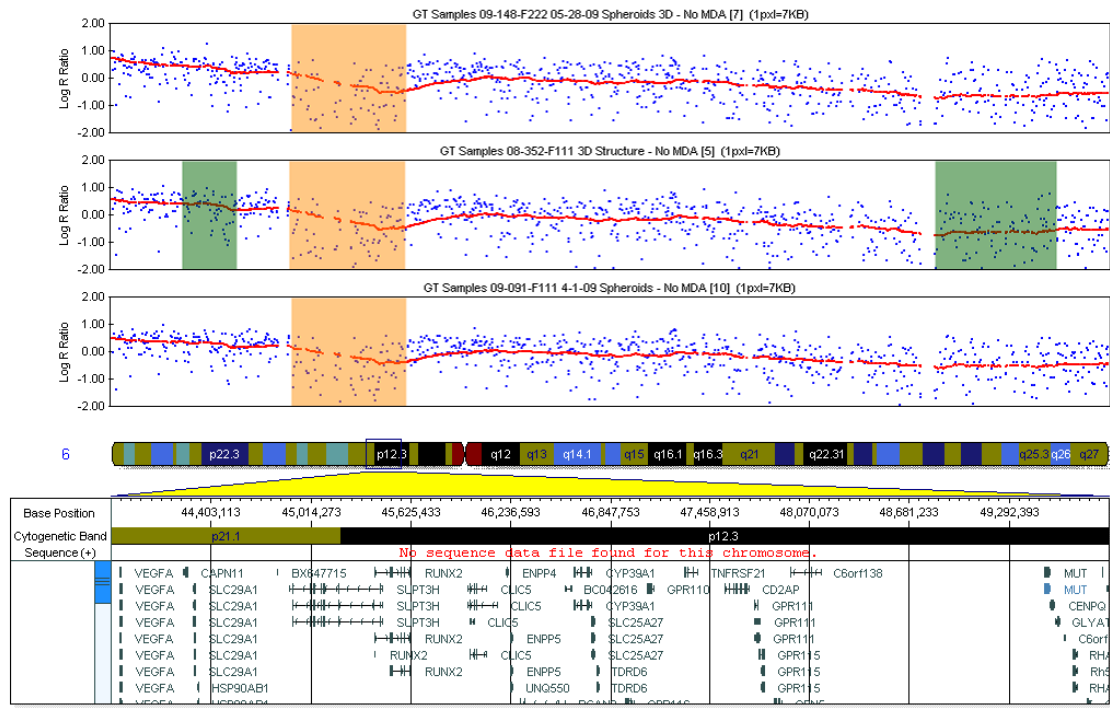


**Figure 17. Three independent patient's DCIS spheroids exhibited the same Chromosome 6p21.1-p12.3 copy number loss (deletion)<sup>10</sup>.**

The upper panels show the log R ratio plots from 3 different patients (top: 09-148 spheroids/3-D structure; middle: 08-352 3-D structure; bottom: 09-091 spheroids/3-D structure). The region of deletion for these 3 patients (orange) corresponds to the transcript for suppressor of Ty 3 homolog (SUPT3H)<sup>10</sup>. The center panel shows the chromosomal ideogram indicating cytological bands with the centromere in red. The small window shows the region expanded in the figure and the nucleotide positions for this region are shown below the ideogram. The lower panel shows the cytogenetic bands and genetic map for genes located in the expanded region.

The log R ratio plots represent DNA ploidy, or copy number, for the displayed chromosomal region with the red line indicating the statistical average value. A log R



ratio of 0.0 equals a DNA copy number of 2 (diploid). Deflection downward of the red line indicates loss of DNA copy number. Each blue dot represents the log R ratio value for each SNP. The shaded regions represent segments of DNA deviating from a copy number of 2 as determined by the Illumina GenomeStudio 2.0 software. The software uses both quantitative fluorescence intensity and qualitative genotypic data for determining copy number values. The color code is as follows: orange indicates a region of 1 copy; red = 0 copies; blue = 3 copies; purple = 4 or more copies; and green = copy-neutral LOH (2 copies)<sup>10</sup>.

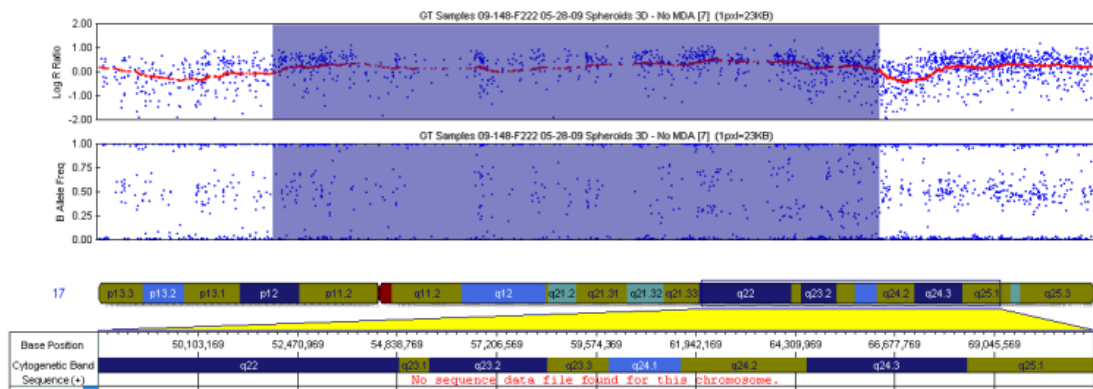


**Figure 18. Chromosome 17q shows extensive regions of copy number variation (gain) for spheroids from case 09-148.**

**Deflection of the red line in the top plot indicates a gain in copy number spanning ~14Mb. The B-allele frequency for heterogeneous SNPs is split into 2 lines above and below 0.5, indicating the presence of 3 copies of DNA in this region<sup>10</sup>.**

**Table 7. Molecular karyotype of cultured human DCIS spheroid showing cytological location of chromosome aberrations (Corrected from reference<sup>10</sup>).**

Sample ID	Gain* of DNA	Loss* of DNA	Copy-neutral LOH
08-352	1p36.3p13.2	2q31.1q32.1	6p21.1.p12.32

	1q21.1q41	4pterp15.2	12pterp12.1
	2(triploid)	8pterp12	12q11.22
	3q11.2	11q14.1q22.1	13q11q33.1
	6q22.31q25.1	14 <sup>b</sup>	17pterp13.1
	8q22.3q24.3	17 <sup>b</sup>	Xq13.1q23
	9p22.3p22.1	19 <sup>b</sup>	
	11q22.1q23.1	Xq25	
	12p11.21q12		
	13q33.2qter		
	14 <sup>a</sup>		
	15q25.2qter		
	17 <sup>a</sup>		
	18(triploid)		
	19 <sup>a</sup>		
	20q13.13q13.2		
	Xq23q26.2		
09-091	8(triploid)	6q21, 6q16.1	22q11.21q11.22
	10q22.3	13q21.31q21.33	
	22q11.23q12.1	21q21.1q21.2	
09-118		5p15.2, 5p15.1p13.3	3q28q29
		10q21.3	5p15.32, 5p15.2p15.1, 5p13.3
		11p11.2p11.12	5q14.1
		12p13.1p12.3	6p21.1.p12.3
			10q21.1q21.2, 10q22.1q22.3, 10q24.1q26.3
		12p12.1p11.22	
		12q12q13.11	12 <sup>c</sup>
			14q31.1-q32.11, 14q32.13q32.2
		15q21.1q21.3	
		18p11.32	15q14q21.1, 15q22.1q22.2
			16p13.3p13.2
			17q25.3
			22q11.23q13.31
			Xp22.33p22.11
			Xq22.1q28
09-148	1q21.1, 1q21.3	5p14.3, 5p14.1	6p21.1
	1q32.1q32.3	6q14.1, 6q24.1	22q13.31qter
	5p15.2, 5p13.3p12	8q2.3, 8q22.3	Xq22.1q22.3, Xq22.3, Xq23
	17q12, 17q21.32q21.33	8p23.2p23.3	
	17q22q23.3	13q21.1	
	20q13.31qter		
09-301			2q21.3q22.1
			4q31.21q31.22
			5q21.3q22.1, 5q23.331.1
			8q23.2
			14q23.2q23.3

Cytological locations are listed as chromosome:arm:band(s)

\* Gain (3 or more copies) or Loss (0 or 1 copy) of DNA > 3 million base pairs

<sup>a</sup> multiple regions of DNA gain

<sup>b</sup> multiple regions of DNA loss

<sup>c</sup> multiple regions of copy neutral (diploid) loss of heterozygosity

At the chromosomal level, some degree of copy number variation and copy-neutral loss of heterozygosity exists in the normal karyotype<sup>187,188</sup>. To demonstrate that our mixed cell culture model was not inducing genetic instability in any of the cell populations, we analyzed fibroblasts from the same culture flasks as those containing the epithelial cell monolayers with spheroids and 3-D pseudoductal structures. Molecular karyotyping, represented in a low resolution copy number variation map for chromosomes 1-22, X and Y, showed copy-neutral LOH with only one area of hemizygous deletion in one sample (Figure 19). Deletion of the Y chromosome confirmed that the fibroblasts were of female origin.

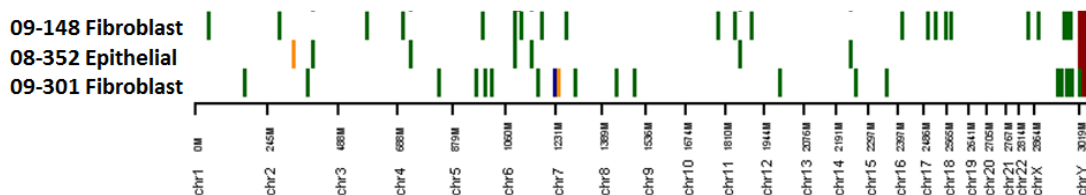


**Figure 19. Cell culture conditions did not induce genetic instability. Fibroblasts in the DCIS culture showed copy-neutral loss of heterozygosity (green) with minimal copy number variations.**

### Temporal comparison of molecular karyotyping

Temporal aspects of cell harvesting such as growth phase, time in culture, ratio of cell types in the culture, etc. could affect the observed cell population and hence the

molecular karyotype. To demonstrate the heterogeneity between and within patient samples in culture, DCIS epithelial cells were harvested from the same patient culture on different days and copy number variation was analyzed with the Illumina CytoSNP chip (Figure 20). The CNV pattern within patients at different time points is more similar than the CNV pattern between patients. In addition, this lack of temporal effect supports the use of the *ex vivo* organoid model as a biosimilar environment to a human breast acinus and will allow comparisons between spheroids and 3-D structures over time. Such comparisons could potentially elucidate the evolution of dominant clones during long-term culture as well as provide evidence either supporting or refuting the clonal evolution model of carcinogenesis.

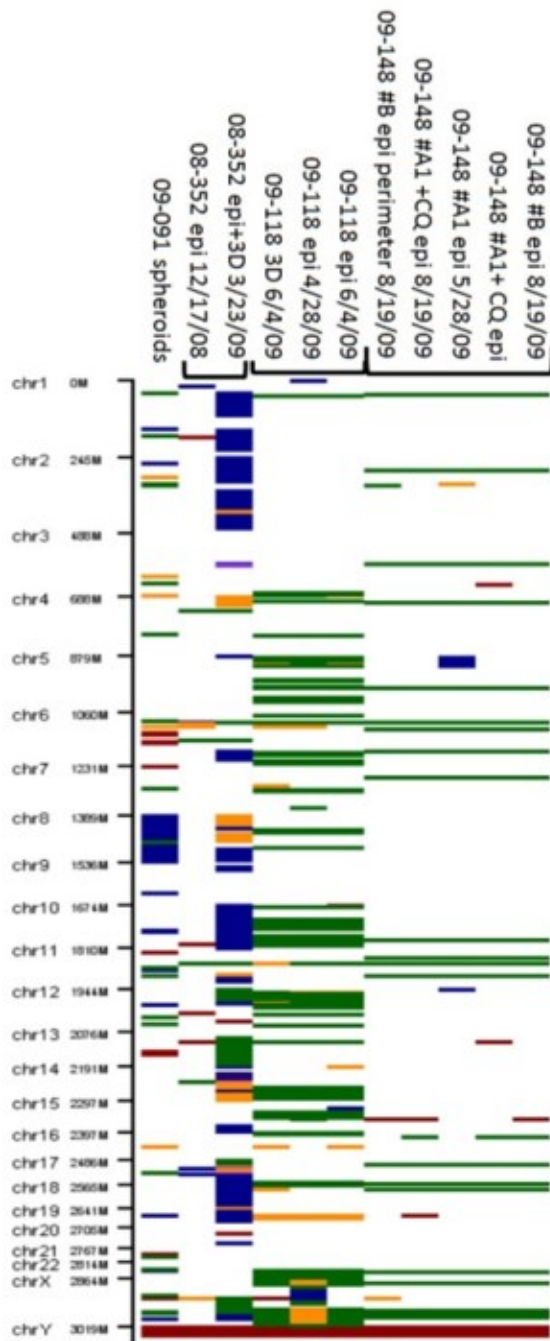


Figure 20. Copy Number Variation (CNV) summary of DCIS organoid cell cultures reflecting temporal aspects of *ex vivo* culture.

DCIS organoids were maintained in culture over a period of months. Copy number variation in organoids from the same patient showed subtle differences, while CNV between patients was much more variable. (Green - copy neutral loss, Blue - gain or amplification, Red - homozygous deletion, Orange - hemizygous deletion).

## Abrogation of genetically unstable cells

On proteomic data indicated that autophagy pathway proteins were up-regulated in the DCIS derived spheroids and that treatment with chloroquine interrupted the autophagic flux in these cells. Chloroquine weakly intercalates with DNA<sup>189,190</sup>. This DNA interaction may potentially increase apoptosis in normal cells and contribute further genetic alterations, although this seems unlikely based on the long-term use of chloroquine as anti-malarial and anti-rheumatic agents<sup>191</sup>.

To determine if chloroquine affected the molecular karyotype of the DCIS organoid cultures, we compared the untreated spheroids and chloroquine (50 $\mu$ M) treated epithelial monolayer from case 09-148. The top plot shows the log R ratio for Chromosome 6 from cell cultures treated with chloroquine phosphate showing normal ploidy, while the lower plot shows a hemizygous deletion (orange) of the SUPT3H locus in cultures displaying spheroid and 3-D structures. (Figure 21).

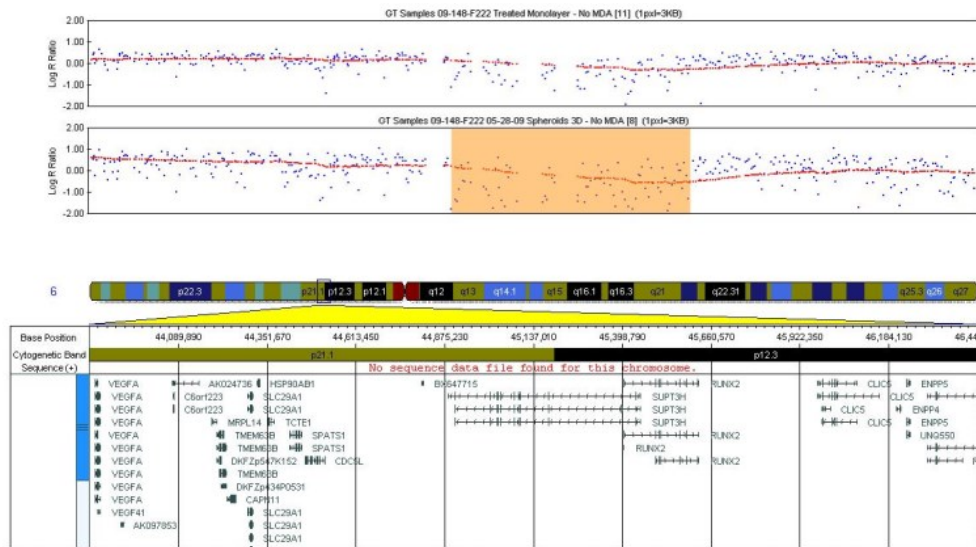


**Figure 21. Copy number variation is not induced by chloroquine treatment in DCIS derived spheroids.**

The molecular karyotype of chromosome 5 from chloroquine treated cultured DCIS epithelial monolayer and untreated spheroids is shown in Figure 22. The upper panel shows log 2 ratio plots of 2 different samples from the same patient (top: 09-148 chloroquine treated epithelial monolayer; bottom: 09-148 untreated spheroids/3-D structure). In the upper panel, the top plot shows the log R ratio from chloroquine treated human DCIS cell cultures showing normal ploidy, while the lower plot shows a number of extended regions of gain and loss of content on chromosome 5. Blue and purple regions in the spheroids/3-D structures show an increase of copy number extending from nucleotide position ~31 Mb to ~43 Mb (12 Mb in total) affecting the dosage of numerous genes. Additional regions of copy number gain are present distally, including subtelomeric regions. Extended regions of copy number loss are indicated in orange (one copy) and red (0 copy). The lower panel shows the cytogenetic banding pattern and the corresponding nucleotide positions beginning with the p-telomere<sup>10</sup>.

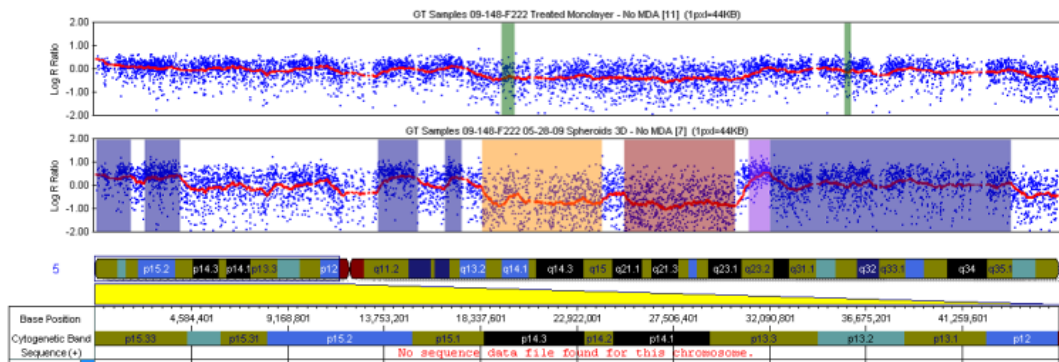


**Figure 22. Molecular karyotype of chromosome 5 from chloroquine treated monolayer or untreated spheroids/3-D structures derived from human DCIS<sup>10</sup>.**

### **Localization of SUPT3H in DCIS lesions**

Immunohistochemistry of SUPT3H was performed to determine the subcellular location and presence/absence of SUPT3H in the DCIS microenvironment. As a transcription factor, SUPT3H would be expected to be localized to the nucleus. However, some transcription factors shuttle between the cytoplasm and the nucleus<sup>192</sup>. We found abundant cytoplasmic staining in numerous cells with only rare cells showing nuclear staining in a DCIS organoid that had been in culture for more than 2 weeks (Figure 23). SUPT3H predominantly was localized to the ductal cells and staining was apparent in the DCIS cells that grew on the surface of the organoid in culture.



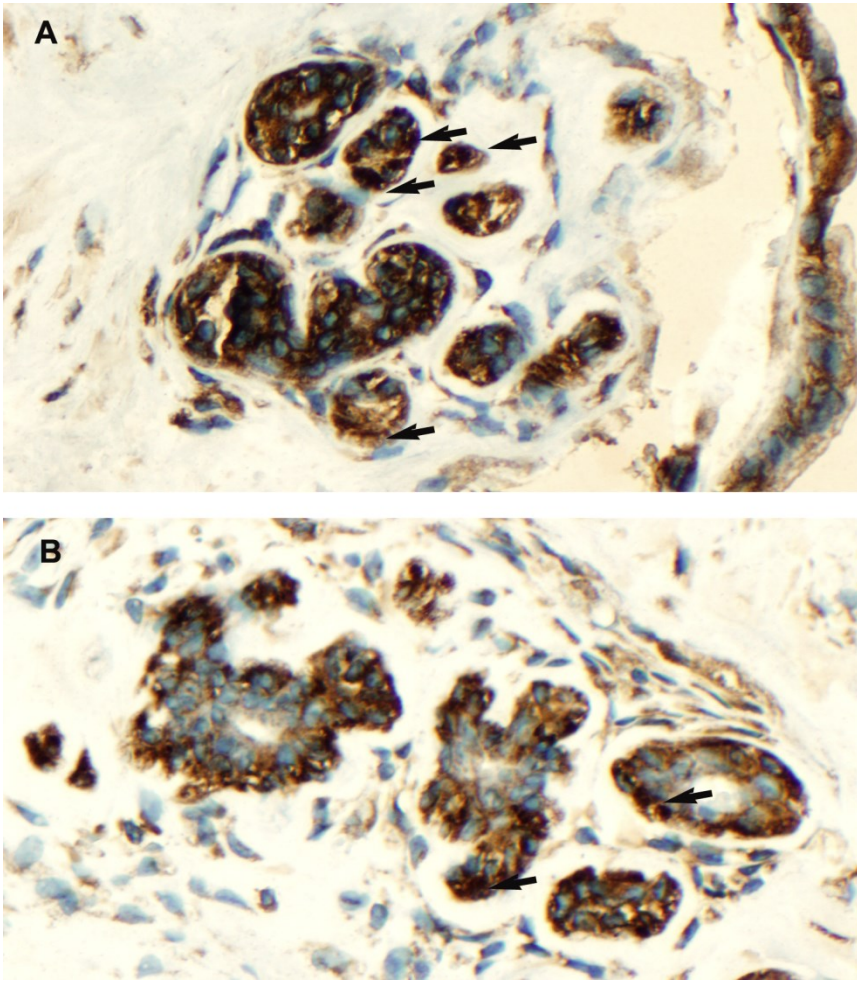


Figure 23. SUPT3H immunohistochemistry of case 09-148 shows rare cells with nuclear staining (black arrows) and numerous cells with cytoplasmic staining. A) SUPT3H positive cells within areas of DCIS and on the surface of the organoid. B) Rare SUPT3H nuclear staining within the ducts.

## Discussion

### Autophagy and genetic instability

Early studies of autophagic flux were conducted with rat hepatocytes<sup>167,193,194</sup>.

Seglen and colleagues found that rat hepatocytes treated with carcinogens unexpectedly contained diploid nuclei rather than the normal tetraploid hepatocyte nuclei and survived longer in culture with less response to amino acid starvation than normal hepatocytes

<sup>195,196</sup>. At the time, autophagy was viewed as a cell death pathway and their conclusions suggested that resistance to autophagy could prolong survival of cancerous cells. Today, we know that autophagy is a bivalent process, either promoting cell survival in times of intracellular stress or as an alternative death pathway<sup>169</sup>.

A mismatch between mitochondrial DNA mutations and nuclear DNA in the same cancer cell may be another route to genetic instability during prolonged periods of autophagy<sup>171,197,198</sup>. Mitochondrial/nuclear DNA mismatch can alter reactive oxygen species and impair ATP generation thereby reducing ATPase function. A third route to genetic instability may be due to insufficient protein production and/or a lack of ribosomes/rRNA if ATP levels are inadequate<sup>199</sup>. ATP requirements for rRNA, mRNA and mitochondrial DNA in isolated human mitochondria showed that rRNA synthesis and lagging strand transcription required more ATP than mRNA synthesis<sup>199</sup>. At low ATP levels, similar to those seen in anaerobic glycolysis, mRNA synthesis was adequate while rRNA synthesis was marginal<sup>199</sup>.

The consequences of autophagy up-regulation are hypothesized to show gene specific patterns of transcription regulation by different proteins depending on which proteins have been degraded. As an example, hypoxia inducible factor 1 $\alpha$  (*HIF-1 $\alpha$* ) promoters associate with SWI/SNF chromatin remodeling complexes and inhibition of SWI/SNF binding to the *HIF-1 $\alpha$*  promoter allows cells to resist cell cycle arrest during hypoxia<sup>200</sup>. Generalized dysregulation of transcription appears unlikely because homeostasis would be disrupted to such an extent that the cell would die, either by apoptosis or via the autophagic death pathway. Recent chromatin profiling studies could

provide a ‘tissue population’ data set for comparing cell-type specific promoter and enhancer states with cells possessing altered metabolic states<sup>201</sup>.

We have shown that breast ductal carcinoma in situ (DCIS) cells up-regulate autophagy while expanding in the breast duct lumen prior to becoming invasive<sup>9,10</sup>. In addition, these DCIS cells possess a progenitor cell phenotype capable of inducing xenograft tumors, and are genetically unstable in the context of single nucleotide polymorphisms and copy number variations compared to patient-matched breast ductal tissue<sup>10</sup>. Factors contributing to our observed genetic instability could be due to inflammation, free radical formation, mutations in mitochondrial DNA (mtDNA), or inefficient base/nucleotide excision repair due to reduced nucleotide pools and/or ATP.

#### **Energy consumption for transcription, translation, remodeling, and DNA repair**

Higher order eukaryotes, such as mammals and birds, require ATP for replication and maintenance of the genome<sup>199,202</sup>. Chromatin remodeling and epigenetic marking are essential processes to ensure that genes are maintained in the desired transcription status for the cell type, function, lineage, and differentiation state<sup>201,203-209</sup>. Chromatin remodeling enzymes are multi-subunit protein complexes containing ATPase subunits that utilize ATP hydrolysis to reposition nucleosomes, insert histones, and condense or open chromatin<sup>165</sup>. SWI/SNF complexes randomize nucleosome position within chromatin by sliding nucleosomes or ejecting nucleosomes via a translocase domain.

An unexplored source of genetic instability in pre-malignant lesions could be alterations in chromatin structure, occupancy, or nucleosome positioning during prolonged autophagy. Basal levels of autophagy ensure removal of damaged organelles

and cell survival<sup>148,210,211</sup>. Cell viability requires a continual source of nutrients and oxidizable substrates to maintain homeostasis. Single cell and multi-cellular organisms have developed autophagy as a mechanism to generate energy (ATP) under stress conditions such as starvation, hypoxia, or chemical/toxic environments. The survival of DCIS cells in the hypoxic, nutrient-deprived intraductal niche could promote genetic instability and the de-repression of the invasive phenotype.

The copy number variations we noted in breast DCIS could be due to genetic changes that precede autophagy or alternatively are a consequence of autophagy. The overall working hypothesis is that autophagy creates a microenvironment that promotes survival but as a consequence may induce ATP insufficiency or surges that alter the homeostasis of DNA repair, chromatin remodeling, nucleotide pool levels, transcription factor subcellular localization, and cell cycle checkpoints<sup>9,10</sup>.

#### **Temporal variation in SNP microarray data**

Variation between patients may be related to temporal conditions such as the time at which spheroids were harvested, the size of the DCIS organoid, the number of organoids in culture, as well as the cellular composition of the culture, e.g. ratio of epithelial cells to fibroblasts, and the size of the spheroid mass. DCIS cells emerging from the duct in culture experience a transition from overcrowding, hypoxia, and nutrient deprivation to one of abundant oxygen, nutrients, and substratum. During this transition time cells may be undergoing different responses to the stresses on DNA replication and repair relating to conditions imposed by autophagy. Preexisting genetically “unstable” cells in situ may have an advantage emerging from this stress, since their preexisting

plasticity can lead to more genetic change and selection during culture outgrowth, before the genomes of the long term population stabilize<sup>9,10</sup>. Illumina CytoSNP data shows a sum-total (average) of all the genotypes present in the population, thus we cannot rule out the possibility that some temporal variation may exist in the organoid culture. If the clonal evolution model of stem cell population growth is correct, we could be missing sub-populations of cells that harbor significant genetic alterations but which don't contribute significantly to the overall SNP intensity signal. This effect can be evaluated by DNA sequencing using spheroids that are harvested from multiple organoid outgrowths from the same patient over time.

### **Chromosome 6 genes implicated in cancer**

Chromosome 6 encompasses 6% of the human genome and contains the major histocompatibility complex (MHC)<sup>212</sup>. MHC comprises a region of 3.6 megabases on band 6p21.3 (33-36 megabases) which typically shows in a low sex-averaged recombination rate<sup>212</sup>. Three hotspots of recombination were observed in the sequencing data, representing segmental duplications, one of which was a pseudogene in the extended MHC region at 6p21.31<sup>212</sup>. Chromosome 6p21.3 is, on a genetic scale, in close proximity to the Chromosome 6p21.1 (44.4-48.6 megabases) area of copy number loss seen in 3/7 of our pre-invasive breast lesion samples. Mutations in the MHC hotspot region could potentially disrupt adjacent areas of the chromosome, although this has not been shown for our genes of interest due to the limitations of our SNP microarrays. The disadvantage of our SNP microarray plots is that for large duplications of a chromosomal region, such as translocations, the region maps back to the donor chromosome. Also, for

a chromosome that appears structurally normal on our plots, it could have insertions or translocations from other genomic regions, but these regions will map back to the donor chromosomes, not the acceptor chromosomes. Thus the acceptor chromosome may appear on the SNP molecular karyotype as normal, as long as none of their material has been duplicated or lost.

From the chromosome 6 sequencing data, several genes implicated in cancer within the 6p21.1 region were: VEGF, HSP 90, NFKBIE, RUNX2, and SUPT3H<sup>212</sup>. RUNX2 is a transcription factor involved in osteoblast differentiation and skeletal morphogenesis, with expression in breast cancer metastatic to bone<sup>213-215</sup>. All RUNX family members bind core binding factor B, which stabilizes RUNX-DNA interactions<sup>216</sup>. Elevated RUNX2 expression is associated with increased levels of MMP-9, MMP-13, Vascular Endothelial Growth Factor, and Osteopontin<sup>213</sup>. A *RUNX2* knock-out mouse model exhibited absence of bone formation in newborn mice and a lack of differentiated osteoblasts<sup>181</sup>. RUNX2 mediates expression of bone sialoprotein in human metastatic breast cancer cells (MDA-MB-231 and LCC15-MB), acting as a positive regulator, but not in normal human mammary epithelial cell lines<sup>180,181</sup>. *RUNX2* lies within the region of Chromosome 6 exhibiting LOH. Although we don't know the mutation status of the second allele in this region, we can hypothesize that the expression of RUNX2 may be elevated to compensate for the LOH. Elevated RUNX2 levels could initiate invasion via modulation of MMPs within the breast niche.

### **SUPT3H, chromatin modifications, epigenetic marks**

Chromatin is lavishly decorated with epigenetic marks including acetylation, methylation, and phosphorylation of histone tails<sup>217,218</sup>. The importance of subtle histone modifications to create diverse chromatin structure and gene transcription states was introduced by Allfrey *et al* in 1964 and 11 years ago the “histone code hypothesis” was postulated to describe the vast effects chromatin epigenetic marks on gene function<sup>217,219-221</sup>. These cis-acting marks provide a plethora of functionality to the chromatin package by: a) controlling access to DNA transcription complexes, b) mediating long-range interactions between promoters, enhancers, insulators, c) modulating receptor binding, and d) providing templates for active repositioning of nucleosomes and histones<sup>201</sup>.

The power of epigenetic modifications such as histone methylation and acetylation to alter cell fate and function is much greater than single gene mutations because epigenetic changes silence or activate not just single genes, but multiple genes in various pathways<sup>165,222</sup>. Actively transcribed genes are associated with acetylation of promoter and enhancer regions, whereas inactive genes are associated with deacetylation<sup>223</sup>. The concept of bivalency, in which a promoter can possess both repressive and active methylation marks, has been shown to be an important regulator of pluripotency in embryonic stem cells<sup>203</sup>. We identified 3/7 patients with the same LOH in the region of SUPT3H, a subunit of a histone acetylase complex, that could modulate the chromatin structure and activity<sup>9,10</sup>.

SUPT3H was identified via molecular cloning as a histone acetyltransferase<sup>185</sup>. Further work revealed SUPT3H to be part of the nuclear STAGA complex which is a transcription co-activator that associates with spliceosome-associated proteins and DNA

UV-damage binding proteins and nucleotide excision repair proteins<sup>186</sup>. The SWISS-MODEL of SUPT3H for residues 107-151 reveals a histone association domain<sup>224-226</sup>. Crystallization structure studies of TAF<sub>II</sub>28- TAF<sub>II</sub>18 complex identified two histone fold motifs with a 120 residue linker that allows creation of a histone pair via intramolecular interactions rather than intermolecular pairing<sup>182</sup>. This atypical histone fold motif was also found in the SPT3 family. This motif presumably forms compact and tight protein-protein-interactions<sup>182</sup>.

Similar to our rate of LOH, LOH at Chromosome 6p21.2 was also found by polymerase chain reaction analysis in 46.8% (29 of 62) of cervical cancer patients<sup>227</sup>. The tumor size and stage was not correlated with the LOH. However, in this patient cohort that was also treated with radiation therapy, LOH at Chromosome 6p21.2 was correlated with cervical cancer recurrence<sup>227</sup>. Further evidence of the role of SUPT3H and STAGA complexes in tumorigenesis was shown in studies of c-Myc association studies in HeLa and HEK293 cells<sup>183</sup>. c-Myc has been shown to promote mammary epithelial differentiation and is a well-characterized proto-oncogene<sup>183,228</sup>. Myc recruits transformation-transactivation domain associated protein and the human histone acetyltransferase GC5N, to the active N-terminus of the STAGA complex<sup>183,184</sup>. The Myc-STAGA-GC5N complex may have broad histone acetylase activity due to the combination of myc histone H4 acetylation and GC5N histone H3 acetylation in a single complex<sup>183</sup>.

Analogous to the transcription factor FOXO, which functions as a tumor suppressor by initiating cell-cycle arrest and apoptosis when it translocates to the nucleus,



SUPT3H may have a cytoplasmic form and a nuclear form based on our immunohistochemical staining of DCIS lesions<sup>192</sup>. Thus further studies of SUPT3H and RUNX2 sequence and function may provide insights into transcriptional regulation/de-regulation in progression of DCIS tumorigenesis.

## CHAPTER 5: AUTOPHAGY AS A THERAPEUTIC TARGET IN DCIS

### Introduction

#### Cytoprotective Autophagy

Otto Warburg predicted in 1956 that the ability of cancer cells to survive with little or no energy “will be of great importance for the behavior of the cancer cells in the body”<sup>229,230</sup>. His concept of a cancer cell energy source can be explained in part by autophagy, a cyclic cellular pathway that can be catabolic, generating ATP in times of cellular stress, or can be apoptotic, leading to cell death<sup>169</sup>. Autophagy regulates cell homeostasis via regulation of cell survival or cell death, via an alternative mechanism to apoptosis. Basal levels of autophagy ensure removal of damaged organelles and cell survival.

Autophagy is a highly conserved constitutive catalytic process; Yeast autophagy genes have orthologous genes in higher eukaryotes and many mutations result in embryonic lethal effects<sup>166</sup>. Over evolutionary time, autophagy may have developed as an immune function. Engulfment of cytoplasmic bacteria within a lysosome could have been a simple method for single cells to eliminate a pathogenic organism. In multicellular organisms, dendritic cells have been shown to utilize autophagy as an unconventional secretory pathway to process pathogens and present them on the cell membrane for recognition by lymphocytes<sup>231</sup>. Autophagy also appears to function in a variety of cell types as a constitutive process for maintaining ATP levels and a free amino acid pool,

degradation of protein aggregates, prevention of neurodegeneration (a neuron specific function)<sup>232</sup>, and for controlling cell death<sup>166,168</sup>.

Autophagy was originally thought to be a generally non-specific degradation of aging organelles (mitochondria, endoplasmic reticulum and golgi apparatus) and long-lived cytoplasmic proteins<sup>122</sup>. The paradox is that well-studied cellular processes such as DNA replication and transcription have been shown to be highly regulated and exquisitely coordinated via DNA structure, epigenetic marks, and trans-acting protein complexes, therefore it seems unlikely that autophagy, which results in a life or death decision for the cell, would be a non-specific recycling of cellular contents. Data now indicate that autophagy can selectively remove specific organelles such as the endoplasmic reticulum (reticulophagy), mitochondria (mitophagy), and ribosomes (ribophagy)<sup>233,234</sup>. Autophagy is now known to be a highly ordered and regulated degradation process at the nutrient, protein complex/organelle level<sup>233</sup>.

Despite a growing appreciation for the importance of autophagy, its role as a cellular survival process in relation to maintenance of chromatin structure, epigenetic marks, and gene activation status is a currently under-explored area. During autophagic cell survival we can speculate that there must be chromatin modifications to prevent transcription/translation of unnecessary genes/proteins. Do levels of chromatin remodeling proteins, histones, and nucleotide/phosphorous pools remain at homeostatic levels during prolonged autophagy?

### **Chloroquine: an anti-lysosomotropic agent**

Current molecular therapies for cancer, used alone or in combination with chemotherapy, are effective for only a short time period, and fail to significantly extend survival for many common cancers. Improvements in the duration of a therapeutic response have been attained by using genomic and proteomic biomarkers to guide cancer therapy. Unfortunately these advances are too often punctuated by treatment failure due to acquired resistance driven by genetic instability or renewed growth of pre-existing therapy-resistant cancer subclones<sup>157</sup>. Based on these therapeutic set-backs, there is a growing recognition that long term improvements in cancer treatment outcomes require new classes of therapy that a) prevent cancer by targeting pre-invasive neoplastic lesions, or b) potentiate drug efficacy, or c) reduce drug resistance with current therapies. These new classes of therapy are envisioned to target mechanisms of carcinogenesis, tumor cell survival, and cancer stem cell function that transcend conventional therapeutic targets. Chloroquine and hydroxychloroquine (HCQ), 4-aminoquinolines, are currently emerging as strong candidate drugs capable of fulfilling these broad transcendent goals of circumventing acquired drug resistance, enhancing drug efficacy, and preventing the transition from pre invasive to invasive cancer<sup>157</sup>.

A strong rationale exists for using lysosomotropic agents for chemoprevention. The safety profile of CQ has been well established for long term prophylaxis, and acute therapy of malaria worldwide<sup>235,236</sup>. CQ has been shown to suppress N-methyl-N-nitrosurea induced mouse breast carcinogenesis<sup>237</sup>, enhances the effectiveness of tyrosine kinase inhibitor treatment of primary CML stem cells<sup>238</sup>, and has been proposed as a potential means to improve the effectiveness of tamoxifen *in vitro* for tamoxifen resistant

breast carcinoma cells by blocking autophagy dependent cell survival<sup>239</sup>. CQ has also been proposed as a therapy for Myc induced lymphomagenesis because CQ induces lysosomal stress, which triggers p53 dependent cell death that does not require caspase mediated apoptosis<sup>240,241</sup>.

Autophagy and lysosomal biogenesis are linked via transcription factor EB (TFEB), a helix-loop-helix leucine zipper family transcription factor, that regulates lysosome function<sup>242</sup>. TFEB directs a complex system (CLEAR network) of lysosomal enzymes that control protein, lipid, and glycoprotein degradation, as well as the biogenesis of autophagosomes in a HeLa cell model<sup>242</sup>.

Cells devoid of an anchoring network or substratum up-regulate autophagy as a survival mechanism. Within the confines of the breast duct, epithelial cell hyperplasia creates overcrowding, which leads the epithelial cells to lose their basement membrane adhesion (Figure 4). Central necrosis, characterized by areas of dead/dying cells, at the center of a hyperproliferating cell mass, creates an intra-ductal environment that favors autophagy, as well as cell migration. Metabolic by-products from the dead cells act as a chemo-repellent for epithelial cells, while attracting macrophages. Furthermore, stretching of the breast duct creates conditions favoring cell migration<sup>9</sup>. Eisenhoffer *et al* recently demonstrated that live cells undergo active extrusion via a Rho-kinase and sphingosine mediated pathway, presenting evidence that cell extrusion serves dual purposes: maintenance of cell number for homeostasis, and removal of apoptotic/necrotic/damaged cells<sup>243</sup>. Thus, DCIS cells could potentially be extruded from the duct but remain viable in the adjacent stroma.

### **Development of medicinal 4-aminoquinolines**

Cinchona bark extract contains the alkaloids quinine, quinidine, cinchonidine and cinchonine which have anti-infective and anti-rheumatic qualities<sup>244</sup>. Cinchona trees comprise several species within the Rubiaceae family, which are indigenous to the lower altitudes of the Andes<sup>245</sup>. Malaria was endemic throughout Europe, including Scandinavia, in the 18<sup>th</sup> and 19<sup>th</sup> centuries. Prior to the identification of malarial parasites, Cinchona bark was widely used as an anti-pyretic to treat the undulating fevers common in malarial infections<sup>245</sup>. By the 1930's chemists were synthesizing various forms of alkylated quinolones. While developing more effective anti-malarials, Hans Andersag, of Bayer AG, synthesized chloroquine by modifying the acridine ring of atabrine with a quinolone ring<sup>245,246</sup>. However, chloroquine was initially considered too toxic for human use. Ten years later, parallel development of the test substance SN-7619, was discovered to be the same chloroquine synthesized previously by Andersag<sup>245,246</sup>. Further structural modifications of chloroquine led to less toxic formulations, including hydroxychloroquine and chloroquine diphosphate<sup>157</sup>.

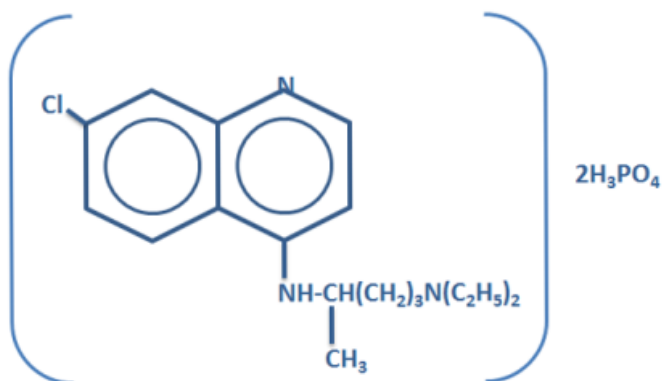


Figure 24. Chemical structure of chloroquine diphosphate (Aralen, Sanofi-Aventis).

Structurally, CQ and HCQ only differ by one hydroxyl group. Chloroquine is usually synthesized as the diphosphate salt of *N'*-(7-chloroquinolin-4-yl)-*N,N*-diethylpentane-1,4-diamine and is a diprotic weak base ( $pK_{a1}=8.1$ ,  $pK_{a2}=10.2$ )<sup>247</sup>. The molecular formula of chloroquine is:  $C_{18}H_{26}ClN_3$ , with a molecular weight of 319.92. The molecular formula of hydroxychloroquine is  $C_{18}H_{26}ClN_3O$ , with a molecular weight of 335.87, and experimentally derived  $pK_{a1}=8.27$ ,  $pK_{a2}=9.67$ <sup>248</sup>.

### **Chloroquine bioavailability/pharmacodynamics**

CQ and HCQ accumulate in tissues due to their weak base property. This di-basic property can be exploited therapeutically to target the acidic extracellular microenvironment of many solid tumors<sup>249,250</sup>. Intracellularly, CQ and HCQ accumulate within the acidic lysosome because they become di-protonated and will not diffuse freely out of the lysosome<sup>157</sup>. Within the lysosome, CQ & HCQ cause an increase in lysosomal pH thus inactivating phospholipase A2, lysophospholipidacylhydrolase and monoacylglycerol lipase<sup>247</sup>. Inhibition of these lysosomal enzymes hinders proteolytic degradation, decreases the pool of available free fatty acids and amino acids, and

subsequently reduces ATP levels which will elevate cellular stress levels which autophagy may not be able to overcome.

Extensive pharmacokinetic studies reveal similarities for the two compounds regarding absorption, protein binding, tissue distribution, but differences in renal clearance and elimination half-life<sup>250-252</sup>. Both CQ and HCQ are rapidly absorbed from the gastrointestinal tract, with an average half-life absorption of 0.57 hours<sup>250</sup>. Bioavailability ranges from 67 to 89%<sup>250,251</sup>. HCQ and CQ are 50 to 65% protein bound, with albumin and  $\alpha_1$  acid-glycoprotein being the major protein binding moieties. Of note,  $\alpha_1$ -acidglycoprotein is an acute phase reactant and CQ/HCQ binding may be affected by the increased levels of  $\alpha_1$ -acidglycoprotein during immune response to cancer or infectious agents<sup>250,252</sup>. CQ and HCQ exhibit a large distribution volume and readily accumulate in tissues such as kidney, liver, lung, spleen, muscle, and melanin-containing cells in the eye and skin<sup>250-252</sup>.

The metabolism and renal excretion of CQ and HCQ are stereoisomer specific. The (R)-stereoisomer of CQ is excreted more slowly than the S-stereoisomer<sup>250</sup>. The renal clearance of HCQ has been calculated as 96 mL/min, with an elimination half-life of 1200 hours, whereas the renal clearance for CQ is 129 mL/min, with an elimination half-life of 288 hours<sup>250-252</sup>. The differences in renal clearance and half-life could be critical parameters in defining dosing regimens as anti-neoplastic agents.

The extensive tissue distribution of chloroquine and hydroxychloroquine is a desirable attribute as an anti-neoplastic agent and could be efficacious in a variety of tissue types. Quinidine, CQ, and HCQ pass Lipinski's "Rule of 5" for qualitatively



assessing the likelihood of oral drug absorption or permeation<sup>253</sup>. Lipinski's Rule of 5 is based on physio-chemical characteristics of the compound. A drug is highly likely to be absorbed or permeate biomolecular membranes if: the relative molecular mass ( $M_r$ ) is <500, the octanol-water partition coefficient ( $\log P$ ) is <5 (indicating lipophilicity), there are <5 hydrogen bond donors, or <10 hydrogen bond acceptors (nitrogen and oxygen atoms)<sup>253,254</sup>.

### **Chloroquine metabolism and excretion**

A high likelihood of drug absorption and permeation are essential for distribution within non-vascularized tissue compartments such as breast duct epithelium. Chloroquine excretion in breast milk indicates that it does indeed accumulate in breast duct epithelium thus supporting its use in breast cancer and DCIS<sup>10,11,255,256</sup>. Chloroquine metabolism occurs in hepatocytes via the cytochrome P450 monooxygenase family<sup>244,257,258</sup>. Chloroquine undergoes de-alkylation to form the major metabolite, desethylchloroquine, which has a similar half-life as chloroquine<sup>244,259,260</sup>. Human liver microsomes studies, HPLC/MS, and chemical inhibition studies identified CYP2C8, CYP3A4 as the major cytochrome oxidases responsible for chloroquine metabolism. CYP2D6 is also involved, but to a lesser extent<sup>257,260</sup>. Tamoxifen metabolism also occurs through the cytochrome P450 oxidases. Tamoxifen is metabolized by CYP2D6 enzymes to endoxifen, which also possesses potent anti-estrogen activity<sup>261</sup>. An important consideration for combinatorial therapy is competitive inhibition of CYP2D6 by chloroquine<sup>260</sup>.

Our preliminary data showing that chloroquine did not induce further genetic instability, and the chemical and biochemical literature suggests that chloroquine would

be an ideal drug for treating DCIS, we explored the effects of chloroquine on signal transduction, and invasion and migration.

## **Materials and Methods**

### **Chloroquine treatment of organoid cultures**

Autophagy was inhibited in organoid cultures by treating cultures with chloroquine diphosphate (CQ) (50  $\mu$ M; Sigma) in serum free DMEM/F12 medium supplemented with human recombinant EGF (10ng/mL; Cell Signaling Technology), insulin (10 $\mu$ g/mL), streptomycin sulfate (100 $\mu$ g/mL) and gentamicin sulfate (20 $\mu$ g/mL; Sigma), with or without 0.36% (v/v) murine Engelbreth-Holm-Swarm (EHS) derived, growth factor reduced, basement membrane extract (Trevigen) at 37°C in a humidified 5.0% CO<sub>2</sub> atmosphere. CQ-containing medium was replaced three times per week for a period of 6 months. Comparable untreated control cultures were maintained in identical medium lacking chloroquine with similar media changes. Chloroquine is water soluble therefore the untreated culture served as the vehicle control.

### **Invasion/migration assay**

The *in vitro* scratch assay for cell migration was performed to compare cell migration and invasion response after chloroquine exposure. Cells were maintained in culture with serum-free DMEM/F12+ factors medium at 37°C, 5% CO<sub>2</sub>, in a humidified environment during prior to, and after, the scratch was made. Matching cultures from the same patient (09-118, atypical ductal hyperplasia) (Table 1), with phenotypically similar epithelial cell outgrowths, were selected for the scratch assay. The CQ treated flask was pre-treated with 50 $\mu$ M chloroquine phosphate (Sigma) for 2 days prior to the scratch assay. A total of 5 scratches in each patch of epithelial cells were made using a sterile

20 $\mu$ L pipette tip. The media was replaced with fresh DMEM/F12+ factors to remove the dislodged cells. The cultures were observed with an inverted microscope (20x objective) 2, 7, 24 and 96 hours after the scratches were made.

### **Reverse Phase Protein Microarray**

Cell procurement and lysis was performed as described in Chapter 3. RPMA construction, staining, and analysis was also performed as described in Chapter 3.

### **Immunohistochemistry**

FFPE tissue blocks of canine mammary lesions, representing normal, atypical, DCIS and invasive cancer were kindly provided by Dr. Sulma Mohammed, Purdue University<sup>262</sup>. Tissue sections were cut at 5 $\mu$ M and IHC was performed as described in Chapter 3.

### **Statistics**

Standard deviation (SD) or standard error of the mean (SEM) was calculated for small group comparisons. The Student t-test, two tailed with Welch's correction, was used to calculate the p-value, and to determine the statistical difference of epithelial outgrowth area before and after CQ treatment and spheroid generation. P values <0.05 were considered significant (GraphPad Prism ver 5.03, GraphPad Software). Wilcoxon rank sum was used to determine the differences between CQ treated and untreated groups for the reverse phase protein arrays (R, SAS Institute). A p=0.1 was considered different for small sample sizes.

## Results

### Autophagy is required for emergence and survival of DCIS tumorigenic spheroid cells

Epithelial cells with their associated spheroids were maintained in culture, then treated with chloroquine phosphate (50  $\mu$ M) for 4 days. The cells were harvested pre and post chloroquine treatment for RPMA analysis. Chloroquine markedly inhibited autophagy associated proteins as shown by a reduction in autophagy induction proteins (Atg5 and APMK $\beta$ 1 Ser108), adhesion proteins (E-Cadherin, Laminin5, Integrin  $\alpha$ 5 $\beta$ 1, FAK Tyr576/577, MMP-9), and proliferation/prosurvival proteins (BAK, C-RAF Ser338, p38 MAPK Thr180/Tyr182) (Wilcoxon  $p=0.1$ ) (Figure 25)<sup>10</sup>.

Chloroquine suppressed outgrowth of DCIS epithelial cells in culture as measured by the diameter of the outgrowth and number of spontaneously generated spheroids (Figure 25). Two axis diameters were measured for multiple organoids for two cases.

The mean diameter of case 09-148-A outgrowth prior to treatment (open circle) was 0.85cm $\pm$ 0.11 (n=15, mean  $\pm$ SEM) and after chloroquine treatment (black circle), the mean diameter was 0.084cm $\pm$ 0.03 (n=23, mean  $\pm$ SEM) ( $p<0.0001$ ). In the second series of organoid cultures, the mean diameter of case 09-148-B outgrowth prior to treatment (open triangle) was 1.36cm $\pm$ 0.25 (n=8, mean  $\pm$ SEM) while the chloroquine treated outgrowth (black triangle) mean diameter was 0.21cm $\pm$ 0.03 (n=7, mean  $\pm$ SEM) ( $p=0.0026$ ). In the untreated cultures (open circle, case 09-148) ranged from 1 to more than 100 for individual duct fragments (mean of 38.7 $\pm$ 11; n=14, mean  $\pm$ SEM). Following chloroquine treatment, 12 out of 14 explants did not have any spheroids (mean number of spheroids post treatment 0.21 $\pm$ 0.15; n=14;  $p=0.0049$ , black circle, mean  $\pm$ SEM). For case

09-301, the mean number of spheroids prior to treatment was  $20.5 \pm 7.8$ ,  $n=14$  (open triangle, mean  $\pm$ SEM) and there were no spheroids observed after treatment ( $n=3$ ; black triangle, mean  $\pm$ SEM). D) DCIS organoid in the presence of chloroquine for 2 weeks showed complete absence of cellular outgrowths and degenerated cells within the duct (arrow 10x magnification)<sup>10</sup>.

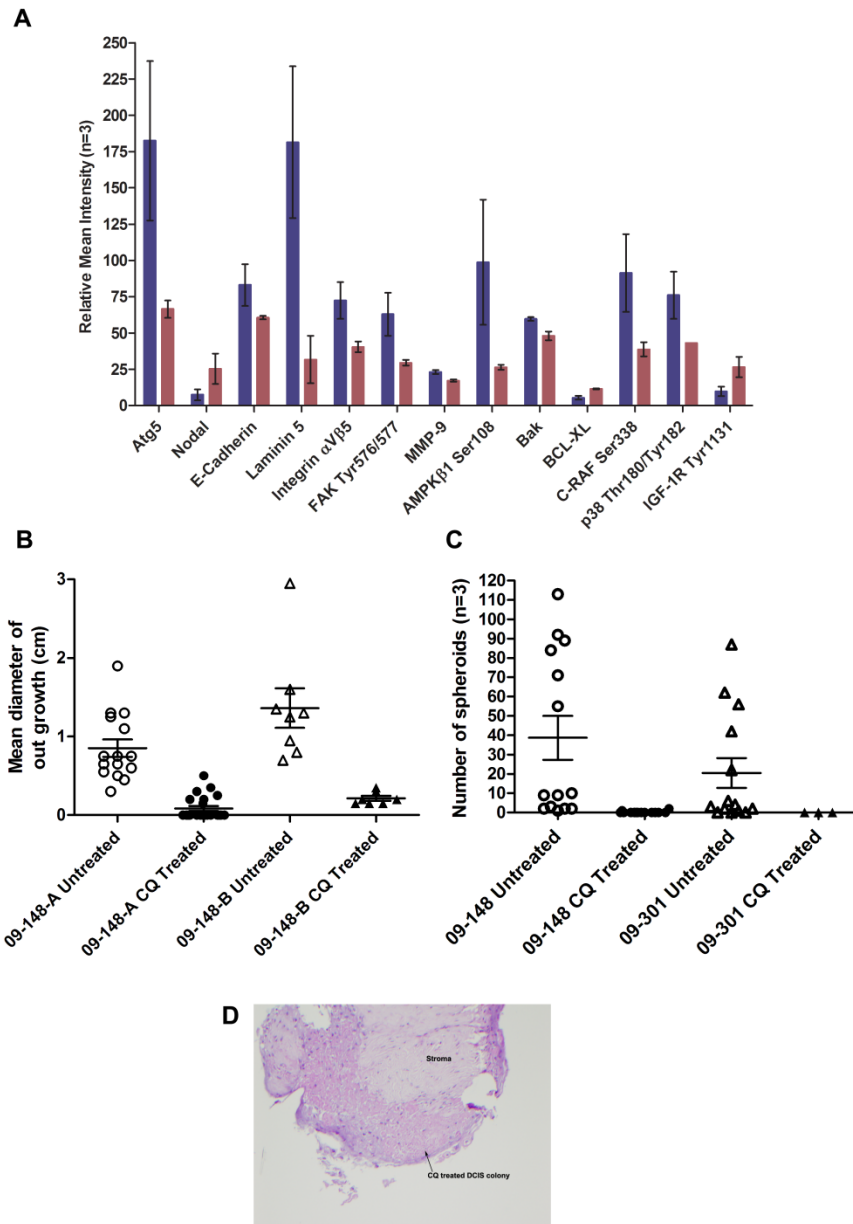


**Figure 25. Chloroquine alters signal transduction pathways, suppresses DCIS neoplastic cell outgrowth, and spheroid formation.**

A) Chloroquine markedly inhibited autophagy associated pathways as shown by a reduction in autophagy pathway proteins (Atg5 and APMK $\beta$ 1 Ser108), adhesion proteins (E-Cadherin, Laminin5, Integrin  $\alpha$ 5 $\beta$ 1, FAK Tyr576/577, MMP-9), and proliferation/prosurvival proteins (BAK, C-RAF Ser338, p38 MAPK Thr180/Tyr182) (Wilcoxon  $p=0.1$ ) (blue=untreated, red=chloroquine 50 $\mu$ M;  $n=3$ ,  $\pm$ SEM). B) The mean diameter of cellular outgrowths was significantly decreased with CQ treatment. C) Chloroquine significantly diminished the number of spheroids in culture<sup>10</sup>.

### **Chloroquine inhibits xenograft tumor formation**

To assess the ability of chloroquine treatment to prevent invasion, chloroquine treated breast epithelial cells were injected into the mammary fat pad of NOD SCID mice (see Chapter 2 for details of injection). Following treatment of the organoid cultures with 50 $\mu$ M chloroquine diphosphate, epithelial cells, and any remaining spheroids, were harvested for transplantation. 0/7 chloroquine treated samples formed a measurable xenograft tumor (Table 8)<sup>10</sup>. Sample 08-352 and 09-148 were highly tumorigenic using untreated cells, however these same cultures failed to induce tumors following chloroquine treatment (Table 2).

**Table 8. Mouse xenograft characteristics for chloroquine treated tissue implants.**

<b>Mouse DOB</b>	<b>NOD SCID Mouse Vendor</b>	<b>Date of Implant</b>	<b>Mouse ID</b>	<b>Chloroquine Treated Tissue ID/Tissue Type/Histology</b>	<b>Xenograft Tumor Formation</b>
3/16/2009	Harlan	05/13/09	<b>172</b>	08-352 cell culture +CQ	No
3/16/2009	Harlan	05/13/09	<b>176/174</b>	08-352 cell culture +CQ	No
4/13/2009	Harlan	06/08/09	<b>580</b>	09-118 spheroids+epithelial cells+CQ	No
4/13/2009	Harlan	06/08/09	<b>583</b>	09-118 spheroids+epithelial cells+CQ	No
7/10/2009	Harlan	08/26/09	<b>679/778/788</b>	09-148 cell culture +CQ	No
7/10/2009	Harlan	08/26/09	<b>791</b>	09-148 cell culture +CQ	No
10/9/2009	Harlan	12/01/09	<b>473</b>	09-118 cell culture +CQ	No

### **Chloroquine inhibits autophagy associated pathway proteins**

Many signal transduction proteins involved in maintaining autophagy also promote cell growth and proliferation. Autophagy and proliferation pathway proteins, phospho-AKT, phospho-mTOR, phospho-IRS-1, phospho-ERK 1/2 and phospho-p38 were suppressed by chloroquine of the DCIS epithelial cell culture. In contrast,

chloroquine treatment increase levels of cleaved PARP Asp214 suggesting that inhibition of autophagy can promote apoptosis in DCIS cells that rely on autophagy for survival.

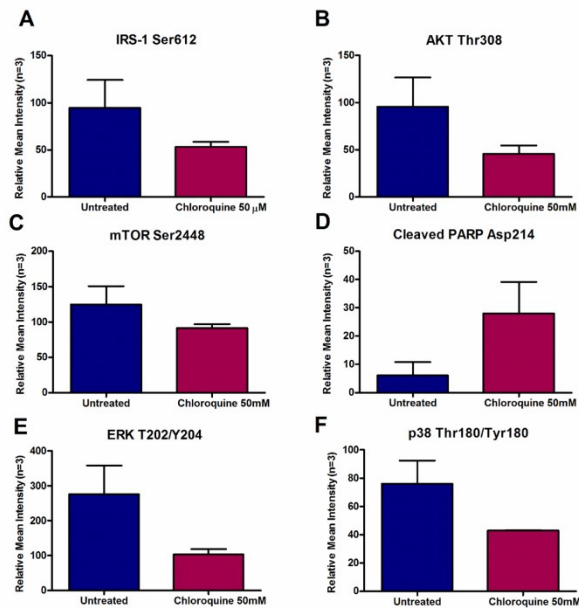


**Figure 26. Chloroquine increased levels of the apoptotic protein cleaved PARP Asp214 in human DCIS cultured cells and suppressed levels of proliferation associated proteins (n=3, mean ±SEM).**

An important source of cellular stress in breast epithelium is the intracellular accumulation of calcium<sup>263,264</sup>. Insoluble calcium induces autophagy<sup>53</sup>. Export of calcium occurs via plasma membrane calcium-ATPase isoform 2 (PMCA2) in myoepithelial cells. In a PMCA2-null mouse model, mammary epithelium underwent apoptosis due to the inability to export calcium<sup>38,265</sup>. Two major DCIS survival mechanisms are 1) the up-regulation of autophagy, and 2) the enhanced export of calcium via plasma membrane PMCA2 efflux pumps. To evaluate whether PMCA2 and autophagy are concurrently up-regulated in cultured human DCIS malignant progenitor cells compared to breast



epithelium, and in human pre-invasive breast lesions, we used RPMA to quantify levels of PMCA2 and LC3B in cells from human DCIS cultures (Figure 27).

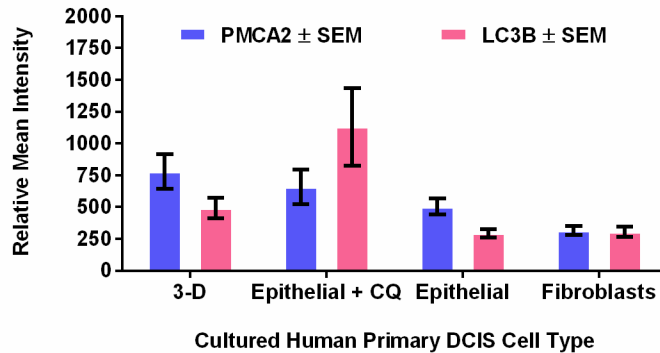
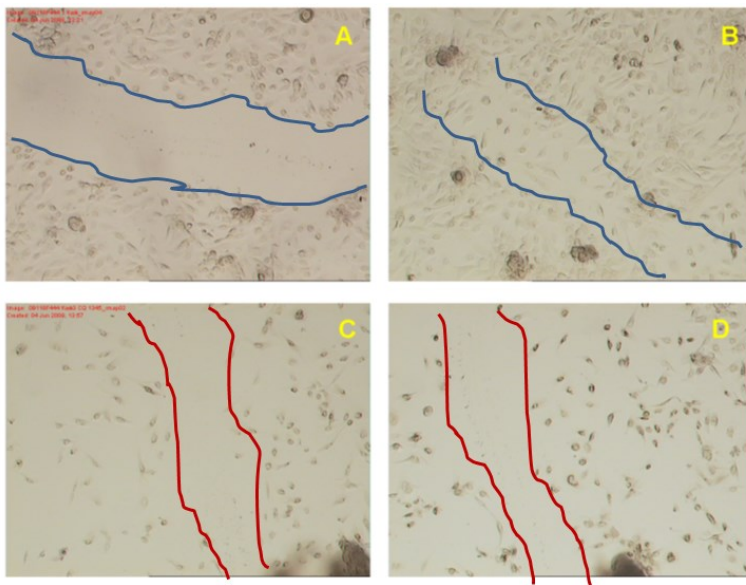


Figure 27. Calcium export protein, PMCA2, is strongly expressed in cultured DCIS malignant progenitor cells.

### **Chloroquine treated cells fail to elicit a wound healing response *in vitro***

Breast epithelium is remodeled by infiltrating macrophages during normal involution cycles. Involution and invasion during carcinogenesis are types of injuries involving inflammation, cell migration, and tissue remodeling. Thus a drug that blocks cell migration or reduces the inflammatory response within the breast epithelium may show efficacy at reducing invasion. To test the migratory capacity of the epithelial cells in organoid culture with or without chloroquine treatment, an *in vitro* scratch assay was performed<sup>266</sup>. Flask #1 (untreated) contained a 19x29mm epithelial cell patch with 566 spheroids prior to the scratch assay. Flask #3 (CQ treated) contained a 16 x16mm epithelial cell patch with 319 spheroids. Chloroquine treated cells exhibited a 35% reduction in spheroids after 4 days in culture (319 spheroids Day 0, 208 spheroids Day

4), indicating the chloroquine permeated the cells. The untreated flask had a slight, but insignificant, increase in total spheroid numbers after 4 days (566 spheroids Day 0, 574 spheroids Day 4). The untreated flask showed complete migration across the scratch zone after within 24 hours (Figure 28 B), whereas the chloroquine treated cells failed to migrate into the scratch area (Figure 28 D). The failure to elicit a migration response in the wound healing assay indicates that chloroquine may prevent invasion *in vivo* (Figure 29).



**Figure 28. Migration assay in organoid culture.** An *in vitro* scratch assay was used to assess effects of chloroquine on cell migration. A) Sample 09-118 untreated, Day 0. B) Sample 09-118 untreated, 24 hours post wounding. C) Sample 09-118 chloroquine treated, Day 0. D) Sample 09-118 chloroquine treated, 24 hours post wounding.

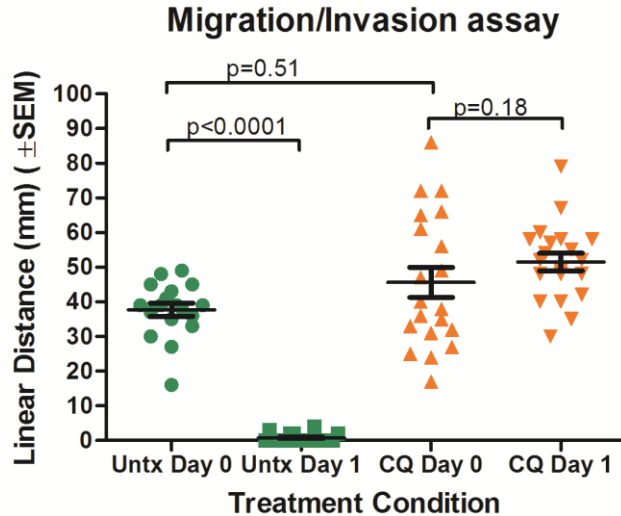
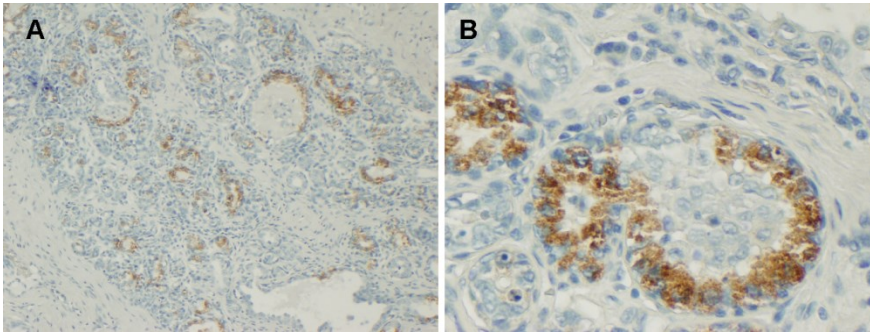


Figure 29. Chloroquine prevented invasion/migration in an *in vitro* scratch assay.. Linear distance across the scratch was measured at 5 different points for case 09-118, (green=untreated, orange=chloroquine treated).

### Autophagy is induced in a canine model of DCIS

The natural progression of breast cancer in dogs follows very similar stages to human breast cancer<sup>262</sup>. Canine breast cancer risk factors are also similar to human reproductive risk factors. To investigate the role of autophagy in canine preinvasive lesions, we performed IHC for autophagy pathway proteins (Figure 30). LC3B was elevated in the canine tissues with ADH and DCIS, with patterns mimicking human breast lesions. Canine models of breast cancer may provide a more robust representation of human breast cancer than the mouse model.



**Figure 30. LC3B immunohistochemistry indicates up-regulation of autophagy in a canine model of breast cancer.**

**A) Atypical Ductal Hyperplasia (10x magnification). B) DCIS (20x magnification).**

## Discussion

### Cellular energy alterations during autophagy

As shown in Chapter 2, *ex vivo* culture systems for DCIS tissue provide a means for monitoring therapy efficacy at the level of molecular signaling from *ex vivo* cultured breast organoids. This system demonstrates that anti-autophagy treatment reduces the invasive potential of DCIS progenitor cells *ex vivo*, in cultured human organoids providing rationale for using Chloroquine as a neoadjuvant therapy for DCIS<sup>9-11</sup>.

Cancer cells adapt to their hypoxic, nutrient depleted microenvironment by switching from aerobic respiration to glycolysis (Warburg effect)<sup>229,230,267</sup>. Autophagy has been shown to induce surges of ATP in cultured glioma cells treated with etoposide thus promoting cell survival<sup>268</sup>. Conversely, surges in ATP levels could be detrimental to cell homeostasis due to increasing levels of reactive oxygen species and on-set of inflammation<sup>170,171</sup>. Autophagy itself is dependent on ATP concentrations as well as amino acid concentration<sup>269</sup>. Autophagosome formation requires an energy dependent sequestration step, in which intracellular components are recruited to form the double-

membrane vesicle, and operation of the lysosomal proton pump utilizes available ATP to redistribute lysosomal contents to the cell membrane<sup>269</sup>. Sustained up-regulation of autophagy may not be able to support continuous high levels of ATP production *in vivo*. But how does the cell decide which pathway/biochemical process should receive this limited supply of ATP? How does a cell decide which proteins should be ubiquitinated and targeted to the lysosome? Initial quantitative proteomic analysis of protein dynamics during starvation induced autophagy in MCF7 breast cancer cell lines suggested that free cytosolic proteins are degraded first, followed by tRNA synthetases, with ribosomal proteins degraded at a later time point<sup>270</sup>. Mitochondrial and nuclear proteins appeared to be degraded last. Interestingly, ER membrane and splicesomal proteins were not found to be degraded during the 36 hour time course<sup>270</sup>. Molecular pathway annotations revealed that purine/pyrimidine metabolism proteins were in the group of proteins degraded at early time points post autophagy induction<sup>270</sup>.

### **Effects of ATP and nucleotide depletion on chromosomal stability**

Higher eukaryotes appear to expend a large amount of energy on maintenance of the genome based on the number of active ATPase proteins involved in DNA repair and chromatin remodeling<sup>165,271-273</sup>. DNA damage can be repaired by four mechanisms: nucleotide excision repair (NER), base excision repair (BER), homologous recombination (HR) and non-homologous end joining (EJ)<sup>274</sup>. NER and BER repair single strand DNA breaks or in the case of BER, replace mismatched purines/pyrimidines. Double strand breaks are more problematic because the ends are “sticky” and can readily bind to alternate DNA sequences. Homologous recombination

occurs in S and G<sub>2</sub> phase when the sister chromatid is present. Non-homologous end joining repair is more error-prone and occurs in mainly in G<sub>1</sub> phase. Although cells have evolved DNA repair mechanisms, it comes with an energy cost: DNA ligase enzymes use ATP to covalently form a ligase-adenylate intermediate<sup>271</sup>. Subsequent steps transfer AMP to another intermediate and the non-adenylated DNA ligase catalyzes phosphodiester bond formation with release of AMP<sup>271</sup>. Human DNA ligase complex IV/XRCC4, a non-homologous end joining (NHEJ) enzyme, was shown to catalyze only a single ligation reaction whether or not ATP was available<sup>271</sup>. This single reaction ligation limitation suggests that non-homologous end joining may occur in strict stoichiometric ratios with the amount of adenylated DNA ligase IV/XRCC4 molecules unless there is a mechanism to reactivate the ligase complex<sup>271</sup>.

Double strand breaks create genetic instability by translocating with neighboring chromosomes. Tobin *et al* recently demonstrated that MCF7 breast cancer cell lines (derived from DCIS) have lower levels of DNA ligase IV with concomitant increased levels of DNA ligase III $\alpha$ <sup>273</sup>. In addition they found that estrogen/progesterone receptor negative cell lines and tamoxifen resistant MCF7 lines possessed significantly higher levels of DNA ligase III $\alpha$ , suggesting dependence on the non-homologous end joining for DNA repair. Dependence on the error prone NHEJ mechanism could account for accumulation of chromosomal deletions in this cell line model<sup>273</sup>. Further evidence that autophagy may affect genetic stability can be inferred from experiments in which 50% of DNA repair events were due to errors in homologous recombination<sup>275</sup>.

Minor DNA mutations and alterations in chromosome structure and number reflect chromosomal instability<sup>276</sup>. Cancer cells with chromosomal instability propagate this instability to daughter cells. LOH on chromosome 18q was observed to frequently cause chromosomal instability in colon cells during the transition from adenoma to carcinoma. Loss of *PIGN*, *MEX3C* and *ZNF516* result in slow replication or stalling of the replication fork<sup>276</sup>. Intriguingly, addition of nucleosides to the colon cancer cell lines attenuated the chromosomal segregation errors<sup>276</sup>.

Zhang *et al* have recently demonstrated that proper nucleosome positioning, spacing and occupancy at the 5' ends of *Saccharomyces cerevisiae* genes requires ATP dependent trans-acting factors<sup>277</sup>. Regulatory elements such as promoters and enhancers reside in the 5' ends thus suggesting that alterations in ATP could potentially affect interactions between regulatory elements and their cognate transcription factors.

Bloom syndrome, characterized by early on-set cancers, is due to mutations in the BLM gene which encode RecQ helicase. In addition to defects in DNA replication, Chabosseau *et al* recently described a reduction in cytidine deaminase and pyrimidine pool imbalances in BLM deficient cells<sup>278</sup>. Restoration of the pyrimidine pool restored replication fork velocity and maintained appropriate homologous recombination<sup>278</sup>. Both these examples support the data showing restoration of a more “normal” molecular karyotype in the cultured DCIS cells over time as they became less dependent on autophagy for survival due to the presence of abundant nutrients and oxygen in culture (Figure 20).

### **Chloroquine for chemoprevention of invasive breast cancer**

From a pharmacology perspective CQ and HCQ are attractive agents because they have outstanding oral bioavailability and there is abundant preclinical data supporting their anti-cancer efficacy: CQ and HCQ a) rapidly diffuse across biomembranes to partition into acidic subcellular vesicles, such as lysosomes<sup>244</sup>, b) interfere with cytoprotective autophagy<sup>166</sup>, c) function as weak DNA intercalating agents<sup>189,190</sup>, d) specifically induce differentiation of tumor/progenitor cells while sparing normal cells<sup>279,280</sup>. More importantly, chloroquine and hydroxychloroquine are well-tolerated with a known safety and toxicity profile based on their widespread use as anti-malarial and anti-rheumatic agents<sup>244</sup>.

Re-purposing chloroquine as an anti-neoplastic agent capitalizes on its broad physiological and biochemical effects which do not depend on a specific molecular target<sup>191,244,247</sup>. Three different approaches are currently being evaluated in Phase I/II clinical trials. The first approach utilizes either chloroquine or hydroxychloroquine as a component of combination therapies to augment molecularly targeted drug efficacy and/or mitigate acquired drug resistance. The second approach involves enhancement of radiotherapy (radiation sensitization) following chloroquine or hydroxychloroquine administration. Chloroquine is a potentiating agent in these first two scenarios<sup>157</sup>. The third approach, presented herein, uses a short course of chloroquine as a neoadjuvant/chemopreventive agent for pre-invasive breast lesions<sup>9-11,157</sup>.



## CHAPTER 6: EFFICACY OF CHLOROQUINE TO TREAT DCIS IN A PHASE I/II CLINICAL TRIAL

### Introduction

#### Rationale for a new clinical trial strategy

A clinical trial provides the ultimate demonstration of safety, efficacy, and comparable treatment outcomes for any new or repurposed drug. National Comprehensive Cancer Network (NCCN) guidelines for DCIS work-up and treatment were formulated based on the results of prospective and retrospective clinical trials (summarized in the review by Boughey *et al*<sup>281</sup>). Current NCCN work-up guidelines recommend history and physical examination, diagnostic bilateral mammogram, tumor pathology review, and tumor estrogen receptor (ER) status, with optional breast MRI or genetic counseling for high risk patients<sup>45</sup>. Treatment guidelines recommend lumpectomy with whole breast radiation or mastectomy with or without sentinel node biopsy<sup>45</sup>. Risk of recurrence is multifactorial. DCIS grade (low, intermediate, high), DCIS size (localized to one breast quadrant or extending into multiple quadrants), surgical margin width, and patient age impact recurrence risks<sup>7,282</sup>. High grade, DCIS in more than one breast quadrant, surgical margins <2mm, and age <50 years may elevate the recurrence risk<sup>45</sup>. However even these guidelines are not without controversy due to conflicting retrospective studies and meta-analyses which suggest that: a) surgical margins <2mm do not increase local DCIS recurrence, and b) wide surgical margins do not reduce

recurrence risk if patients also receive radiation with breast conserving surgery<sup>45</sup>.

Furthermore, administration of tamoxifen as a postsurgical therapy to reduce the risk of ipsilateral breast recurrence is only effective for patients with ER positive DCIS<sup>45</sup>.

Therefore a Phase I/II clinical trial was initiated using chloroquine phosphate as a short-term, low toxicity therapy for DCIS regardless of hormone receptor status<sup>9,11</sup>.

The strategy for using chloroquine as neoadjuvant therapy for DCIS is derived directly from data shown in chapters 2-5 which revealed that a) invasive DCIS progenitor cells could be harvested, for the first time, directly from patient DCIS lesions, b) the autophagy pathway was up-regulated in human DCIS lesions, c) chloroquine phosphate inhibition of autophagy abolished survival of DCIS neoplastic cells in culture and xenograft models, and d) chloroquine treatment of cultured organoids did not induce additional genetic variation in the mammary epithelial cells from the source patient<sup>10</sup>.

DCIS might never progress to an invasive breast carcinoma, therefore any DCIS treatment must be of low general toxicity. Chloroquine has been used for decades for the treatment of malaria, rheumatoid arthritis, and lupus<sup>257,283,284</sup>. The attributes of chloroquine for augmentation of cytotoxic activity when used in combination with standard anti-neoplastic agents have also been recently documented in human studies of glioblastoma multiforme and melanoma<sup>247,285,286</sup>. Chloroquine is ideally suited for a short-term chemoprevention clinical trial because it is an oral, low cost, clinically well-studied compound, with an acceptable safety profile.

A clinical trial evaluating the safety and efficacy of neoadjuvant chloroquine treatment for patients with DCIS provides multiple paradigms for breast cancer treatment

and prevention. Firstly, the trial provides safety information regarding chloroquine use in the DCIS patient population. Secondly, the unique trial design provides efficacy data for short-term treatment regimens. Unlike typical cancer prevention trials which require that new cancer-preventive drugs must first be shown to be efficacious in reducing cancer incidence or mortality and have proven safety for long-term administration, this trial design assesses efficacy in each patient by comparing pathological parameters before and immediately after treatment<sup>287</sup>. Thirdly, short-term treatment does not expose patients to potential toxicities of chronic chloroquine administration, whereas typical chemoprevention trials evaluate long-term exposure to cancer-preventive drug regimens. Finally, chloroquine targets the entire breast epithelial field rather than a specific cell population, genetic mutation, or functional phenotype that may or may not be driving proliferation of DCIS cells<sup>288</sup>.

Therapy that prevents progression to invasion or induces regression of occult or overt premalignant lesions could constitute an efficient chemoprevention agent that blocks the subsequent emergence of overtly invasive, metastatic breast cancer without the need for validating biomarkers predictive of progression and/or recurrence. Therefore, treating DCIS with chloroquine constitutes a potential shortcut to the realization of a general chemoprevention strategy for all breast cancer.

### **Preventing Invasive Neoplasia with Chloroquine (PINC) trial**

The PINC trial is an ongoing clinical study (clinicaltrials.gov identifier NCT01023477) (Figure 31) examining the safety and effectiveness of chloroquine phosphate (Aralen; Sanofi-Aventis, NJ) administration for a one month period to patients

with low, intermediate, or high grade DCIS regardless of hormone receptor status (Figure 31)<sup>11</sup>. Chloroquine is known to rapidly enter the lysosomal compartment of cells and remain detectable in the plasma for up to 23 days<sup>149,251,252,257</sup>. Chloroquine and hydroxychloroquine are excreted in human milk thus supporting the use of these agents in breast disease<sup>255,256</sup>. Although the reported concentration-fold differences between milk and blood vary, the milk concentration of chloroquine is greater than that of plasma or whole blood indicating that, at least during lactation, sufficient quantities of chloroquine enter the breast lumen<sup>255,256</sup>.

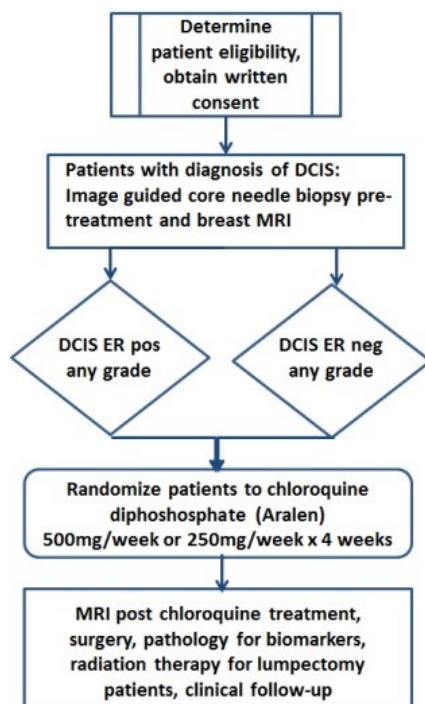


Figure 31. PINC trial design.

Chloroquine diphosphate (Aralen) neoadjuvant therapy is being evaluated for all grades of estrogen receptor positive and estrogen receptor negative breast DCIS lesions (Adapted from Women’s Health, March 2013, Vol. 9, No. 2, Pages 157-170 with permission of Future Medicine Ltd<sup>11</sup>).

Patients with DCIS who are ER negative (expected to be approximately one half of the high grade DCIS cases) or who are ER positive, are eligible for the neoadjuvant trial. Patients, regardless of histologic grade, are randomized to receive chloroquine at one of two doses: 500 mg/week, or 250 mg/week, for four weeks<sup>11</sup>. MRI studies are performed on each patient at enrollment and just before surgical therapy following one month of Aralen treatment. Each group of 10 patients is randomized to the chloroquine doses to allow statistical analysis at incremental accrual rates, as well as at the conclusion of the trial. At the completion of the one month treatment period, all patients receive standard of care surgical therapy: mastectomy or lumpectomy depending on the size and confluence of the primary DCIS lesion<sup>45</sup>. The PINC trial design takes advantage of the typical waiting period between the initial pathologic diagnosis of DCIS and the subsequent surgical therapy. Based on anecdotal patient feedback, 4 weeks is an acceptable timeframe for neoadjuvant therapy without contributing excess emotional distress.

Outcome measures, assessed by comparing the pre-treatment and post-treatment specimens, include: a) reduction in DCIS lesion volume by MRI, b) pathologic regression, c) the reduction or elimination of genetically abnormal tumorigenic DCIS stem like cells, d) and the suppression of cellular proliferation, induction of apoptosis, or disruption of autophagy, as measured by changes in proteomic markers in the post treatment versus the pre-treatment specimen<sup>11</sup>. Molecular measures of efficacy in the pre-versus post-treatment lesion include: a) a reduction in proliferation index by IHC using PCNA or Ki-67, b) an increase in apoptosis index by IHC using cleaved PARP and

activated caspases, and c) disruption of autophagy by IHC using LC3B staining of autophagosomes<sup>9-11</sup>.

Each patient serves as her own control, because therapy efficacy is based on a comparison of the pre-treatment versus post-treatment specimen for each patient.

Additional control patients include females with a diagnosis of DCIS undergoing similar surgical procedures (diagnostic biopsy, followed by lumpectomy or mastectomy) at the same institution. These surgical controls provide an assessment of the effects of the diagnostic biopsy procedures and surgical preparation of the patient on the induction of autophagy in the *in vivo* lesion. In addition, the control cohort provides a comparator for reduction in lesion volume judged by pathological response.

In the neoadjuvant trial design, the DCIS lesions are evaluated radiologically before therapy at the time of diagnostic biopsy, and then again, after therapy, prior to surgical standard of care excision of the neoplasm (Figure 32).

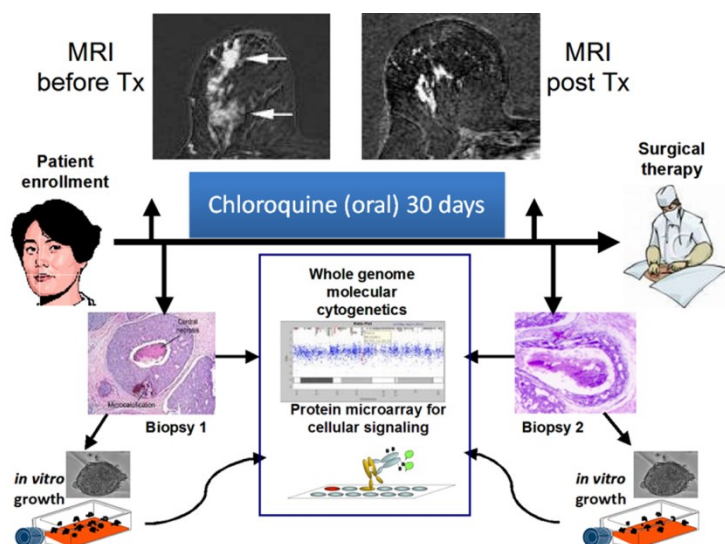


**Figure 32. PINC trial workflow.**

Patients receive an MRI at diagnosis, prior to initiating Aralen treatment. A Second MRI is performed following completion of the 4 week Aralen regimen. Proteomic cell signaling cascades and whole genome molecular cytogenetics are analyzed from the surgical samples and the organoid cultures.

Radiologic measurement of efficacy is based on standard RECIST (Response Evaluation Criteria In Solid Tumors) criteria<sup>289</sup>. Tumor shrinkage is an important endpoint in phase II trials for screening new agents or validating efficacy of off-label agents for anti-tumor effects. Tumor regression measurements are supported by years of evidence in solid tumors showing that tumor shrinkage has a reasonable chance of demonstrating improvement in overall survival in subsequent phase III trials<sup>289</sup>.

The PINC trial design can be modified to test other potential therapies, alone or in combination with CQ. Thus, the PINC trial scheme provides a template for evaluating monotherapy or combination therapies that can be documented to kill or suppress DCIS lesions following short-term therapy.

## **Methods**

### **Patient recruitment and tissue collection**

Patients with a suspected or confirmed diagnosis of DCIS based on mammography/core needle biopsy, and meeting the inclusion criteria, are enrolled in the trial following written informed consent under the institutional review board approved protocol. Control patients are females >18 years of age undergoing similar breast surgical procedures, at the same institution, but who have not taken chloroquine (Table 1).

Patients are randomized within groups of ten to Arm 1 (chloroquine 500mg/week x4 weeks), or Arm 2 (250mg/week x 4 weeks). The diagnostic breast core needle biopsy is formalin fixed and processed into paraffin blocks. FFPE slides are evaluated for ER/PR, histologic grade, and morphology at a central laboratory. Recut FFPE slides representing the pre-treatment baseline sample are provided for research purposes.

At the time of surgical treatment, breast tissue is excised and gross pathology assessment is performed following sterile technique. Areas of tissue harboring discernible DCIS lesions are dissected into organoids approximately 3 mm<sup>2</sup>, containing one or more visible duct segments with associated stroma. This tissue is designated as a “research specimen”. At least one organoid is formalin fixed and processed into a paraffin block. The remaining organoids are rinsed briefly in serum-free sterile medium (DMEM/F12, streptomycin sulfate (0.1mg/mL, Sigma) and gentamicin sulfate (0.02 mg/mL, Sigma)), then stored in DMEM/F12 plus antibiotics until the time of culture. The remaining surgical tissue is processed into formalin fixed, paraffin embedded tissue blocks following standard diagnostic procedures. H&E stained sections from the FFPE research sample are returned to the diagnostic pathology department for quality assurance to



confirm absence of microinvasion. Recut FFPE slides from the post-treatment diagnostic surgical specimen are provided for research purposes for comparison with the pre-treatment samples.

### **Ex vivo organoid culture**

Intact organoids, containing one or more discernable duct segments with associated stroma, were grown in 115cm<sup>2</sup> TPP re-closeable flasks (MidSci) in serum free DMEM/F12 medium supplemented with human recombinant EGF (10ng/mL, Cell Signaling Technology), insulin (10µg/mL, Roche), streptomycin sulfate (100µg/mL, Sigma) and gentamicin sulfate (20µg/mL), with or without 0.36% (v/v) murine Engelbreth-Holm-Swarm (EHS) derived, growth factor reduced, basement membrane extract (Trevigen) at 37°C in a humidified 5.0% CO<sub>2</sub> atmosphere. Medium was replaced three times per week. Organoids were submerged in a minimum volume of medium (just enough to cover the duct fragments) to maximize gas exchange. Non-adherent organoids were removed from the culture flask. Periodically, organoids/cells were removed, under microscopic visualization, for propagation into new culture flasks or phenotypic and molecular analysis.

### **Zymography of conditioned medium**

Several organoids from patient PINC6 were distributed in wells of a 24-well culture plate with DMEM/F12+ factors. Conditioned medium (approximately 500µL) was harvested from the *ex vivo* organoid culture for patient #PINC6. The medium was evaporated overnight in a SpeedVac (Thermo) at low heat. The residual medium was reconstituted in Novex 2X SDS tris-glycine loading buffer (Invitrogen) in a ratio of 2:1.

One organoid was removed from the culture well, placed in extraction buffer (T-PER, Novex 2X SDS tris-glycine loading buffer, TCEP) and pulverized. The lysate was heated at 95°C for 5 minutes and cleared by centrifugation at 14,000rpm for 20 seconds.

10µL of the reconstituted conditioned medium was loaded on a 10% Zymogram gel (0.1% gelatin) in individual lanes. 20µL of the organoid lysate was loaded in a single lane. SeeBlue prestained molecular weight marker (Invitrogen) was loaded in lane 1. The samples were separated by electrophoresis for 90 minutes at 125V (constant). The gel was renatured, developed for 4 hours at 37°C, and visualized with SimplyBlue Safe Stain (Invitrogen) following manufacturer's directions, and imaged on a flat bed scanner.

#### **Proliferation Index: Immunohistochemistry**

Immunohistochemistry was performed as described in Chapter 3: Proteomic analysis of DCIS Cells using Envision+ streptavidin-biotin amplification chemistry with diaminobenzidine (DAB) detection. FFPE tissue sections were probed with Ki-67 (Dako clone MIB-1, 1:30, HIER pH9), or PCNA (Dako clone PC10, 1:3,000, HIER pH6), or LC3B (Cell Signaling Technology #3868, 1:25, HIER pH6). Sections were mounted in aqueous mounting medium (Faramount, Dako) with a glass coverslip. Positive stained cells were enumerated by visual examination and manual counting of the total number of cells (nuclei) within a duct and the total number of positive (brown) cells in the same duct. Control tissue sections were stained simultaneously with PINC patient samples as appropriate. The proliferation index was calculated for each patient sample, pre and post-treatment (Equation 2).

**Equation 2. Proliferation Index**

$$\text{Proliferation Index} = (\text{Number of positive cells in DCIS duct} / \text{Total number of cells in DCIS duct}) / (\text{Number of positive cells in normal duct} / \text{Total number of cells in normal duct}) * 100$$

## Results

### Patient enrollment

Eight patients have been enrolled in the study and completed the study treatment since May 2012 (Table 9). No adverse side effects due to Aralen treatment have been reported. Control patients are females, greater than 18 years of age, undergoing surgical therapy, at the same institution, for pathologically confirmed DCIS or ADH (Table 1).

**Table 9. Clinical data for PINC patients enrolled to date.**

<b>Patient ID</b>	<b>ER</b>	<b>PR</b>	<b>Calcifications</b>	<b>Nuclear Grade</b>	<b>Necrosis</b>
PINC 1	Pos	Pos	Yes	Intermediate	Present
PINC 2	Pos	Pos	Yes	Intermediate	Present
PINC 3	Pos	Pos	Yes	Intermediate	Present
PINC 4	Pos	Pos	Yes	Intermediate	Present
PINC 5	Pos	Pos	Yes	Low	Absent
PINC 6	Neg	Neg	Yes	High	Present
PINC 7	Pos	Neg	Intraluminal	Low	Absent
PINC 8	Pos	Pos	Yes	Intermediate	Focal

### Diminished spheroid formation post treatment in *ex vivo* organoid culture

Fresh tissue at the time of surgery was not available for patients PINC1, PINC2, and PINC7. The tissue for patient PINC4 was not processed in a sterile environment.

Despite attempts to rinse the tissue multiple times in antibiotic containing culture

medium, the organoid culture developed bacterial contamination on Day 2 post incubation. The culture was terminated, the tissue was rinsed in antibiotic containing medium, and fixed in 10% neutral buffered formalin for processing into a paraffin block.

Surgical tissue procured following Aralen treatment from patients PINC3, PINC5, PINC6, and PINC8 were processed for organoid culture as described for the pre-clinical tissue samples (Chapter 2: Isolation and Propagation of DCIS progenitor cells). Estrogen supplementation of the culture was not necessary. The culture duration for each PINC patient tissue to date is: PINC3 = 10 months, PINC5 = 7 months, PINC6 = 5 months, and PINC8 = 3 months. Observations regarding cellular outgrowths post Aralen treatment include: a) minimal cellular outgrowth as measured by the radial distance of the cellular outgrowths in two dimensions, b) minimal (<5) spheroid formation per organoid (Figure 33), c) absence of large, complex 3-D cellular structures, d) numerous organoid patches supporting only fibroblast outgrowth rather than mixed epithelial/fibroblast outgrowths, e) asymmetrical outgrowth compared to the untreated pre-clinical controls (Table 10). The data indicate an overall reduced capacity for epithelial cell proliferation following Aralen treatment.

**Table 10. Characteristics of organoid cultures from surgical tissue harvested post Aralen treatment.**

	<u>PINC3</u>	<u>PINC5</u>	<u>PINC6</u>	<u>PINC8</u>
<b># of organoids in culture</b>	11	5	6	8
<b># of cellular outgrowths</b>	10	5	6	6
<b># of outgrowths with epithelial cells</b>	9	3	5	2
<b>largest radial distance (mm) of epithelial cell growth</b>	5	10	1.5	1.5
<b>average radial distance (mm) of outgrowth</b>	2.5	5	1	1

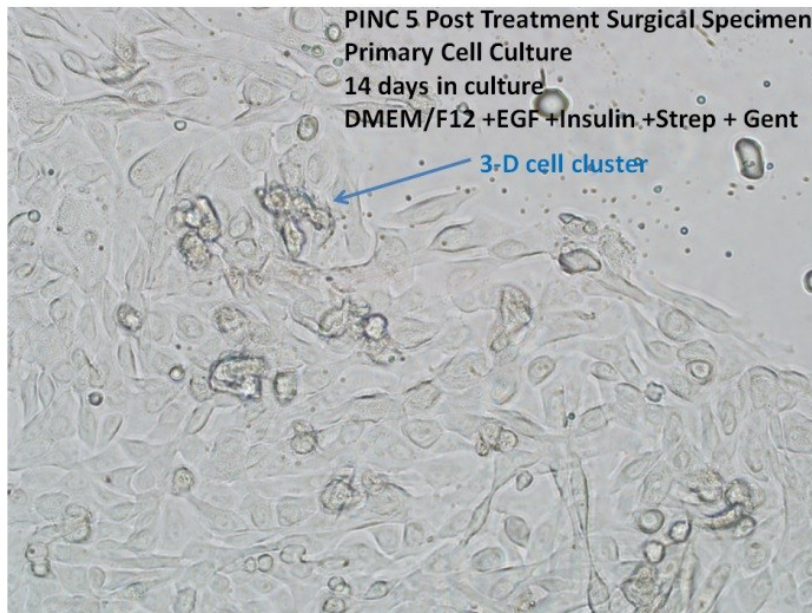


**Figure 33. Lack of extensive 3-D structure formation and spheroid development in the organoid culture following 4 weeks of *in vivo* Chloroquine diphosphate (Aralen) therapy.**

An additional observation noted in the cultures derived from the patients enrolled in the PINC trial was the lack of invasion/migration across the culture flask following cell harvesting. Periodically cells/organoids are harvested from the culture by opening the flask lid and removing populations of cells and some of the surrounding medium for further analysis. As described in Chapter 5, the untreated control cultures exhibit a typical *in vitro* response to wounding, with cells migrating to, and filling-in, the gap (Figure 28). Cell harvesting failed to elicit cell migration into the site devoid of cells in cultures derived from the PINC patients treated with Aralen (data not shown). This demonstrates that chloroquine may inhibit *in vivo* migration as well.

### **Matrix metalloproteinases in organoids and conditioned medium**

Gelatin zymography was used to determine the presence of MMP in the organoids and conditioned medium of the chloroquine treated patients<sup>290</sup>. MMP were present in the conditioned medium from cultures with epithelial cells (epi+), spheroids, and the organoid lysate but were absent from conditioned medium that failed to support any cellular outgrowths in culture and the media only. Lane 12 (cells-) had a large number of epithelial cells but did not have an organoid during the time the conditioned medium was collected. The organoid had been removed for propagation in another well. The zymogram band pattern potentially indicates the presence of activated MMP-2 (65-62kDa) and MMP-7 (28kDa), or possibly MMP-1 (54kDa). Definitive identification of the specific MMP will require further analysis with recombinant MMP standards. This screening zymogram indicates the presence of active MMP, capable of basement membrane degradation, in the conditioned medium and organoids with cellular outgrowths.

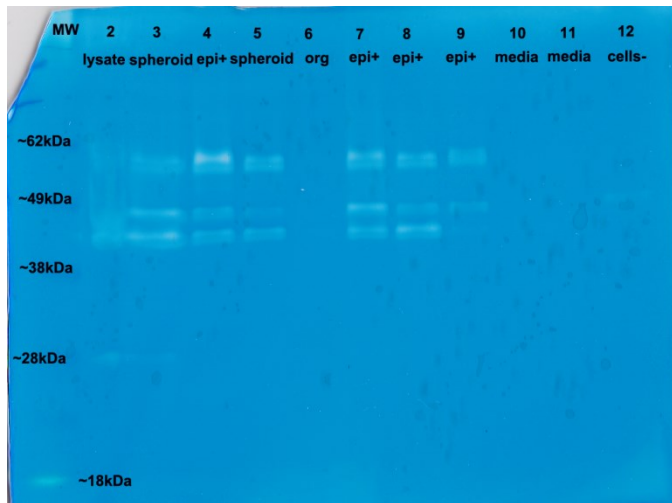


Figure 34. Matrix metalloproteinases are present in conditioned medium harvested from *ex vivo* cultures of patients treated with Aralen for 4 weeks.

Lane 2 lysate was prepared from an intact organoid. Lanes 3 & 5 contained an organoid with spheroids. Lanes 4, 7, 8 & 9 contained an organoid with epithelial cells (no spheroids). Lane 6 did not have any cellular outgrowths from a single organoid. Lanes 10 & 11 were media only controls. Lane 12 contained epithelial cells only. The organoid had been removed several days prior to harvesting the conditioned medium.

### Proliferation index reduction post anti-autophagy therapy

DCIS cells accumulating within the duct require up-regulation of autophagy for survival<sup>10</sup>. Anti-autophagy therapy induces apoptosis *ex vivo* in the cultured tumorigenic DCIS cells, but its effect on the proliferative capacity of the *in vivo* DCIS epithelial cells and stromal cells is unknown. To assess the effect of the 4 week anti-autophagy therapy on the proliferative capacity of DCIS and stromal cells, immunohistochemistry with anti-Proliferating Cell Nuclear Antigen (PCNA) or anti-Ki-67 was performed to calculate a proliferation index (Equation 2. Proliferation Index)<sup>291</sup>.

Formalin fixed paraffin embedded (FFPE) tissue sections for PINC trial patients 4, 6, 7, and 8, plus four treatment control tissues, were probed with anti-PCNA (Dako, clone PC10, 1:3,000) following heat induced antigen retrieval at pH 6 using a streptavidin-biotin method (Envision+, Dako). Residual DCIS tissue in the FFPE sections

was absent or insufficient for staining for PINC patients PINC1, PINC2 and PINC5. PINC3 FFPE tissue sections were probed with anti-Ki-67. Compared to control samples and the pre-treatment tissue, the PCNA proliferation index was significantly ( $p < 0.001$ ) reduced in the *in vivo* DCIS lesions post chloroquine treatment (Figure 35). The proliferation index for each patient's individual DCIS lesion is shown in Figure 36.

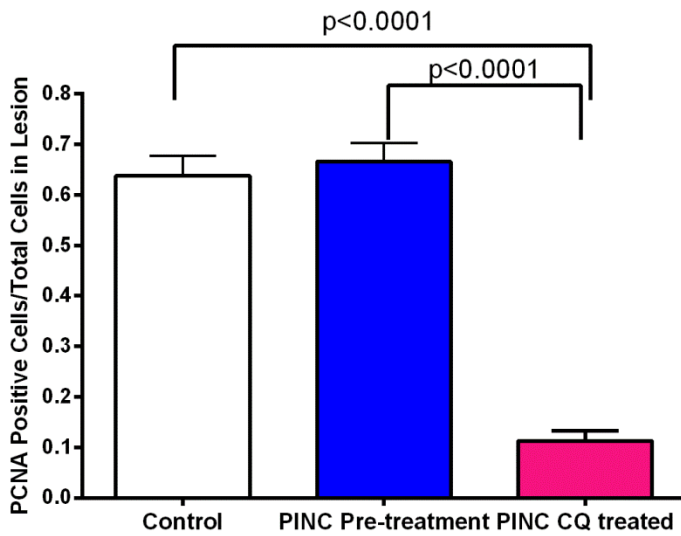


Figure 35. The proliferation index is significantly reduced following a 4 week course of Aralen therapy in patients diagnosed with breast ductal carcinoma in situ.



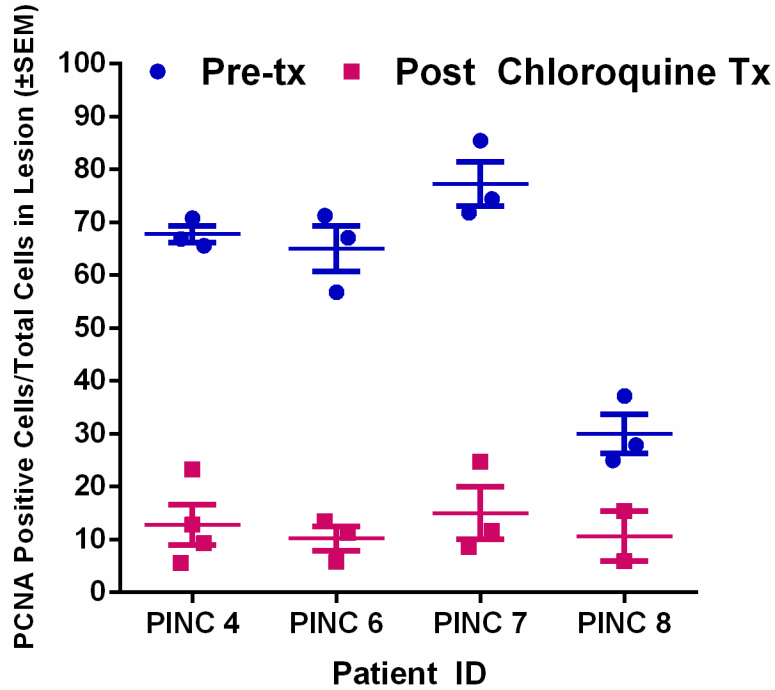


Figure 36. PCNA proliferation index for PINC patients before (blue circles) and after Aralen treatment (red squares).

**Pathologic response: Decrease in DCIS lesion volume**

To demonstrate pathologic response following Aralen treatment, the lesion size documented in the diagnostic biopsy pathology report was compared to the lesion size documented on the surgical (post treatment) pathology report (Table 11). The proliferation index for PINC 3 was calculated with Ki-67 data. All other cases were calculated using PCNA data. In addition, the tissue provided for research was evaluated by H&E staining for the number of DCIS lesions (data not shown).

PINC 6 was described in the pre-treatment pathology report as 5 cm in area by MRI with extensive DCIS extending into the lobules. The post treatment DCIS was estimated as being 3.0 cm in maximum area in the report. PINC 7 had no residual DCIS

per the pathology report. In the research specimen, one small DCIS lesion was present, which was stained and scored for proliferative index. According to the diagnostic pre-treatment report, lesions for PINC 8 had an aggregate dimension of 4.5 x 3.0 x 0.4 cm. In the post treatment report the maximum dimensions of DCIS measured from 0.2 to 1.0 cm in greatest dimension. The PINC 8 pre-treatment sample was subdivided into seven cassettes (FFPE blocks). Recut sections were only provided from one tissue block, therefore a conservative estimate of 50% was made pending further recuts and MRI evaluation.

**Table 11. Pathologic response for PINC patients based on reduction in lesion area and proliferation index.**

Patient ID	ER	PR	Nuclear Grade	Pathologic Area Reduction	Proliferation Index by IHC		Fold Change
					Pre-tx	Post-tx	
PINC 1	Pos	Pos	Intermediate	>75%	N/A	N/A	N/A
PINC 2	Pos	Pos	Intermediate	>90%	N/A	N/A	N/A
PINC 3	Pos	Pos	Intermediate	100%	41.4	2.3	-18.2
PINC 4	Pos	Pos	Intermediate	>50%	67.8	12.8	-5.3
PINC 5	Pos	Pos	Low	>75%	N/A	N/A	N/A
PINC 6	Neg	Neg	High	>33%	65.0	10.2	-6.4
PINC 7	Pos	Neg	Intermediate	100%	77.3	15.0	-5.1
PINC 8	Pos	Pos	Intermediate	>50%	29.7	10.0	-3.0

To demonstrate a reduction in both proliferation index and autophagy following *in vivo* chloroquine treatment, FFPE tissue sections from the PINC patient's diagnostic specimen were stained with PCNA or LC3B (Figure 37). PINC 4 showed a 5.3 fold reduction in proliferation in the DCIS lesions with a qualitative reduction in punctate LC3B staining compared to her pre-treatment tissue. These data demonstrate the

profound effect of chloroquine treatment on the proliferative capacity of the carcinoma in situ cells while showing minimal effect on the proliferative capacity of the normal ducts and adjacent stroma.

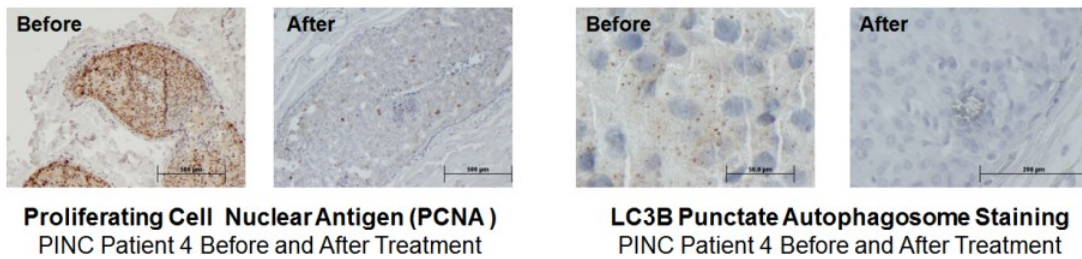


**Figure 37. Immunohistochemistry reveals a reduction in breast DCIS cell proliferation and autophagy following *in vivo* chloroquine treatment.**

## **Discussion**

### **Clinical trial progress to date**

Eight patients have completed treatment to date (March 2013). Based on the safety and efficacy demonstrated to date, negotiations are underway to expand the trial to an additional site (University of Pittsburgh) to increase the rate of patient enrollment. Long-term follow-up of the patients will proceed over the next two years.

Testing of the hypothesis for this study poses extensive possibilities for data analysis. The variables follow distributions from nominal to interval and challenge the formation of multivariable statistical models (Table 12). In addition to exploring bivariate associations between predictor and outcome variables using appropriate statistical tests (t-test, Spearman's rho correlation, Fisher's Exact), multi-variable models will be constructed using logistic regression or a mixed model where appropriate. A mixed

model will be particularly useful in this analysis where some predictor variables are repeated measures with cases having an unequal number of evaluations. The main measurement of efficacy is tumor response on MRI using RECIST criteria. RECIST criteria applied to DCIS is 20% reduction to qualify as partial response.

All analysis will assume a 2-tailed alpha = 0.05. The following key models will be explored:

**Outcome:** Invasion (Yes/No or degree); **Predictor class #1:** Tissue antigen markers, pathologic grade, signal pathway activation; **Predictor class #2:** Treatment category (chloroquine 500mg/week or 250mg/week).

**Outcome:** Tumorigenicity; **Predictor class #1:** Invasion *in vitro*, Tissue IHC antigen markers, pathologic grade, signal pathway activation; **Predictor class #2:** Treatment category.

**Outcome:** Invasion (Yes/No or degree), Activation or suppression state of signal pathways, cell proliferation index *in vitro*; **Predictors:** Treatment category.

**Table 12. PINC trial outcome variables and statistical methods.**

<b>Outcome variables</b>	<b>Form</b>
Generation of <i>in vitro</i> invasive cells from a pre-malignant lesion ductal organoid number of invasive foci per perimeter length	Interval, ordinal, nominal
Generation of a growing tumor in a xenograft model	Nominal Yes/No
Activated cellular signal pathways by RPMA	Interval
<b>MRI image score</b>	Interval, ordinal, nominal
<b>Predictor variables</b>	

Pathologic grade: low, intermediate, high	Interval, ordinal, nominal
Ki-67, PCNA, HER2, LC3B, CD68, ER, PR	Nominal: Yes/No
Treatment with Aralen (500mg/week or 250mg/week)	Nominal: Yes/No
<b>Covariates</b>	
Age, Menopausal status, Ethnicity	Interval, ordinal, nominal

### **Proliferation index markers**

Although both Ki-67 and PCNA levels are considered to reflect the relative proliferative capacity of the cells, each antibody and its cognate antigen has individual immunogenic properties that warrant the use of both markers<sup>292,293</sup>.

Ki-67 is a non-histone nuclear protein first isolated in sera from patients with Systemic Lupus Erythematosus<sup>294-296</sup>. Ki-67 antigen is only expressed in G<sub>1</sub>, S, G<sub>2</sub> and mitosis, but not G<sub>0</sub> phase of the cell cycle<sup>294</sup>. Antibodies to Ki-67 have been validated in numerous studies for assessing the cellular growth fraction<sup>295</sup>. Chen *et al* showed the utility of Ki-67 immunofluorescence as a proliferation marker in spheroids from a PI3K mutant cell line treated with combinations of CQ and/or rapamycin<sup>297</sup>. Lazova *et al* applied Ki-67 and LC3B IHC to breast cancer tissue microarrays as markers of proliferation and cytoprotective autophagy induction<sup>298</sup>. The caveats to measuring Ki-67 include well-known pre-analytical factors that decrease staining intensity, such as fixation delays, freezing tissue prior to fixation, and use of EDTA or acid decalcification methods. False negative results with Ki-67 immunohistochemistry occur in tissue

sections stored on glass slides for more than 3 months<sup>292</sup>. In the PINC trial workflow, the pre-treatment and post-treatment tissue sections were stained at the same time to minimize experimental variables. However, the pre-analytical variables for the PINC patient tissue samples were unknown because the diagnostic biopsy was analyzed by a central laboratory, with unknown timing between tissue acquisition and tissue processing. Thus, PCNA was also assessed to rule out potential loss of Ki-67 due to technical issues rather than biological function.

Proliferating Cell Nuclear Antigen (PCNA), is also an autoantibody found in patients with SLE, but distinctly different than Ki-67<sup>299</sup>. PCNA is an auxiliary protein of the DNA transcription complex (DNA Polymerases  $\delta$  and  $\epsilon$ ), which functions as a sliding clamp to increase the fidelity of transcription on the leading and lagging strands<sup>299,300</sup>. PCNA serves as a scaffold protein during DNA repair and chromatin assembly. PCNA regulation by ubiquitylation/deubiquitylation provides maintenance of genomic stability during DNA replication and repair<sup>301</sup>. Expression of PCNA increases during the G<sub>1</sub>-phase, peaks during the S-phase, and declines during the G<sub>2</sub>/M-phase, thus subtle variations in PCNA levels may be detectable between cells in different phases of the cell cycle<sup>301</sup>.

### **Epidemiologic study of breast cancer prevalence in relation to Chloroquine use**

Treating DCIS constitutes a potential shortcut to the realization of a general chemoprevention strategy for all breast cancer. Therapy that induces regression of occult or overt premalignant lesions could constitute an efficient chemoprevention agent that blocks the subsequent emergence of overtly invasive, metastatic breast cancer without the

need for validating biomarkers predictive of progression and/or recurrence. This strategy is analogous to prevention of cervical cancer or colon cancer via polypectomy of pre-invasive lesions, but may provide a non-surgical treatment option for DCIS.

A natural extension of neoadjuvant Chloroquine therapy for DCIS is an epidemiological study which could provide population-based evidence that CQ will prevent invasive breast cancer. The hypothesis is that breast cancer prevalence is lower in women who have been treated with CQ, or its derivatives, for malaria, lupus, or rheumatoid arthritis. Scant evidence exists in the literature correlating the association of malignancy and Chloroquine use<sup>302</sup>. Therefore a cross-sectional study of the breast cancer prevalence in relation to chloroquine (CQ) use could be conducted concurrently with neoadjuvant trials studying the safety and efficacy of chloroquine in DCIS to provide complementary and independent information regarding the hypothesized association between prevention of breast cancer and CQ use.

An epidemiological study would evaluate the association in a free-living population of individuals taking CQ for malaria prophylaxis, compared to sociodemographically and age matched control individuals. The clinical study supports the value of chloroquine as a means of treating pre-malignant lesions and the epidemiological survey would provide evidence regarding CQ use and breast cancer prevention. Outcome data from the epidemiologic survey could be used to guide the design of future CQ chemoprevention trials, and may point to subpopulations which can derive the most benefit from the treatment.

**Proposed epidemiologic study**

A web-based “Women’s Breast Health” survey will be developed based on a questionnaire. The questionnaire will be pre-tested before distribution. The Center for Social Science Research (CSSR) at George Mason University will use the *OnQ* (*Online Questionnaire*) web-based survey system held on a dedicated Linux based secure server. Originally developed with support from the National Science Foundation (Grant IIS-0082750, "ITR: Survey2001: Information Technology's Impact on Community, Culture and Conservation."), *OnQ* combines a user-friendly, Java-based client respondent interface and the flexibility of a database back-end that manages questions and answer options. The database structure for *OnQ* is organized around the logic of questions and answers. For self-administered web surveys *OnQ* evaluates respondent input and selects the appropriate skip patterns to approximate the intelligence of a skilled interviewer. *OnQ* supports complex skip patterns to branch individuals through a survey and provides a graphic representation of the skip patterns to assist the survey author. The questionnaire contains internal repeat questions that should return the same answer, providing a quality assurance metric.

The survey instrument is designed to be automated and will protect confidentiality. Each respondent will be sent an individualized link to the form and a unique respondent number. Provided with a list of email addresses and invitation text, the *OnQ* program creates the email and sends it along with a unique number for each person. This link will insure confidentiality but will still allow the study team to judge whether a participant responds more than once.



Statistical Methods: Percentages and means will be computed to evaluate sociodemographic, clinical, and health characteristics of the respondents. Logistic regression will be used to evaluate the odds of breast cancer in relation to CQ use. The primary outcomes will be breast cancer diagnosis. We will evaluate diagnosis at any time in the past, as well as a category restricted to women diagnosed in the previous five years. The primary drug exposures will be ever/never use of CQ, years of CQ use, age at first CQ exposure, and type of exposure (short-term use vs. long-term use). The primary analysis will be the relationship between age-adjusted breast cancer prevalence and CQ exposure. It is not established that breast cancer risk factors influence CQ use, so other factors are unlikely to be confounders. However, additional analyses will be adjusted for breast cancer risk factors (hormone use, family history, race, anthropometry, health status, reproductive history, and health behaviors) in order to evaluate whether adjustment for any of these factors influences the interpretation of the age-adjusted analyses.

Sample Size and Power: The estimated prevalence of women in the US who have a history of breast cancer is 2,747,459 women<sup>60</sup>. The 2010 population of women aged 21+ in the US was 220,958,853<sup>303</sup>. This gives us a prevalence of 1.2%. In a sample of 1000 women, we would expect only 12 women to have a personal history of breast cancer. Published results using web surveys in health care professionals or health educators, indicate response rate ranging from 23-55%<sup>304-306</sup>. Given all of this information, we will target the sample size to 10,000 women and assume the response rate to be between 23-55%. An estimate of the absolute difference in percentages

(between women with history of breast cancer vs. women without history of breast cancer) that we could detect would be about 10-18%. Therefore if the percentage of chloroquine exposure in the women with a history of breast cancer is 30%, we would have 90% power to statistically detect 40-48% chloroquine exposure in the women without breast cancer (depending on the response rate). If a notable difference is observed, but not statistically significant, this will provide key preliminary data for future studies. With all cross-sectional surveys of diseased vs. non-diseased individuals, there is a possibility of recall or reporting bias. We have inserted a question into the questionnaire in order to evaluate the possibility of these biases. Lactose intolerance will be queried; this factor is not a known risk factor for breast cancer, but has a high enough prevalence to evaluate potential reporting bias.

Residual confounding is a likely source of bias in the multivariate (beyond age) adjustment. As described in the statistical methods, many of these factors are unlikely to be strong confounders of a relationship between CQ use and breast cancer prevalence. The primary focus will be the age-adjusted analyses, and further adjustment will be conducted on an exploratory basis.

### **Neuroendocrine axis and calcium regulation as new therapeutic targets**

Beyond autophagy, alternative chemoprevention strategies to prevent DCIS from progressing to invasive cancer may involve neuroendocrine modulation of the breast ductal microenvironment or induction of calcium related stress to induce apoptosis. The neuroendocrine system harbors desirable therapeutic targets due to breast anatomy, the propensity for breast cancer to metastasize to bone, and the availability of neuroendocrine

modulators. Extrapolating facets of pathophysiology from multiple myeloma and breast cancer provides evidence that autophagy, neuroendocrine signaling, and endoplasmic reticulum stress could potentially be future drug targets for DCIS.

Breast ducts are known to be innervated with parasympathetic nerves and possess neurohormone receptors to estrogen receptor, progesterone receptor, prolactin, oxytocin and growth hormone<sup>22,307</sup>. Bone is a frequent metastatic site for primary breast tumors, which contributes to increased morbidity and mortality of breast cancer patients<sup>308,309</sup>. Evidence from our recent study of 159 bone metastasis samples from eight different primary tumors, including breast cancer, demonstrates that the neuroendocrine axis, specifically cellular levels of Tumor Necrosis Factor Receptor (TNFR1) and serotonin, were correlated with patient survival<sup>310</sup>.

Bone colonization by malignant plasma cells is a common pathological feature of multiple myeloma. Multiple myeloma manifests itself as a clonal proliferation of antibody producing B cells (plasma cells)<sup>311</sup>. A hallmark of multiple myeloma is secretion of vast quantities of mis-folded immunoglobulins<sup>311</sup>. Bortezomib (Velcade), a proteasome inhibitor, is routinely used for treatment of patients with multiple myeloma<sup>311</sup>. Peripheral neuropathy is a frequent side-effect of Bortezomib treatment. Schoenlein *et al* reported that bortezomib blocks catabolic autophagy in MCF7 and T47-D breast cancer cell line models, induces an unfolded protein response and leads to apoptosis<sup>239,312</sup>. The molecular mechanisms underlying peripheral neuropathy due to Bortezomib treatment are not completely known but one can hypothesize that it may be related to autophagy inhibition. These disparate findings, when considered in a

pathophysiologic context, may indicate that a cell signaling network between neuroendocrine axis, autophagy, and proteasome (protein folding) interact in such a manner that inhibition of one or more critical components of these pathways may have therapeutic efficacy in DCIS<sup>309</sup>. Thus, *ex vivo* treatment of breast spheroids and epithelial/fibroblast co-cultures with serotonin, bortezomib, and/or serotonin inhibitors may elucidate previously unexplored neuroendocrine cell signaling pathways relevant to breast cancer progression.

A hallmark of DCIS is the presence of microcalcifications within the DCIS lesion<sup>49</sup>. The role of calcium in promoting breast cancer progression is not completely known, however the presence of calcium phosphate/hydroxyapatite within the breast ductal tree has diagnostic significance for intermediate and high grade DCIS lesions<sup>5,46,47</sup>. Recent electron microscopic studies of mammalian cell culture revealed that autophagosomes are closely interconnected with the endoplasmic reticulum during the unfolded protein response in which endoplasmic reticulum-derived membrane stacks are sequestered into autophagosome-like structures<sup>313</sup>. The initial synthesis of autophagosome formation is still unknown but one model proposes autophagosome formation by de novo lipid synthesis or transport. These early autophagic membranes appear to be surrounded by a fragment of the endoplasmic reticulum cisternae<sup>314,315</sup>. Intracellular calcium is regulated in part by release of calcium stores from the endoplasmic reticulum suggesting a role for endoplasmic reticulum stress in the development of intra-ductal calcifications.

Calcium plays a vital role in wound repair. Calcium has been shown to be concentrated at intracellular junctions and at a distance from the site of the injury. Wound healing is a process of developing new intracellular junctions via Abr protein – a dual GEF/GAP kinase<sup>316</sup>. GEF activates Rho, while GAP inactivates Rho. Rho activation initiates a contractile ring that recruits neighboring cells to contribute to wound repair<sup>317</sup>. Abr localizes to the center of the Rho contractile zone and Rho activation recruits Abr. The GAP domain of Abr inactivates Cdc42, and the GEF domain activates Rho. Abr is recruited to the junction with the neighbor cell. A lack of Abr causes cell lysis. In DCIS central necrosis could be a product of dis-regulated wound healing, potentially due to Abr deficiency/modulation within the center of the ductal cell mass, resulting in cell lysis.

### **Summary**

Strong links exist between calcium, autophagy, and cellular homeostasis in breast DCIS. As shown in chapters 2-4, *ex vivo* culture systems, proteomic analysis, and molecular karyotyping provide methods for assessing the biologic invasive potential of an individual patient's DCIS cells *ex vivo*, before and after treatment. Fresh human DCIS lesions contain carcinoma cells with breast cancer stem-like cell properties, which possess invasive properties<sup>9-11</sup>. Human breast DCIS cells: a) possess spheroid forming neoplastic cells that can be harvested and propagated in organoid culture, b) have stem-like properties and generate invasive tumors in mouse xenografts, thus they can be classified as carcinoma precursors, c) up-regulate autophagy *in vivo* and *in vitro*, and d) undergo apoptosis in the presence of chloroquine. Within the breast duct, DCIS cells up-regulate autophagy as a survival mechanism in the presence of anoikis, calcium

imbalance, hypoxia, oxidative stress, and nutrient deprivation. Genetic instability at the DCIS stage, as shown by loss of heterozygosity or gene duplication in multiple chromosomal regions, is sufficient to promote tumorigenesis. A phase I/II clinical trial evaluating the efficacy of neoadjuvant oral chloroquine anti-autophagy therapy for DCIS is actively recruiting patients. In the future, other therapeutics can be combined with anti-autophagy therapy, such as modulators of calcium efflux, to improve therapy effectiveness, and/or reduce the number of repeated treatments over a woman's lifetime.

## INDEX

- Aralen. 92, 112, 113, 116, 120, 121, 122, 124, 125, 126, 130
- ATP. xiv, 49, 63, 79, 80, 81, 87, 93, 105, 106, 107, 108, 160
- atypical ductal hyperplasia..... 13, 15
- Autophagy.... xiv, 58, 63, 78, 87, 88, 105
- bioavailability ..... 92, 109
- BRCA1..... xiv, 1, 20, 41, 143, 150, 152
- calcium..... 9, 11, 12, 101, 135, 137, 138, 146, 147, 165
- Calcium..... 138
- Canine..... 104
- CD24..... 18
- CD44..... 18
- CD68..... 47, 55, 56, 130
- chemoprevention 89, 109, 111, 112, 131, 132, 135
- chloroquine 111, 112, 114, 132, 135, 139
- chromatin . 10, 11, 41, 42, 63, 79, 80, 81, 84, 88, 106, 131, 152, 158, 160, 161
- cleaved PARP ..... 101
- collagenase..... 23
- DCIS ... xiv, 1, 13, 17, 21, 23, 29, 32, 37, 41, 58, 62, 69, 70, 73, 74, 80, 81, 87, 90, 105, 107, 110, 111, 112, 113, 114, 115, 116, 119, 121, 124, 131, 132, 135, 137, 138
- EpCAM..... xiv, 25, 32, 33, 38, 151
- epidemiological..... 132
- FOXO..... xiv, 85
- Genetic instability ..... 63, 139
- histone.... 41, 84, 85, 130, 158, 160, 161, 166, 168
- Histone..... 10
- Hox*..... 41, 42
- hydroxychloroquine ..... 109
- Immunofluorescence..... xiv, 25, 47
- institutional review board ..... 23
- Jak/Stat..... 10
- Ki-67 .. 57, 114, 119, 124, 125, 126, 130, 131, 167, 168
- loss-of-heterozygosity..... 13
- lysosomal ..... *See* lysosome
- lysosome ..... 57, 60, 87, 90, 92, 106
- LysoTracker Red..... 47, 54, 56, 57
- mammary fat pad ..... 24, 32, 36, 100
- Methylation ..... 41, 161
- MHC ..... xv, 82
- microcalcifications.... 9, 11, 12, 137, 147
- microenvironment 5, 19, 62, 81, 105, 135
- Migration..... 103
- MMP . xv, 21, 45, 50, 51, 83, 97, 99, 123
- Molecular karyotyping.... xvii, 64, 65, 72
- myoepithelial..... 19
- NCCN ..... 110
- NF- $\kappa$ B ..... xv, 10
- NOD SCID..... xv, 32
- PCNA. xv, 114, 119, 124, 126, 127, 130, 131, 168
- pharmacodynamics ..... 92
- PMCA2 ..... xv, 101, 102, 165
- progenitor..... 17, 37, 62, 80, 105, 111
- proliferation index..... 119
- proteomic ..... 1, 58, 106, 114, 138
- RECIST..... xv, 116
- recurrence..... 110
- Reverse Phase Protein Microarrayxv, 42, 43, 96
- RUNX2 ..... xv, 67, 83, 86, 161
- single nucleotide polymorphism... 64, 67
- spheroids xvii, 24, 26, 28, 31, 32, 34, 36, 37, 39, 42, 48, 49, 50, 52, 54, 56, 57,

65, 67, 68, 69, 70, 72, 73, 75, 76, 77,  
81, 97, 99, 100, 102, 123, 130, 137  
Statistics ..... 48, 96, 148  
stem cells..... 17, 37, 84, 89  
stroma..... 19, 23, 29, 117  
SUPT3H... xv, 46, 47, 51, 66, 67, 69, 75,  
77, 78, 83, 84, 85, 86

SWI/SNF ..... xv, 10, 79  
xanthine oxidoreductase..... 9  
Xenograft ..... 24, 33  
Zymography ..... 118  
 $\beta$ -casein ..... 10



## REFERENCES

## REFERENCES

1. Campbell LL, Polyak K. Breast tumor heterogeneity: cancer stem cells or clonal evolution? *Cell Cycle* 2007;6(19):2332-8.
2. Simpson PT, Reis-Filho JS, Gale T, Lakhani SR. Molecular evolution of breast cancer. *J Pathol* 2005;205(2):248-54.
3. Arun B, Vogel KJ, Lopez A, Hernandez M, Atchley D, Broglio KR, Amos CI, Meric-Bernstam F, Kuerer H, Hortobagyi GN and others. High prevalence of preinvasive lesions adjacent to BRCA1/2-associated breast cancers. *Cancer Prev Res (Phila Pa)* 2009;2(2):122-7.
4. Betsill WL, Jr., Rosen PP, Lieberman PH, Robbins GF. Intraductal carcinoma. Long-term follow-up after treatment by biopsy alone. *JAMA* 1978;239(18):1863-7.
5. Boecker W. *Preneoplasia of the Breast*. Munich: Elsevier GmbH; 2006. 650 p.
6. Collins LC, Tamimi RM, Baer HJ, Connolly JL, Colditz GA, Schnitt SJ. Outcome of patients with ductal carcinoma in situ untreated after diagnostic biopsy: results from the Nurses' Health Study. *Cancer* 2005;103(9):1778-84.
7. Fisher B, Land S, Mamounas E, Dignam J, Fisher ER, Wolmark N. Prevention of invasive breast cancer in women with ductal carcinoma in situ: an update of the National Surgical Adjuvant Breast and Bowel Project experience. *Semin Oncol* 2001;28(4):400-18.
8. Page DL, Dupont WD, Rogers LW, Landenberger M. Intraductal carcinoma of the breast: follow-up after biopsy only. *Cancer* 1982;49(4):751-8.
9. Espina V, Liotta LA. What is the malignant nature of human ductal carcinoma in situ? *Nat Rev Cancer* 2011.
10. Espina V, Mariani BD, Gallagher RI, Tran K, Banks S, Wiedemann J, Huryk H, Mueller C, Adamo L, Deng J and others. Malignant precursor cells pre-exist in human breast DCIS and require autophagy for survival. *PLoS One* 2010;5(4):e10240.
11. Espina V, Wysolmerski J, Edmiston K, Liotta LA. Attacking breast cancer at the preinvasion stage by targeting autophagy. *Women's Health* 2013;9(2):1-14.

12. Sanders ME, Schuyler PA, Dupont WD, Page DL. The natural history of low-grade ductal carcinoma in situ of the breast in women treated by biopsy only revealed over 30 years of long-term follow-up. *Cancer* 2005;103(12):2481-4.
13. Allegra C, Aberle D, Ganschow P, Hahn S, Lee C, Millon-Underwood S, Pike M, Reed S, Saftlas A, Scarvalone S and others. National Institutes of Health State-of-the-Science Conference Statement: Diagnosis and Management of Ductal Carcinoma In Situ *J Natl Cancer Inst.* 2009;102(3):161-169.
14. Castro NP, Osorio CA, Torres C, Bastos EP, Mourao-Neto M, Soares FA, Brentani HP, Carraro DM. Evidence that molecular changes in cells occur before morphological alterations during the progression of breast ductal carcinoma. *Breast Cancer Res* 2008;10(5):R87.
15. Damonte P, Hodgson JG, Chen JQ, Young LJ, Cardiff RD, Borowsky AD. Mammary carcinoma behavior is programmed in the precancer stem cell. *Breast Cancer Res* 2008;10(3):R50.
16. Ma XJ, Dahiya S, Richardson E, Erlander M, Sgroi DC. Gene expression profiling of the tumor microenvironment during breast cancer progression. *Breast Cancer Res* 2009;11(1):R7.
17. Ma XJ, Salunga R, Tuggle JT, Gaudet J, Enright E, McQuary P, Payette T, Pistone M, Stecker K, Zhang BM and others. Gene expression profiles of human breast cancer progression. *Proc Natl Acad Sci U S A* 2003;100(10):5974-9.
18. Namba R, Maglione JE, Davis RR, Baron CA, Liu S, Carmack CE, Young LJ, Borowsky AD, Cardiff RD, Gregg JP. Heterogeneity of mammary lesions represent molecular differences. *BMC Cancer* 2006;6:275.
19. Sgroi DC. Preinvasive breast cancer. *Annu Rev Pathol* 2010;5:193-221.
20. Smalley M, Ashworth A. Stem cells and breast cancer: A field in transit. *Nat Rev Cancer* 2003;3(11):832-44.
21. Campbell PJ, Pleasance ED, Stephens PJ, Dicks E, Rance R, Goodhead I, Follows GA, Green AR, Futreal PA, Stratton MR. Subclonal phylogenetic structures in cancer revealed by ultra-deep sequencing. *Proc Natl Acad Sci U S A* 2008;105(35):13081-6.
22. Pandya S, Moore RG. Breast development and anatomy. *Clin Obstet Gynecol* 2011;54(1):91-5.
23. Ramsay DT, Kent JC, Hartmann RA, Hartmann PE. Anatomy of the lactating human breast redefined with ultrasound imaging. *J Anat* 2005;206(6):525-34.

24. Wicha MS, Liotta LA, Garbisa S, Kidwell WR. Basement membrane collagen requirements for attachment and growth of mammary epithelium. *Exp Cell Res* 1979;124(1):181-90.
25. Adriance MC, Inman JL, Petersen OW, Bissell MJ. Myoepithelial cells: good fences make good neighbors. *Breast Cancer Res* 2005;7(5):190-7.
26. Claus EB, Chu P, Howe CL, Davison TL, Stern DF, Carter D, DiGiovanna MP. Pathobiologic findings in DCIS of the breast: morphologic features, angiogenesis, HER-2/neu and hormone receptors. *Exp Mol Pathol* 2001;70(3):303-16.
27. Gudjonsson T, Adriance MC, Sternlicht MD, Petersen OW, Bissell MJ. Myoepithelial cells: their origin and function in breast morphogenesis and neoplasia. *J Mammary Gland Biol Neoplasia* 2005;10(3):261-72.
28. Tavassoli F. Intraductal Proliferative Lesions. In: Tavassoli F, Devilee P, editors. *Tumors of the Breast and Female Genital Organs*. Lyon: IARC-Press; 2003. p 63-73.
29. Mayr NA, Staples JJ, Robinson RA, Vanmetre JE, Hussey DH. Morphometric studies in intraductal breast carcinoma using computerized image analysis. *Cancer* 1991;67(11):2805-12.
30. Villadsen R, Fridriksdottir AJ, Ronnov-Jessen L, Gudjonsson T, Rank F, LaBarge MA, Bissell MJ, Petersen OW. Evidence for a stem cell hierarchy in the adult human breast. *J Cell Biol* 2007;177(1):87-101.
31. Ohtake T, Kimijima I, Fukushima T, Yasuda M, Sekikawa K, Takenoshita S, Abe R. Computer-assisted complete three-dimensional reconstruction of the mammary ductal/lobular systems: implications of ductal anastomoses for breast-conserving surgery. *Cancer* 2001;91(12):2263-72.
32. Going JJ, Moffat DF. Escaping from Flatland: clinical and biological aspects of human mammary duct anatomy in three dimensions. *J Pathol* 2004;203(1):538-44.
33. Izumori A, Horii R, Akiyama F, Iwase T. Proposal of a novel method for observing the breast by high-resolution ultrasound imaging: understanding the normal breast structure and its application in an observational method for detecting deviations. *Breast Cancer* 2013;20(1):83-91.
34. Iyengar P, Espina V, Williams TW, Lin Y, Berry D, Jelicks LA, Lee H, Temple K, Graves R, Pollard J and others. Adipocyte-derived collagen VI affects early mammary tumor progression in vivo, demonstrating a critical interaction in the tumor/stroma microenvironment. *J Clin Invest* 2005;115(5):1163-76.

35. Sorokin L. The impact of the extracellular matrix on inflammation. *Nat Rev Immunol* 2010;10(10):712-23.
36. Yamada T, Mori N, Watanabe M, Kimijima I, Okumoto T, Seiji K, Takahashi S. Radiologic-pathologic correlation of ductal carcinoma in situ. *Radiographics* 2010;30(5):1183-98.
37. Jenness R. The composition of human milk. *Semin Perinatol* 1979;3(3):225-39.
38. VanHouten JN, Neville MC, Wysolmerski JJ. The calcium-sensing receptor regulates plasma membrane calcium adenosine triphosphatase isoform 2 activity in mammary epithelial cells: a mechanism for calcium-regulated calcium transport into milk. *Endocrinology* 2007;148(12):5943-54.
39. Razzell W, Evans IR, Martin P, Wood W. Calcium Flashes Orchestrate the Wound Inflammatory Response through DUOX Activation and Hydrogen Peroxide Release. *Curr Biol* 2013;23(5):424-9.
40. Artlett CM. Inflammasomes in wound healing and fibrosis. *J Pathol* 2013;229(2):157-67.
41. Vorbach C, Capecchi MR, Penninger JM. Evolution of the mammary gland from the innate immune system? *Bioessays* 2006;28(6):606-16.
42. Andrechek ER, Mori S, Rempel RE, Chang JT, Nevins JR. Patterns of cell signaling pathway activation that characterize mammary development. *Development* 2008;135(14):2403-13.
43. Marusyk A, Polyak K. Tumor heterogeneity: causes and consequences. *Biochim Biophys Acta* 2009;1805(1):105-17.
44. Xu R, Spencer VA, Bissell MJ. Extracellular matrix-regulated gene expression requires cooperation of SWI/SNF and transcription factors. *J Biol Chem* 2007;282(20):14992-9.
45. Theriault RL, Carlson RW, Allred C, Anderson BO, Burstein HJ, Edge SB, Farrar WB, Forero A, Giordano SH, Goldstein LJ and others. 2013 March 30, 2013. NCCN Breast Cancer Guidelines Version 2.2013. National Comprehensive Cancer Network <[http://www.nccn.org/professionals/physician\\_gls/pdf/breast.pdf](http://www.nccn.org/professionals/physician_gls/pdf/breast.pdf)>. Accessed 2013 March 30, 2013.
46. Evans A, Pinder S, Wilson R, Sibbering M, Poller D, Elston C, Ellis I. Ductal carcinoma in situ of the breast: correlation between mammographic and pathologic findings. *AJR Am J Roentgenol* 1994;162(6):1307-11.

47. Holland R, Hendriks JH, Vebeek AL, Mravunac M, Schuurmans Stekhoven JH. Extent, distribution, and mammographic/histological correlations of breast ductal carcinoma in situ. *Lancet* 1990;335(8688):519-22.
48. Cox RF, Hernandez-Santana A, Ramdass S, McMahon G, Harmey JH, Morgan MP. Microcalcifications in breast cancer: novel insights into the molecular mechanism and functional consequence of mammary mineralisation. *Br J Cancer* 2012;106(3):525-37.
49. Foschini MP, Fornelli A, Peterse JL, Mignani S, Eusebi V. Microcalcifications in ductal carcinoma in situ of the breast: histochemical and immunohistochemical study. *Hum Pathol* 1996;27(2):178-83.
50. Hermann G, Keller RJ, Drossman S, Caravella BA, Tartter P, Panetta RA, Bleiweiss IJ. Mammographic pattern of microcalcifications in the preoperative diagnosis of comedo ductal carcinoma in situ: histopathologic correlation. *Can Assoc Radiol J* 1999;50(4):235-40.
51. Cox A, Dunning AM, Garcia-Closas M, Balasubramanian S, Reed MW, Pooley KA, Scollen S, Baynes C, Ponder BA, Chanock S and others. A common coding variant in CASP8 is associated with breast cancer risk. *Nat Genet* 2007;39(3):352-8.
52. Lev-Toaff AS, Feig SA, Saitas VL, Finkel GC, Schwartz GF. Stability of malignant breast microcalcifications. *Radiology* 1994;192(1):153-6.
53. Gao W, Ding WX, Stolz DB, Yin XM. Induction of macroautophagy by exogenously introduced calcium. *Autophagy* 2008;4(6):754-61.
54. Lagios MD. Heterogeneity of duct carcinoma in situ (DCIS): relationship of grade and subtype analysis to local recurrence and risk of invasive transformation. *Cancer Lett* 1995;90(1):97-102.
55. Mommers EC, Poulin N, Sangulin J, Meijer CJ, Baak JP, van Diest PJ. Nuclear cytometric changes in breast carcinogenesis. *J Pathol* 2001;193(1):33-9.
56. Reis-Filho JS, Lakhani SR. The diagnosis and management of pre-invasive breast disease: genetic alterations in pre-invasive lesions. *Breast Cancer Res* 2003;5(6):313-9.
57. Moinfar F, Man YG, Arnould L, Bratthauer GL, Ratschek M, Tavassoli FA. Concurrent and independent genetic alterations in the stromal and epithelial cells of mammary carcinoma: implications for tumorigenesis. *Cancer Res* 2000;60(9):2562-6.
58. Wulfkühle JD, Speer R, Pierobon M, Laird J, Espina V, Deng J, Mammano E, Yang SX, Swain SM, Nitti D and others. Multiplexed cell signaling analysis of human breast cancer applications for personalized therapy. *J Proteome Res* 2008;7(4):1508-17.

59. Hanahan D, Weinberg RA. Hallmarks of cancer: the next generation. *Cell* 2011;144(5):646-74.
60. Howlander N, Noone AM, Krapcho M, Neyman N, Aminou R, Altekruse SF, Kosary CL, Ruhl J, Tatalovich Z, Cho CH and others. SEER Cancer Statistics Review, 1975-2009 (Vintage 2009 Populations). Bethesda, MD: National Cancer Institute; 2009 April 2012.
61. Kuhl CK, Schrading S, Bieling HB, Wardelmann E, Leutner CC, Koenig R, Kuhn W, Schild HH. MRI for diagnosis of pure ductal carcinoma in situ: a prospective observational study. *Lancet* 2007;370(9586):485-92.
62. Hu M, Yao J, Carroll DK, Weremowicz S, Chen H, Carrasco D, Richardson A, Violette S, Nikolskaya T, Nikolsky Y and others. Regulation of in situ to invasive breast carcinoma transition. *Cancer Cell* 2008;13(5):394-406.
63. Berman HK, Gauthier ML, Tlsty TD. Premalignant breast neoplasia: a paradigm of interlesional and intralesional molecular heterogeneity and its biological and clinical ramifications. *Cancer Prev Res (Phila Pa)* 2010;3(5):579-87.
64. Schnitt SJ. The transition from ductal carcinoma in situ to invasive breast cancer: the other side of the coin. *Breast Cancer Res* 2009;11(1):101.
65. Schnitt SJ, Harris JR, Smith BL. Developing a prognostic index for ductal carcinoma in situ of the breast. Are we there yet? *Cancer* 1996;77(11):2189-92.
66. Esserman L, Shieh Y, Thompson I. Rethinking screening for breast cancer and prostate cancer. *JAMA* 2009;302(15):1685-92.
67. Esserman LJ, Kumar AS, Herrera AF, Leung J, Au A, Chen YY, Moore DH, Chen DF, Hellawell J, Wolverson D and others. Magnetic resonance imaging captures the biology of ductal carcinoma in situ. *J Clin Oncol* 2006;24(28):4603-10.
68. Wicha MS, Liu S, Dontu G. Cancer stem cells: an old idea--a paradigm shift. *Cancer Res* 2006;66(4):1883-90; discussion 1895-6.
69. Stingl J, Eaves CJ, Kuusk U, Emerman JT. Phenotypic and functional characterization in vitro of a multipotent epithelial cell present in the normal adult human breast. *Differentiation* 1998;63(4):201-13.
70. Kalirai H, Clarke RB. Human breast epithelial stem cells and their regulation. *J Pathol* 2006;208(1):7-16.

71. Al-Hajj M, Wicha MS, Benito-Hernandez A, Morrison SJ, Clarke MF. Prospective identification of tumorigenic breast cancer cells. *Proc Natl Acad Sci U S A* 2003;100(7):3983-8.
72. Celis JE, Gromova I, Cabezon T, Gromov P, Shen T, Timmermans-Wielenga V, Rank F, Moreira JM. Identification of a subset of breast carcinomas characterized by expression of cytokeratin 15: relationship between CK15+ progenitor/amplified cells and pre-malignant lesions and invasive disease. *Mol Oncol* 2007;1(3):321-49.
73. Ginestier C, Hur MH, Charafe-Jauffret E, Monville F, Dutcher J, Brown M, Jacquemier J, Viens P, Kleer CG, Liu S and others. ALDH1 is a marker of normal and malignant human mammary stem cells and a predictor of poor clinical outcome. *Cell Stem Cell* 2007;1(5):555-67.
74. Huang EH, Hynes MJ, Zhang T, Ginestier C, Dontu G, Appelman H, Fields JZ, Wicha MS, Boman BM. Aldehyde dehydrogenase 1 is a marker for normal and malignant human colonic stem cells (SC) and tracks SC overpopulation during colon tumorigenesis. *Cancer Res* 2009;69(8):3382-9.
75. Hwang-Verslues WW, Kuo WH, Chang PH, Pan CC, Wang HH, Tsai ST, Jeng YM, Shew JY, Kung JT, Chen CH and others. Multiple lineages of human breast cancer stem/progenitor cells identified by profiling with stem cell markers. *PLoS One* 2009;4(12):e8377.
76. Hill RP. Identifying cancer stem cells in solid tumors: case not proven. *Cancer Res* 2006;66(4):1891-5; discussion 1890.
77. Ponti D, Zaffaroni N, Capelli C, Daidone MG. Breast cancer stem cells: an overview. *Eur J Cancer* 2006;42(9):1219-24.
78. Clarke MF, Fuller M. Stem cells and cancer: two faces of eve. *Cell* 2006;124(6):1111-5.
79. Dick JE. Breast cancer stem cells revealed. *Proc Natl Acad Sci U S A* 2003;100(7):3547-9.
80. Dirks PB. Brain tumor stem cells: the cancer stem cell hypothesis writ large. *Mol Oncol* 2010;4(5):420-30.
81. Hemmati HD, Nakano I, Lazareff JA, Masterman-Smith M, Geschwind DH, Bronner-Fraser M, Kornblum HI. Cancerous stem cells can arise from pediatric brain tumors. *Proc Natl Acad Sci U S A* 2003;100(25):15178-83.
82. Singh S, Dirks PB. Brain tumor stem cells: identification and concepts. *Neurosurg Clin N Am* 2007;18(1):31-8, viii.



83. Abraham BK, Fritz P, McClellan M, Hauptvogel P, Athelougou M, Brauch H. Prevalence of CD44+/CD24-/low cells in breast cancer may not be associated with clinical outcome but may favor distant metastasis. *Clin Cancer Res* 2005;11(3):1154-9.
84. Zoller M. CD44: can a cancer-initiating cell profit from an abundantly expressed molecule? *Nat Rev Cancer* 2011;11(4):254-67.
85. Bissell MJ, Labarge MA. Context, tissue plasticity, and cancer: are tumor stem cells also regulated by the microenvironment? *Cancer Cell* 2005;7(1):17-23.
86. Hennessy BT, Gonzalez-Angulo A-M, Stemke-Hale K, Gilcrease MZ, Krishnamurthy S, Lee J-S, Fridlyand J, Sahin A, Agarwal R, Joy C and others. Characterization of a naturally occurring breast cancer subset enriched in epithelial-to-mesenchymal transition and stem cell characteristics. *Cancer Research* 2009;69(10):4116-4124.
87. Liotta LA, Kohn EC. The microenvironment of the tumour-host interface. *Nature* 2001;411(6835):375-9.
88. Molyneux G, Geyer FC, Magnay FA, McCarthy A, Kendrick H, Natrajan R, Mackay A, Grigoriadis A, Tutt A, Ashworth A and others. BRCA1 basal-like breast cancers originate from luminal epithelial progenitors and not from basal stem cells. *Cell Stem Cell* 2010;7(3):403-17.
89. Franks SE, Campbell CI, Barnett EF, Siwicky MD, Livingstone J, Cory S, Moorehead RA. Transgenic IGF-IR overexpression induces mammary tumors with basal-like characteristics, whereas IGF-IR-independent mammary tumors express a claudin-low gene signature. *Oncogene* 2012;31(27):3298-309.
90. Perou CM, Sorlie T, Eisen MB, van de Rijn M, Jeffrey SS, Rees CA, Pollack JR, Ross DT, Johnsen H, Akslen LA and others. Molecular portraits of human breast tumours. *Nature* 2000;406(6797):747-52.
91. Meijnen P, Peterse JL, Antonini N, Rutgers EJ, van de Vijver MJ. Immunohistochemical categorisation of ductal carcinoma in situ of the breast. *Br J Cancer* 2008;98(1):137-42.
92. Kim J, Villadsen R, Sorlie T, Fogh L, Gronlund SZ, Fridriksdottir AJ, Kuhn I, Rank F, Wielenga VT, Solvang H and others. Tumor initiating but differentiated luminal-like breast cancer cells are highly invasive in the absence of basal-like activity. *Proc Natl Acad Sci U S A* 2012;109(16):6124-9.
93. Park ES, Rabinovsky R, Carey M, Hennessy BT, Agarwal R, Liu W, Ju Z, Deng W, Lu Y, Woo HG and others. Integrative analysis of proteomic signatures, mutations,

and drug responsiveness in the NCI 60 cancer cell line set. *Molecular Cancer Therapeutics* 2010;9(2):257-267.

94. Gonzalez LO, Junquera S, del Casar JM, Gonzalez L, Marin L, Gonzalez-Reyes S, Andicoechea A, Gonzalez-Fernandez R, Gonzalez JM, Perez-Fernandez R and others. Immunohistochemical study of matrix metalloproteinases and their inhibitors in pure and mixed invasive and in situ ductal carcinomas of the breast. *Hum Pathol* 2010;41(7):980-9.
95. Mueller C, Edmiston KH, Carpenter C, Gaffney E, Ryan C, Ward R, White S, Memeo L, Colarossi C, Petricoin EF, 3rd and others. One-step preservation of phosphoproteins and tissue morphology at room temperature for diagnostic and research specimens. *PLoS One* 2011;6(8):e23780.
96. Espina V, Edmiston KH, Heiby M, Pierobon M, Sciro M, Merritt B, Banks S, Deng J, VanMeter AJ, Geho DH and others. A portrait of tissue phosphoprotein stability in the clinical tissue procurement process. *Mol Cell Proteomics* 2008;7(10):1998-2018.
97. Espina V, Mueller C, Edmiston K, Sciro M, Petricoin EF, Liotta LA. Tissue is alive: New technologies are needed to address the problems of protein biomarker pre-analytical variability. *Proteomics Clin Appl* 2009;3(8):874-882.
98. Mueller C, Liotta LA, Espina V. Reverse phase protein microarrays advance to use in clinical trials. *Mol Oncol* 2010;4(6):461-81.
99. Dontu G, Abdallah WM, Foley JM, Jackson KW, Clarke MF, Kawamura MJ, Wicha MS. In vitro propagation and transcriptional profiling of human mammary stem/progenitor cells. *Genes Dev* 2003;17(10):1253-70.
100. Pechoux C, Gudjonsson T, Ronnov-Jessen L, Bissell MJ, Petersen OW. Human mammary luminal epithelial cells contain progenitors to myoepithelial cells. *Dev Biol* 1999;206(1):88-99.
101. Beckhove P, Schutz F, Diel IJ, Solomayer EF, Bastert G, Foerster J, Feuerer M, Bai L, Sinn HP, Umansky V and others. Efficient engraftment of human primary breast cancer transplants in nonconditioned NOD/Scid mice. *Int J Cancer* 2003;105(4):444-53.
102. Berenbaum MC, Sheard CE, Reittie JR, Bundick RV. The growth of human tumours in immunosuppressed mice and their response to chemotherapy. *Br J Cancer* 1974;30(1):13-32.
103. Martowicz A, Spizzo G, Gastl G, Untergasser G. Phenotype-dependent effects of EpCAM expression on growth and invasion of human breast cancer cell lines. *BMC Cancer* 2012;12:501.

104. Chaparro RJ, Konigshofer Y, Beilhack GF, Shizuru JA, McDevitt HO, Chien YH. Nonobese diabetic mice express aspects of both type 1 and type 2 diabetes. *Proc Natl Acad Sci U S A* 2006;103(33):12475-80.
105. Christianson SW, Shultz LD, Leiter EH. Adoptive transfer of diabetes into immunodeficient NOD-scid/scid mice. Relative contributions of CD4+ and CD8+ T-cells from diabetic versus prediabetic NOD.NON-Thy-1a donors. *Diabetes* 1993;42(1):44-55.
106. Gabut M, Samavarchi-Tehrani P, Wang X, Slobodeniuc V, O'Hanlon D, Sung HK, Alvarez M, Talukder S, Pan Q, Mazzoni EO and others. An alternative splicing switch regulates embryonic stem cell pluripotency and reprogramming. *Cell* 2011;147(1):132-46.
107. Lee MG, Villa R, Trojer P, Norman J, Yan KP, Reinberg D, Di Croce L, Shiekhatar R. Demethylation of H3K27 regulates polycomb recruitment and H2A ubiquitination. *Science* 2007;318(5849):447-50.
108. Lemon B, Inouye C, King DS, Tjian R. Selectivity of chromatin-remodelling cofactors for ligand-activated transcription. *Nature* 2001;414(6866):924-8.
109. Margueron R, Reinberg D. The Polycomb complex PRC2 and its mark in life. *Nature* 2011;469(7330):343-9.
110. Noordermeer D, Leleu M, Splinter E, Rougemont J, De Laat W, Duboule D. The dynamic architecture of Hox gene clusters. *Science* 2011;334(6053):222-5.
111. Zhu Q, Pao GM, Huynh AM, Suh H, Tonnu N, Nederlof PM, Gage FH, Verma IM. BRCA1 tumour suppression occurs via heterochromatin-mediated silencing. *Nature* 2011;477(7363):179-84.
112. Goetz MP, Suman VJ, Ingle JN, Nibbe AM, Visscher DW, Reynolds CA, Lingle WL, Erlander M, Ma XJ, Sgroi DC and others. A two-gene expression ratio of homeobox 13 and interleukin-17B receptor for prediction of recurrence and survival in women receiving adjuvant tamoxifen. *Clin Cancer Res* 2006;12(7 Pt 1):2080-7.
113. Ma XJ, Hilsenbeck SG, Wang W, Ding L, Sgroi DC, Bender RA, Osborne CK, Allred DC, Erlander MG. The HOXB13:IL17BR expression index is a prognostic factor in early-stage breast cancer. *J Clin Oncol* 2006;24(28):4611-9.
114. Ma XJ, Salunga R, Dahiya S, Wang W, Carney E, Durbecq V, Harris A, Goss P, Sotiropoulos C, Erlander M and others. A five-gene molecular grade index and HOXB13:IL17BR are complementary prognostic factors in early stage breast cancer. *Clin Cancer Res* 2008;14(9):2601-8.

115. Magnani L, Ballantyne EB, Zhang X, Lupien M. PBX1 Genomic Pioneer Function Drives ERalpha Signaling Underlying Progression in Breast Cancer. *PLoS Genet* 2011;7(11):e1002368.
116. Paweletz CP, Charboneau L, Bichsel VE, Simone NL, Chen T, Gillespie JW, Emmert-Buck MR, Roth MJ, Petricoin IE, Liotta LA. Reverse phase protein microarrays which capture disease progression show activation of pro-survival pathways at the cancer invasion front. *Oncogene* 2001;20(16):1981-9.
117. Petricoin EF, 3rd, Espina V, Araujo RP, Midura B, Yeung C, Wan X, Eichler GS, Johann DJ, Jr., Qualman S, Tsokos M and others. Phosphoprotein pathway mapping: Akt/mammalian target of rapamycin activation is negatively associated with childhood rhabdomyosarcoma survival. *Cancer Res* 2007;67(7):3431-40.
118. VanMeter AJ, Rodriguez AS, Bowman ED, Jen J, Harris CC, Deng J, Calvert VS, Silvestri A, Fredolini C, Chandhoke V and others. Laser capture microdissection and protein microarray analysis of human non-small cell lung cancer: differential epidermal growth factor receptor (EGFR) phosphorylation events associated with mutated EGFR compared with wild type. *Mol Cell Proteomics* 2008;7(10):1902-24.
119. Hoyer-Hansen M, Jaattela M. Autophagy: an emerging target for cancer therapy. *Autophagy* 2008;4(5):574-80.
120. Huang J, Klionsky DJ. Autophagy and human disease. *Cell Cycle* 2007;6(15):1837-49.
121. Lum JJ, DeBerardinis RJ, Thompson CB. Autophagy in metazoans: cell survival in the land of plenty. *Nat Rev Mol Cell Biol* 2005;6(6):439-48.
122. De Duve C, Wattiaux R. Functions of lysosomes. *Annu Rev Physiol* 1966;28:435-92.
123. Deter RL, Baudhuin P, De Duve C. Participation of lysosomes in cellular autophagy induced in rat liver by glucagon. *J Cell Biol* 1967;35(2):C11-6.
124. Deter RL, De Duve C. Influence of glucagon, an inducer of cellular autophagy, on some physical properties of rat liver lysosomes. *J Cell Biol* 1967;33(2):437-49.
125. Klionsky DJ. Autophagy revisited: a conversation with Christian de Duve. *Autophagy* 2008;4(6):740-3.
126. Seglen PO, Gordon PB. Effects of lysosomotropic monoamines, diamines, amino alcohols, and other amino compounds on protein degradation and protein synthesis in isolated rat hepatocytes. *Mol Pharmacol* 1980;18(3):468-75.

127. Klionsky DJ, Abdalla FC, Abeliovich H, Abraham RT, Acevedo-Arozena A, Adeli K, Agholme L, Agnello M, Agostinis P, Aguirre-Ghiso JA and others. Guidelines for the use and interpretation of assays for monitoring autophagy. *Autophagy* 2012;8(4):445-544.
128. Gyorki DE, Asselin-Labat ML, van Rooijen N, Lindeman GJ, Visvader JE. Resident macrophages influence stem cell activity in the mammary gland. *Breast Cancer Res* 2009;11(4):R62.
129. O'Brien J, Schedin P. Macrophages in breast cancer: do involution macrophages account for the poor prognosis of pregnancy-associated breast cancer? *J Mammary Gland Biol Neoplasia* 2009;14(2):145-57.
130. Hussein MR, Hassan HI. Analysis of the mononuclear inflammatory cell infiltrate in the normal breast, benign proliferative breast disease, in situ and infiltrating ductal breast carcinomas: preliminary observations. *J Clin Pathol* 2006;59(9):972-7.
131. Moreira JM, Cabezon T, Gromova I, Gromov P, Timmermans-Wielenga V, Machado I, Llombart-Bosch A, Kroman N, Rank F, Celis JE. Tissue proteomics of the human mammary gland: towards an abridged definition of the molecular phenotypes underlying epithelial normalcy. *Mol Oncol* 2010;4(6):539-61.
132. Sheri A, Dowsett M. Developments in Ki67 and other biomarkers for treatment decision making in breast cancer. *Ann Oncol* 2012;23 Suppl 10:x219-27.
133. Walker RA. Immunohistochemical markers as predictive tools for breast cancer. *J Clin Pathol* 2008;61(6):689-96.
134. Zagouri F, Sergentanis TN, Zografos GC. Precursors and preinvasive lesions of the breast: the role of molecular prognostic markers in the diagnostic and therapeutic dilemma. *World J Surg Oncol* 2007;5:57.
135. de Roos MA, van der Vegt B, de Vries J, Wesseling J, de Bock GH. Pathological and biological differences between screen-detected and interval ductal carcinoma in situ of the breast. *Ann Surg Oncol* 2007;14(7):2097-104.
136. Silverstein MJ, Craig PH, Lagios MD, Waisman JK, Lewinsky BS, Colburn WJ, Poller DN. Developing a prognostic index for ductal carcinoma in situ of the breast. Are we there yet? *Cancer* 1996;78(5):1138-40.
137. Silverstein MJ, Lagios MD, Craig PH, Waisman JR, Lewinsky BS, Colburn WJ, Poller DN. A prognostic index for ductal carcinoma in situ of the breast. *Cancer* 1996;77(11):2267-74.

138. Pinder SE. Ductal carcinoma in situ (DCIS): pathological features, differential diagnosis, prognostic factors and specimen evaluation. *Mod Pathol* 2010;23 Suppl 2:S8-13.
139. Liotta LA, Espina V, Mehta AI, Calvert V, Rosenblatt K, Geho D, Munson PJ, Young L, Wulfkuhle J, Petricoin EF, 3rd. Protein microarrays: meeting analytical challenges for clinical applications. *Cancer Cell* 2003;3(4):317-25.
140. Liotta LA, Tryggvason K, Garbisa S, Hart I, Foltz CM, Shafie S. Metastatic potential correlates with enzymatic degradation of basement membrane collagen. *Nature* 1980;284(5751):67-8.
141. Witkiewicz AK, Dasgupta A, Sotgia F, Mercier I, Pestell RG, Sabel M, Klee CG, Brody JR, Lisanti MP. An absence of stromal caveolin-1 expression predicts early tumor recurrence and poor clinical outcome in human breast cancers. *Am J Pathol* 2009;174(6):2023-34.
142. Chen L, Shen R, Ye Y, Pu XA, Liu X, Duan W, Wen J, Zimmerer J, Wang Y, Liu Y and others. Precancerous stem cells have the potential for both benign and malignant differentiation. *PLoS One* 2007;2(3):e293.
143. Tlsty T. Cancer: whispering sweet somethings. *Nature* 2008;453(7195):604-5.
144. Gong C, Bauvy C, Tonelli G, Yue W, Delomenie C, Nicolas V, Zhu Y, Domergue V, Marin-Esteban V, Tharinger H and others. Beclin 1 and autophagy are required for the tumorigenicity of breast cancer stem-like/progenitor cells. *Oncogene* 2012.
145. Kondo Y, Kondo S. Autophagy and cancer therapy. *Autophagy* 2006;2(2):85-90.
146. Jin S, DiPaola RS, Mathew R, White E. Metabolic catastrophe as a means to cancer cell death. *J Cell Sci* 2007;120(Pt 3):379-83.
147. Jin S, White E. Tumor suppression by autophagy through the management of metabolic stress. *Autophagy* 2008;4(5):563-6.
148. Liang XH, Jackson S, Seaman M, Brown K, Kempkes B, Hibshoosh H, Levine B. Induction of autophagy and inhibition of tumorigenesis by beclin 1. *Nature* 1999;402(6762):672-6.
149. Vazquez-Martin A, Oliveras-Ferreros C, Menendez JA. Autophagy facilitates the development of breast cancer resistance to the anti-HER2 monoclonal antibody trastuzumab. *PLoS One* 2009;4(7):e6251.

150. Mantovani A, Biswas SK, Galdiero MR, Sica A, Locati M. Macrophage plasticity and polarization in tissue repair and remodelling. *J Pathol* 2013;229(2):176-85.
151. O'Brien J, Lyons T, Monks J, Lucia MS, Wilson RS, Hines L, Man YG, Borges V, Schedin P. Alternatively activated macrophages and collagen remodeling characterize the postpartum involuting mammary gland across species. *Am J Pathol* 2010;176(3):1241-55.
152. Lotze MT, Buchser WJ, Liang X. Blocking the interleukin 2 (IL2)-induced systemic autophagic syndrome promotes profound antitumor effects and limits toxicity. *Autophagy* 2012;8(8):1264-6.
153. Tang D, Kang R, Livesey KM, Cheh CW, Farkas A, Loughran P, Hoppe G, Bianchi ME, Tracey KJ, Zeh HJ, 3rd and others. Endogenous HMGB1 regulates autophagy. *J Cell Biol* 2010;190(5):881-92.
154. Vakkila J, Lotze MT. Inflammation and necrosis promote tumour growth. *Nat Rev Immunol* 2004;4(8):641-8.
155. Liang X, De Vera ME, Buchser WJ, Romo de Vivar Chavez A, Loughran P, Beer Stolz D, Basse P, Wang T, Van Houten B, Zeh HJ, 3rd and others. Inhibiting systemic autophagy during interleukin 2 immunotherapy promotes long-term tumor regression. *Cancer Res* 2012;72(11):2791-801.
156. Pollard JW. Trophic macrophages in development and disease. *Nat Rev Immunol* 2009;9(4):259-70.
157. Espina V, Liotta LA. Chloroquine enjoys a renaissance as an anti-neoplastic therapy. *Clinical Investigation* 2013 (submitted).
158. Nik-Zainal S, Van Loo P, Wedge DC, Alexandrov LB, Greenman CD, Lau KW, Raine K, Jones D, Marshall J, Ramakrishna M and others. The life history of 21 breast cancers. *Cell* 2012;149(5):994-1007.
159. Polyak K. Breast cancer: origins and evolution. *J Clin Invest* 2007;117(11):3155-63.
160. Paik S, Shak S, Tang G, Kim C, Baker J, Cronin M, Baehner FL, Walker MG, Watson D, Park T and others. A multigene assay to predict recurrence of tamoxifen-treated, node-negative breast cancer. *N Engl J Med* 2004;351(27):2817-26.
161. Paik S, Tang G, Shak S, Kim C, Baker J, Kim W, Cronin M, Baehner FL, Watson D, Bryant J and others. Gene expression and benefit of chemotherapy in women with node-negative, estrogen receptor-positive breast cancer. *J Clin Oncol* 2006;24(23):3726-34.

162. Lengauer C, Kinzler KW, Vogelstein B. Genetic instabilities in human cancers. *Nature* 1998;396(6712):643-9.
163. Pihan GA, Purohit A, Wallace J, Knecht H, Woda B, Quesenberry P, Doxsey SJ. Centrosome defects and genetic instability in malignant tumors. *Cancer Res* 1998;58(17):3974-85.
164. Pihan GA, Wallace J, Zhou Y, Doxsey SJ. Centrosome abnormalities and chromosome instability occur together in pre-invasive carcinomas. *Cancer Res* 2003;63(6):1398-404.
165. Ho L, Crabtree GR. Chromatin remodelling during development. *Nature* 2010;463(7280):474-84.
166. Levine B, Klionsky DJ. Development by self-digestion: molecular mechanisms and biological functions of autophagy. *Dev Cell* 2004;6(4):463-77.
167. Seglen PO, Gordon PB, Tolleshaug H, Hoyvik H. Use of [<sup>3</sup>H]raffinose as a specific probe of autophagic sequestration. *Exp Cell Res* 1986;162(1):273-7.
168. Shintani T, Klionsky DJ. Autophagy in health and disease: a double-edged sword. *Science* 2004;306(5698):990-5.
169. White E, DiPaola RS. The double-edged sword of autophagy modulation in cancer. *Clin Cancer Res* 2009;15(17):5308-16.
170. Green DR, Galluzzi L, Kroemer G. Mitochondria and the autophagy-inflammation-cell death axis in organismal aging. *Science* 2011;333(6046):1109-12.
171. Lane N. Evolution. The costs of breathing. *Science* 2011;334(6053):184-5.
172. Stephens PJ, McBride DJ, Lin ML, Varela I, Pleasance ED, Simpson JT, Stebbings LA, Leroy C, Edkins S, Mudie LJ and others. Complex landscapes of somatic rearrangement in human breast cancer genomes. *Nature* 2009;462(7276):1005-10.
173. Peiffer DA, Le JM, Steemers FJ, Chang W, Jenniges T, Garcia F, Haden K, Li J, Shaw CA, Belmont J and others. High-resolution genomic profiling of chromosomal aberrations using Infinium whole-genome genotyping. *Genome Res* 2006;16(9):1136-48.
174. Perkel J. SNP genotyping: six technologies that keyed a revolution. *Nature Methods* 2008;5(5):447-454.
175. Rasmussen M, Sundstrom M, Goransson Kultima H, Botling J, Micke P, Birgisson H, Glimelius B, Isaksson A. Allele-specific copy number analysis of tumor samples with aneuploidy and tumor heterogeneity. *Genome Biol* 2011;12(10):R108.



176. Shlien A, Malkin D. Copy number variations and cancer. *Genome Med* 2009;1(6):62.
177. Mardis ER. The impact of next-generation sequencing technology on genetics. *Trends Genet* 2008;24(3):133-41.
178. Rao SK, Edwards J, Joshi AD, Siu IM, Riggins GJ. A survey of glioblastoma genomic amplifications and deletions. *J Neurooncol* 2010;96(2):169-79.
179. Smith DR, Quinlan AR, Peckham HE, Makowsky K, Tao W, Woolf B, Shen L, Donahue WF, Tusneem N, Stromberg MP and others. Rapid whole-genome mutational profiling using next-generation sequencing technologies. *Genome Res* 2008;18(10):1638-42.
180. Barnes GL, Hebert KE, Kamal M, Javed A, Einhorn TA, Lian JB, Stein GS, Gerstenfeld LC. Fidelity of Runx2 activity in breast cancer cells is required for the generation of metastases-associated osteolytic disease. *Cancer Res* 2004;64(13):4506-13.
181. Barnes GL, Javed A, Waller SM, Kamal MH, Hebert KE, Hassan MQ, Bellahcene A, Van Wijnen AJ, Young MF, Lian JB and others. Osteoblast-related transcription factors Runx2 (Cbfa1/AML3) and MSX2 mediate the expression of bone sialoprotein in human metastatic breast cancer cells. *Cancer Res* 2003;63(10):2631-7.
182. Birk C, Poch O, Romier C, Ruff M, Mengus G, Lavigne AC, Davidson I, Moras D. Human TAF(II)28 and TAF(II)18 interact through a histone fold encoded by atypical evolutionary conserved motifs also found in the SPT3 family. *Cell* 1998;94(2):239-49.
183. Liu X, Tesfai J, Evrard YA, Dent SY, Martinez E. c-Myc transformation domain recruits the human STAGA complex and requires TRRAP and GCN5 acetylase activity for transcription activation. *J Biol Chem* 2003;278(22):20405-12.
184. Liu X, Vorontchikhina M, Wang YL, Faiola F, Martinez E. STAGA recruits Mediator to the MYC oncoprotein to stimulate transcription and cell proliferation. *Mol Cell Biol* 2008;28(1):108-21.
185. Martinez E, Kundu TK, Fu J, Roeder RG. A human SPT3-TAFII31-GCN5-L acetylase complex distinct from transcription factor IID. *J Biol Chem* 1998;273(37):23781-5.
186. Martinez E, Palhan VB, Tjernberg A, Lyman ES, Gamper AM, Kundu TK, Chait BT, Roeder RG. Human STAGA complex is a chromatin-acetylating transcription coactivator that interacts with pre-mRNA splicing and DNA damage-binding factors in vivo. *Mol Cell Biol* 2001;21(20):6782-95.

187. Redon R, Ishikawa S, Fitch KR, Feuk L, Perry GH, Andrews TD, Fiegler H, Shapero MH, Carson AR, Chen W and others. Global variation in copy number in the human genome. *Nature* 2006;444(7118):444-54.
188. Sebat J, Lakshmi B, Troge J, Alexander J, Young J, Lundin P, Maner S, Massa H, Walker M, Chi M and others. Large-scale copy number polymorphism in the human genome. *Science* 2004;305(5683):525-8.
189. O'Brien RL, Allison JL, Hahn FE. Evidence for intercalation of chloroquine into DNA. *Biochim Biophys Acta* 1966;129(3):622-4.
190. O'Brien RL, Olenick JG, Hahn FE. Reactions of quinine, chloroquine, and quinacrine with DNA and their effects on the DNA and RNA polymerase reactions. *Proc Natl Acad Sci U S A* 1966;55(6):1511-7.
191. Fox R. Anti-malarial drugs: possible mechanisms of action in autoimmune disease and prospects for drug development. *Lupus* 1996;5 Suppl 1:S4-10.
192. Wu Y, Shang X, Sarkissyan M, Slamon D, Vadgama JV. FOXO1A is a target for HER2-overexpressing breast tumors. *Cancer Res* 2010;70(13):5475-85.
193. Hoyvik H, Gordon PB, Seglen PO. Use of a hydrolysable probe, [<sup>14</sup>C]lactose, to distinguish between pre-lysosomal and lysosomal steps in the autophagic pathway. *Exp Cell Res* 1986;166(1):1-14.
194. Seglen PO, Gordon PB, Hoyvik H. Radiolabelled sugars as probes of hepatocytic autophagy. *Biomed Biochim Acta* 1986;45(11-12):1647-56.
195. Schwarze PE, Pettersen EO, Seglen PO. Characterization of hepatocytes from carcinogen-treated rats by two-parametric flow cytometry. *Carcinogenesis* 1986;7(1):171-3.
196. Seglen PO, Schwarze PE, Saeter G. Changes in cellular ploidy and autophagic responsiveness during rat liver carcinogenesis. *Toxicol Pathol* 1986;14(3):342-8.
197. He Y, Wu J, Dressman DC, Iacobuzio-Donahue C, Markowitz SD, Velculescu VE, Diaz LA, Jr., Kinzler KW, Vogelstein B, Papadopoulos N. Heteroplasmic mitochondrial DNA mutations in normal and tumour cells. *Nature* 2010;464(7288):610-4.
198. Wallace DC. Colloquium paper: bioenergetics, the origins of complexity, and the ascent of man. *Proc Natl Acad Sci U S A* 2010;107 Suppl 2:8947-53.

199. Gaines G, Rossi C, Attardi G. Markedly different ATP requirements for rRNA synthesis and mtDNA light strand transcription versus mRNA synthesis in isolated human mitochondria. *J Biol Chem* 1987;262(4):1907-15.
200. Kenneth NS, Mudie S, van Uden P, Rocha S. SWI/SNF regulates the cellular response to hypoxia. *J Biol Chem* 2009;284(7):4123-31.
201. Ernst J, Kheradpour P, Mikkelsen TS, Shoresh N, Ward LD, Epstein CB, Zhang X, Wang L, Issner R, Coyne M and others. Mapping and analysis of chromatin state dynamics in nine human cell types. *Nature* 2011;473(7345):43-9.
202. Sawadogo M, Roeder RG. Energy requirement for specific transcription initiation by the human RNA polymerase II system. *J Biol Chem* 1984;259(8):5321-6.
203. Barski A, Cuddapah S, Cui K, Roh TY, Schones DE, Wang Z, Wei G, Chepelev I, Zhao K. High-resolution profiling of histone methylations in the human genome. *Cell* 2007;129(4):823-37.
204. Hawkins RD, Hon GC, Lee LK, Ngo Q, Lister R, Pelizzola M, Edsall LE, Kuan S, Luu Y, Klugman S and others. Distinct epigenomic landscapes of pluripotent and lineage-committed human cells. *Cell Stem Cell* 2010;6(5):479-91.
205. Jin C, Zang C, Wei G, Cui K, Peng W, Zhao K, Felsenfeld G. H3.3/H2A.Z double variant-containing nucleosomes mark 'nucleosome-free regions' of active promoters and other regulatory regions. *Nat Genet* 2009;41(8):941-5.
206. Jothi R, Cuddapah S, Barski A, Cui K, Zhao K. Genome-wide identification of in vivo protein-DNA binding sites from ChIP-Seq data. *Nucleic Acids Res* 2008;36(16):5221-31.
207. Martinez-Garcia E, Popovic R, Min DJ, Sweet SM, Thomas PM, Zamdborg L, Heffner A, Will C, Lamy L, Staudt LM and others. The MMSET histone methyl transferase switches global histone methylation and alters gene expression in t(4;14) multiple myeloma cells. *Blood* 2011;117(1):211-20.
208. Takeuchi JK, Bruneau BG. Directed transdifferentiation of mouse mesoderm to heart tissue by defined factors. *Nature* 2009;459(7247):708-11.
209. Wang Z, Zang C, Rosenfeld JA, Schones DE, Barski A, Cuddapah S, Cui K, Roh TY, Peng W, Zhang MQ and others. Combinatorial patterns of histone acetylations and methylations in the human genome. *Nat Genet* 2008;40(7):897-903.
210. Aita VM, Liang XH, Murty VV, Pincus DL, Yu W, Cayanis E, Kalachikov S, Gilliam TC, Levine B. Cloning and genomic organization of beclin 1, a candidate tumor suppressor gene on chromosome 17q21. *Genomics* 1999;59(1):59-65.

211. Qu X, Zou Z, Sun Q, Luby-Phelps K, Cheng P, Hogan RN, Gilpin C, Levine B. Autophagy gene-dependent clearance of apoptotic cells during embryonic development. *Cell* 2007;128(5):931-46.
212. Mungall AJ, Palmer SA, Sims SK, Edwards CA, Ashurst JL, Wilming L, Jones MC, Horton R, Hunt SE, Scott CE and others. The DNA sequence and analysis of human chromosome 6. *Nature* 2003;425(6960):805-11.
213. Akech J, Wixted JJ, Bedard K, van der Deen M, Hussain S, Guise TA, van Wijnen AJ, Stein JL, Languino LR, Altieri DC and others. Runx2 association with progression of prostate cancer in patients: mechanisms mediating bone osteolysis and osteoblastic metastatic lesions. *Oncogene* 2010;29(6):811-21.
214. Kilbey A, Terry A, Jenkins A, Borland G, Zhang Q, Wakelam MJ, Cameron ER, Neil JC. Runx regulation of sphingolipid metabolism and survival signaling. *Cancer Res* 2010;70(14):5860-9.
215. van der Deen M, Akech J, Lapointe D, Gupta S, Young DW, Montecino MA, Galindo M, Lian JB, Stein JL, Stein GS and others. Genomic promoter occupancy of runt-related transcription factor RUNX2 in Osteosarcoma cells identifies genes involved in cell adhesion and motility. *J Biol Chem* 2012;287(7):4503-17.
216. Collins A, Littman DR, Taniuchi I. RUNX proteins in transcription factor networks that regulate T-cell lineage choice. *Nat Rev Immunol* 2009;9(2):106-15.
217. Gardner KE, Allis CD, Strahl BD. Operating on chromatin, a colorful language where context matters. *J Mol Biol* 2011;409(1):36-46.
218. Allis CD, Muir TW. Spreading Chromatin into Chemical Biology. *Chembiochem* 2011;12:264-279.
219. Allfrey VG, Faulkner R, Mirsky AE. Acetylation and Methylation of Histones and Their Possible Role in the Regulation of Rna Synthesis. *Proc Natl Acad Sci U S A* 1964;51:786-94.
220. Strahl BD, Allis CD. The language of covalent histone modifications. *Nature* 2000;403(6765):41-5.
221. Wolffe AP, Hayes JJ. Chromatin disruption and modification. *Nucleic Acids Res* 1999;27(3):711-20.
222. Northrup DL, Zhao K. Application of ChIP-Seq and related techniques to the study of immune function. *Immunity* 2011;34(6):830-42.

223. Wang Z, Zang C, Cui K, Schones DE, Barski A, Peng W, Zhao K. Genome-wide mapping of HATs and HDACs reveals distinct functions in active and inactive genes. *Cell* 2009;138(5):1019-31.
224. Arnold K, Bordoli L, Kopp J, Schwede T. The SWISS-MODEL workspace: a web-based environment for protein structure homology modelling. *Bioinformatics* 2006;22(2):195-201.
225. Guex N, Peitsch MC. SWISS-MODEL and the Swiss-PdbViewer: an environment for comparative protein modeling. *Electrophoresis* 1997;18(15):2714-23.
226. Schwede T, Kopp J, Guex N, Peitsch MC. SWISS-MODEL: An automated protein homology-modeling server. *Nucleic Acids Res* 2003;31(13):3381-5.
227. Harima Y, Harima K, Sawada S, Tanaka Y, Arita S, Ohnishi T. Loss of heterozygosity on chromosome 6p21.2 as a potential marker for recurrence after radiotherapy of human cervical cancer. *Clin Cancer Res* 2000;6(3):1079-85.
228. Blakely CM, Sintasath L, D'Cruz CM, Hahn KT, Dugan KD, Belka GK, Chodosh LA. Developmental stage determines the effects of MYC in the mammary epithelium. *Development* 2005;132(5):1147-60.
229. Warburg O. On respiratory impairment in cancer cells. *Science* 1956;124(3215):269-70.
230. Warburg O. On the origin of cancer cells. *Science* 1956;123(3191):309-14.
231. Klein L, Munz C, Lunemann JD. Autophagy-mediated antigen processing in CD4(+) T cell tolerance and immunity. *FEBS Lett* 2010;584(7):1405-10.
232. Jaeger PA, Wyss-Coray T. All-you-can-eat: autophagy in neurodegeneration and neuroprotection. *Mol Neurodegener* 2009;4:16.
233. Dengjel J, Kristensen AR, Andersen JS. Ordered bulk degradation via autophagy. *Autophagy* 2008;4(8):1057-9.
234. Zimmermann AC, Zarei M, Eiselein S, Dengjel J. Quantitative proteomics for the analysis of spatio-temporal protein dynamics during autophagy. *Autophagy* 2010;6(8):1009-16.
235. Mzayek F, Deng H, Mather FJ, Wasilevich EC, Liu H, Hadi CM, Chansolme DH, Murphy HA, Melek BH, Tenaglia AN and others. Randomized dose-ranging controlled trial of AQ-13, a candidate antimalarial, and chloroquine in healthy volunteers. *PLoS Clin Trials* 2007;2(1):e6.

236. Schlitzer M. Malaria chemotherapeutics part I: History of antimalarial drug development, currently used therapeutics, and drugs in clinical development. *ChemMedChem* 2007;2(7):944-86.
237. Loehberg CR, Thompson T, Kastan MB, Maclean KH, Edwards DG, Kittrell FS, Medina D, Conneely OM, O'Malley BW. Ataxia telangiectasia-mutated and p53 are potential mediators of chloroquine-induced resistance to mammary carcinogenesis. *Cancer Res* 2007;67(24):12026-33.
238. Bellodi C, Lidonnici MR, Hamilton A, Helgason GV, Soliera AR, Ronchetti M, Galavotti S, Young KW, Selmi T, Yacobi R and others. Targeting autophagy potentiates tyrosine kinase inhibitor-induced cell death in Philadelphia chromosome-positive cells, including primary CML stem cells. *J Clin Invest* 2009;119(5):1109-23.
239. Schoenlein PV, Periyasamy-Thandavan S, Samaddar JS, Jackson WH, Barrett JT. Autophagy facilitates the progression of ERalpha-positive breast cancer cells to antiestrogen resistance. *Autophagy* 2009;5(3):400-3.
240. Amaravadi RK, Yu D, Lum JJ, Bui T, Christophorou MA, Evan GI, Thomas-Tikhonenko A, Thompson CB. Autophagy inhibition enhances therapy-induced apoptosis in a Myc-induced model of lymphoma. *J Clin Invest* 2007;117(2):326-36.
241. Degtyarev M, De Maziere A, Orr C, Lin J, Lee BB, Tien JY, Prior WW, van Dijk S, Wu H, Gray DC and others. Akt inhibition promotes autophagy and sensitizes PTEN-null tumors to lysosomotropic agents. *J Cell Biol* 2008;183(1):101-16.
242. Palmieri M, Impey S, Kang H, di Ronza A, Pelz C, Sardiello M, Ballabio A. Characterization of the CLEAR network reveals an integrated control of cellular clearance pathways. *Hum Mol Genet* 2011;20(19):3852-66.
243. Eisenhoffer GT, Loftus PD, Yoshigi M, Otsuna H, Chien CB, Morcos PA, Rosenblatt J. Crowding induces live cell extrusion to maintain homeostatic cell numbers in epithelia. *Nature* 2012;484(7395):546-9.
244. O'Neill PM, Bray PG, Hawley SR, Ward SA, Park BK. 4-Aminoquinolines--past, present, and future: a chemical perspective. *Pharmacol Ther* 1998;77(1):29-58.
245. Jensen M, Mehlhorn H. Seventy-five years of Resochin in the fight against malaria. *Parasitol Res* 2009;105(3):609-27.
246. Krafts K, Hempelmann E, Skorska-Stania A. From methylene blue to chloroquine: a brief review of the development of an antimalarial therapy. *Parasitol Res* 2012;111(1):1-6.

247. Solomon VR, Lee H. Chloroquine and its analogs: a new promise of an old drug for effective and safe cancer therapies. *Eur J Pharmacol* 2009;625(1-3):220-33.
248. Warhurst DC, Steele JC, Adagu IS, Craig JC, Cullander C. Hydroxychloroquine is much less active than chloroquine against chloroquine-resistant *Plasmodium falciparum*, in agreement with its physicochemical properties. *J Antimicrob Chemother* 2003;52(2):188-93.
249. Boyer MJ, Tannock IF. Regulation of intracellular pH in tumor cell lines: influence of microenvironmental conditions. *Cancer Res* 1992;52(16):4441-7.
250. Furst DE. Pharmacokinetics of hydroxychloroquine and chloroquine during treatment of rheumatic diseases. *Lupus* 1996;5 Suppl 1:S11-5.
251. Gustafsson LL, Walker O, Alvan G, Beermann B, Estevez F, Gleisner L, Lindstrom B, Sjoqvist F. Disposition of chloroquine in man after single intravenous and oral doses. *Br J Clin Pharmacol* 1983;15(4):471-9.
252. Walker O, Birkett DJ, Alvan G, Gustafsson LL, Sjoqvist F. Characterization of chloroquine plasma protein binding in man. *Br J Clin Pharmacol* 1983;15(3):375-7.
253. Lipinski CA, Lombardo F, Dominy BW, Feeney PJ. Experimental and computational approaches to estimate solubility and permeability in drug discovery and development settings. *Adv Drug Deliv Rev* 2001;46(1-3):3-26.
254. Bickerton GR, Paolini GV, Besnard J, Muresan S, Hopkins AL. Quantifying the chemical beauty of drugs. *Nat Chem* 2012;4(2):90-8.
255. Boelaert JR, Yaro S, Augustijns P, Meda N, Schneider YJ, Schols D, Mols R, De Laere EA, Van de Perre P. Chloroquine accumulates in breast-milk cells: potential impact in the prophylaxis of postnatal mother-to-child transmission of HIV-1. *AIDS* 2001;15(16):2205-7.
256. Nation RL, Hackett LP, Dusci LJ, Ilett KF. Excretion of hydroxychloroquine in human milk. *Br J Clin Pharmacol* 1984;17(3):368-9.
257. Ducharme J, Farinotti R. Clinical pharmacokinetics and metabolism of chloroquine. Focus on recent advancements. *Clin Pharmacokinet* 1996;31(4):257-74.
258. Preissner S, Kroll K, Dunkel M, Senger C, Goldsobel G, Kuzman D, Guenther S, Winnenburg R, Schroeder M, Preissner R. SuperCYP: a comprehensive database on Cytochrome P450 enzymes including a tool for analysis of CYP-drug interactions. *Nucleic Acids Res* 2009;38(Database issue):D237-43.

259. Kim KA, Park JY, Lee JS, Lim S. Cytochrome P450 2C8 and CYP3A4/5 are involved in chloroquine metabolism in human liver microsomes. *Arch Pharm Res* 2003;26(8):631-7.
260. Projean D, Baune B, Farinotti R, Flinois JP, Beaune P, Taburet AM, Ducharme J. In vitro metabolism of chloroquine: identification of CYP2C8, CYP3A4, and CYP2D6 as the main isoforms catalyzing N-desethylchloroquine formation. *Drug Metab Dispos* 2003;31(6):748-54.
261. Goetz MP, Knox SK, Suman VJ, Rae JM, Safgren SL, Ames MM, Visscher DW, Reynolds C, Couch FJ, Lingle WL and others. The impact of cytochrome P450 2D6 metabolism in women receiving adjuvant tamoxifen. *Breast Cancer Res Treat* 2007;101(1):113-21.
262. Antuofermo E, Miller MA, Pirino S, Xie J, Badve S, Mohammed SI. Spontaneous mammary intraepithelial lesions in dogs--a model of breast cancer. *Cancer Epidemiol Biomarkers Prev* 2007;16(11):2247-56.
263. Berridge MJ, Bootman MD, Roderick HL. Calcium signalling: dynamics, homeostasis and remodelling. *Nat Rev Mol Cell Biol* 2003;4(7):517-29.
264. Carafoli E. Intracellular calcium homeostasis. *Annu Rev Biochem* 1987;56:395-433.
265. VanHouten J, Sullivan C, Bazinet C, Ryoo T, Camp R, Rimm DL, Chung G, Wysolmerski J. PMCA2 regulates apoptosis during mammary gland involution and predicts outcome in breast cancer. *Proc Natl Acad Sci U S A* 2010;107(25):11405-10.
266. Liang CC, Park AY, Guan JL. In vitro scratch assay: a convenient and inexpensive method for analysis of cell migration in vitro. *Nat Protoc* 2007;2(2):329-33.
267. Rabinowitz JD, White E. Autophagy and metabolism. *Science* 2010;330(609):1344-8.
268. Katayama M, Kawaguchi T, Berger MS, Pieper RO. DNA damaging agent-induced autophagy produces a cytoprotective adenosine triphosphate surge in malignant glioma cells. *Cell Death Differ* 2007;14(3):548-58.
269. Plomp PJ, Wolvetang EJ, Groen AK, Meijer AJ, Gordon PB, Seglen PO. Energy dependence of autophagic protein degradation in isolated rat hepatocytes. *Eur J Biochem* 1987;164(1):197-203.
270. Kristensen AR, Schandorff S, Hoyer-Hansen M, Nielsen MO, Jaattela M, Dengjel J, Andersen JS. Ordered organelle degradation during starvation-induced autophagy. *Mol Cell Proteomics* 2008;7(12):2419-28.



271. Chen X, Ballin JD, Della-Maria J, Tsai MS, White EJ, Tomkinson AE, Wilson GM. Distinct kinetics of human DNA ligases I, IIIalpha, IIIbeta, and IV reveal direct DNA sensing ability and differential physiological functions in DNA repair. *DNA Repair (Amst)* 2009;8(8):961-8.
272. Soutoglou E, Dorn JF, Sengupta K, Jasin M, Nussenzweig A, Ried T, Danuser G, Misteli T. Positional stability of single double-strand breaks in mammalian cells. *Nat Cell Biol* 2007;9(6):675-82.
273. Tobin LA, Robert C, Nagaria P, Chumsri S, Twaddell W, Ioffe OB, Greco GE, Brodie AH, Tomkinson AE, Rassool FV. Targeting abnormal DNA repair in therapy-resistant breast cancers. *Mol Cancer Res* 2011.
274. Dinant C, Houtsmuller AB, Vermeulen W. Chromatin structure and DNA damage repair. *Epigenetics Chromatin* 2008;1(1):9.
275. Liang F, Han M, Romanienko PJ, Jasin M. Homology-directed repair is a major double-strand break repair pathway in mammalian cells. *Proc Natl Acad Sci U S A* 1998;95(9):5172-7.
276. Burrell RA, McClelland SE, Endesfelder D, Groth P, Weller MC, Shaikh N, Domingo E, Kanu N, Dewhurst SM, Gronroos E and others. Replication stress links structural and numerical cancer chromosomal instability. *Nature* 2013;494(7438):492-6.
277. Zhang Z, Wippo CJ, Wal M, Ward E, Korber P, Pugh BF. A packing mechanism for nucleosome organization reconstituted across a eukaryotic genome. *Science* 2011;332(6032):977-80.
278. Chabosseau P, Buhagiar-Labarchede G, Onclercq-Delic R, Lambert S, Debatisse M, Brison O, Amor-Gueret M. Pyrimidine pool imbalance induced by BLM helicase deficiency contributes to genetic instability in Bloom syndrome. *Nat Commun* 2011;2:368.
279. Martirosyan AR, Rahim-Bata R, Freeman AB, Clarke CD, Howard RL, Strobl JS. Differentiation-inducing quinolines as experimental breast cancer agents in the MCF-7 human breast cancer cell model. *Biochem Pharmacol* 2004;68(9):1729-38.
280. Rahim R, Strobl JS. Hydroxychloroquine, chloroquine, and all-trans retinoic acid regulate growth, survival, and histone acetylation in breast cancer cells. *Anticancer Drugs* 2009.
281. Boughey JC, Gonzalez RJ, Bonner E, Kuerer HM. Current treatment and clinical trial developments for ductal carcinoma in situ of the breast. *Oncologist* 2007;12(11):1276-87.

282. Fisher ER, Dignam J, Tan-Chiu E, Costantino J, Fisher B, Paik S, Wolmark N. Pathologic findings from the National Surgical Adjuvant Breast Project (NSABP) eight-year update of Protocol B-17: intraductal carcinoma. *Cancer* 1999;86(3):429-38.
283. Augustijns P, Geusens P, Verbeke N. Chloroquine levels in blood during chronic treatment of patients with rheumatoid arthritis. *Eur J Clin Pharmacol* 1992;42(4):429-33.
284. Wozniacka A, Cygankiewicz I, Chudzik M, Sysa-Jedrzejowska A, Wranicz JK. The cardiac safety of chloroquine phosphate treatment in patients with systemic lupus erythematosus: the influence on arrhythmia, heart rate variability and repolarization parameters. *Lupus* 2006;15(8):521-5.
285. Savarino A, Lucia MB, Giordano F, Cauda R. Risks and benefits of chloroquine use in anticancer strategies. *Lancet Oncol* 2006;7(10):792-3.
286. Sotelo J, Briceno E, Lopez-Gonzalez MA. Adding chloroquine to conventional treatment for glioblastoma multiforme: a randomized, double-blind, placebo-controlled trial. *Ann Intern Med* 2006;144(5):337-43.
287. Kelloff GJ, Sigman CC. Assessing intraepithelial neoplasia and drug safety in cancer-preventive drug development. *Nat Rev Cancer* 2007;7(7):508-18.
288. O'Shaughnessy JA, Kelloff GJ, Gordon GB, Dannenberg AJ, Hong WK, Fabian CJ, Sigman CC, Bertagnolli MM, Stratton SP, Lam S and others. Treatment and prevention of intraepithelial neoplasia: an important target for accelerated new agent development. *Clin Cancer Res* 2002;8(2):314-46.
289. Eisenhauer EA, Therasse P, Bogaerts J, Schwartz LH, Sargent D, Ford R, Dancey J, Arbuck S, Gwyther S, Mooney M and others. New response evaluation criteria in solid tumours: revised RECIST guideline (version 1.1). *Eur J Cancer* 2009;45(2):228-47.
290. Snoek-van Beurden PA, Von den Hoff JW. Zymographic techniques for the analysis of matrix metalloproteinases and their inhibitors. *Biotechniques* 2005;38(1):73-83.
291. Matsubara N, Mukai H, Fujii S, Wada N. Different prognostic significance of Ki-67 change between pre- and post-neoadjuvant chemotherapy in various subtypes of breast cancer. *Breast Cancer Res Treat* 2012;137(1):203-12.
292. Dowsett M, Nielsen TO, A'Hern R, Bartlett J, Coombes RC, Cuzick J, Ellis M, Henry NL, Hugh JC, Lively T and others. Assessment of Ki67 in breast cancer: recommendations from the International Ki67 in Breast Cancer working group. *J Natl Cancer Inst* 2011;103(22):1656-64.

293. Anderson H, Hills M, Zabaglo L, A'Hern R, Leary AF, Haynes BP, Smith IE, Dowsett M. Relationship between estrogen receptor, progesterone receptor, HER-2 and Ki67 expression and efficacy of aromatase inhibitors in advanced breast cancer. *Ann Oncol* 2011;22(8):1770-6.
294. Gerdes J, Lemke H, Baisch H, Wacker HH, Schwab U, Stein H. Cell cycle analysis of a cell proliferation-associated human nuclear antigen defined by the monoclonal antibody Ki-67. *J Immunol* 1984;133(4):1710-5.
295. Gerdes J, Li L, Schlueter C, Duchrow M, Wohlenberg C, Gerlach C, Stahmer I, Kloth S, Brandt E, Flad HD. Immunobiochemical and molecular biologic characterization of the cell proliferation-associated nuclear antigen that is defined by monoclonal antibody Ki-67. *Am J Pathol* 1991;138(4):867-73.
296. Gerdes J, Schwab U, Lemke H, Stein H. Production of a mouse monoclonal antibody reactive with a human nuclear antigen associated with cell proliferation. *Int J Cancer* 1983;31(1):13-20.
297. Chen N, Eritja N, Lock R, Debnath J. Autophagy restricts proliferation driven by oncogenic phosphatidylinositol 3-kinase in three-dimensional culture. *Oncogene* 2012.
298. Lazova R, Camp RL, Klump V, Siddiqui SF, Amaravadi RK, Pawelek JM. Punctate LC3B expression is a common feature of solid tumors and associated with proliferation, metastasis, and poor outcome. *Clin Cancer Res* 2012;18(2):370-9.
299. Miyachi K, Fritzler MJ, Tan EM. Autoantibody to a nuclear antigen in proliferating cells. *J Immunol* 1978;121(6):2228-34.
300. Muskhelishvili L, Latendresse JR, Kodell RL, Henderson EB. Evaluation of cell proliferation in rat tissues with BrdU, PCNA, Ki-67(MIB-5) immunohistochemistry and in situ hybridization for histone mRNA. *J Histochem Cytochem* 2003;51(12):1681-8.
301. Fox JT, Lee KY, Myung K. Dynamic regulation of PCNA ubiquitylation/deubiquitylation. *FEBS Lett* 2011;585(18):2780-5.
302. Sulkes A, Naparstek Y. The infrequent association of systemic lupus erythematosus and solid tumors. *Cancer* 1991;68(6):1389-93.
303. Howden LM, Meyer JA. Age and Sex Composition: 2010 Census Briefs. In: Commerce USDo, editor 2010 Census Summary File 1 (SF1). Washington, D.C.: United States Census Bureau; 2011. p 16.
304. Chen LS, Goodson P. Web-based survey of US health educators: challenges and lessons. *Am J Health Behav* 2010;34(1):3-11.

305. Dobrow MJ, Orchard MC, Golden B, Holowaty E, Paszat L, Brown AD, Sullivan T. Response audit of an Internet survey of health care providers and administrators: implications for determination of response rates. *J Med Internet Res* 2008;10(4):e30.
306. Gilmour JA, Scott SD, Huntington N. Nurses and Internet health information: a questionnaire survey. *J Adv Nurs* 2008;61(1):19-28.
307. Sapino A, Righi L, Cassoni P, Papotti M, Pietribiasi F, Bussolati G. Expression of the neuroendocrine phenotype in carcinomas of the breast. *Semin Diagn Pathol* 2000;17(2):127-37.
308. Campbell JP, Merkel AR, Masood-Campbell SK, Elefteriou F, Sterling JA. Models of bone metastasis. *J Vis Exp* 2012(67):e4260.
309. Campbell JP, Karolak MR, Ma Y, Perrien DS, Masood-Campbell SK, Penner NL, Munoz SA, Zijlstra A, Yang X, Sterling JA and others. Stimulation of host bone marrow stromal cells by sympathetic nerves promotes breast cancer bone metastasis in mice. *PLoS Biol* 2012;10(7):e1001363.
310. Chiechi A, Novello C, Magagnoli G, Deng J, Benassi MS, Picci P, Vaisman I, Espina V, Liotta LA. Elevated TNFR1 and Serotonin in bone metastasis are correlated with poor survival following bone metastasis diagnosis for both carcinoma and sarcoma primary tumors. *Clinical Cancer Research: An Official Journal of the American Association for Cancer Research* 2013:(in press).
311. Rajkumar SV. Multiple myeloma: 2013 update on diagnosis, risk-stratification, and management. *Am J Hematol* 2013;88(3):225-35.
312. Periyasamy-Thandavan S, Jackson WH, Samaddar JS, Erickson B, Barrett JR, Raney L, Gopal E, Ganapathy V, Hill WD, Bhalla KN and others. Bortezomib blocks the catabolic process of autophagy via a cathepsin-dependent mechanism, affects endoplasmic reticulum stress and induces caspase-dependent cell death in antiestrogen-sensitive and resistant ER+ breast cancer cells. *Autophagy* 2010;6(1):19-35.
313. Bernales S, McDonald KL, Walter P. Autophagy counterbalances endoplasmic reticulum expansion during the unfolded protein response. *PLoS Biol* 2006;4(12):e423.
314. Axe EL, Walker SA, Manifava M, Chandra P, Roderick HL, Habermann A, Griffiths G, Ktistakis NT. Autophagosome formation from membrane compartments enriched in phosphatidylinositol 3-phosphate and dynamically connected to the endoplasmic reticulum. *J Cell Biol* 2008;182(4):685-701.
315. Hayashi-Nishino M, Fujita N, Noda T, Yamaguchi A, Yoshimori T, Yamamoto A. A subdomain of the endoplasmic reticulum forms a cradle for autophagosome formation. *Nat Cell Biol* 2009;11(12):1433-7.

316. Tan EC, Leung T, Manser E, Lim L. The human active breakpoint cluster region-related gene encodes a brain protein with homology to guanine nucleotide exchange proteins and GTPase-activating proteins. *J Biol Chem* 1993;268(36):27291-8.
317. Clark AG, Miller AL, Vaughan E, Yu HY, Penkert R, Bement WM. Integration of single and multicellular wound responses. *Curr Biol* 2009;19(16):1389-95.

## **CURRICULUM VITAE**

Virginia Espina received her Bachelor of Science in Medical Technology from Rochester Institute of Technology in 1982. She was employed as a Medical Technologist, in the Chemistry/Special Chemistry laboratory at West Virginia University Hospital, Morgantown, WV, for 8 years. She was employed at Suburban Hospital, Bethesda, MD for the following 3 years, working in all areas of the clinical laboratory. For the next 9 years, she held several positions at Shady Grove Adventist Hospital, including Blood Bank Technologist, Blood Bank Lead Tech, Proficiency Improvement Coordinator, and Interim Laboratory Director. She received her Master of Science in Biotechnology from Johns Hopkins University in 1999. Virginia then began her research career at the National Institutes of Health/National Cancer Institute in the Laboratory of Pathology as the manager of the Laser Capture Microdissection Core Facility. She was recruited to George Mason University in 2005 as Research Faculty in the Center for Applied Proteomics and Molecular Medicine.